

https://dspace.org/

An Analysis of Avian Trunk Neural Crest Cell Migration In Vitro: Investigating the Role and Arrangement of Actin in Migrating Neural Crest Cells

Sahib, Mariam Bibi

2025
University of the Witwatersrand, Johannesburg
https://hdl.handle.net/10539/49836

Sahib, Mariam Bibi. (2025). An Analysis of Avian Trunk Neural Crest Cell Migration In Vitro: Investigating the Role and Arrangement of Actin in Migrating Neural Crest Cells [Master's dissertation, University of the Witwatersrand, Johannesburg]. WIReDSpace. https://hdl.handle.net/10539/49836

Downloaded from a DSpace repository. https://dspace.org/

AN ANALYSIS OF AVIAN TRUNK NEURAL CREST CELL MIGRATION *IN VITRO*: INVESTIGATING THE ROLE AND ARRANGEMENT OF ACTIN IN MIGRATING NEURAL CREST CELLS

Mariam Bibi Sahib

Student number: 1892562



A Dissertation submitted to the Faculty of Health Science, University of the Witwatersrand, in fulfilment of the requirements for the degree of Master of Science.

Johannesburg, 2025

DECLARATION

I Mariam Bibi Sahib declare that this Dissertation is my own, unaided work. It is being submitted for the Degree of at the Master of Science at the University of the Witwatersrand, Johannesburg. It has not been submitted before for any degree or examination at any other University.

: Mariam Bibi Sahib

(Signature of candidate)

_____28____day of____AUGUST_____2025_____in__Johannesburg_____

ABSTRACT

Neural crest (NC) cells are multipotent and highly migratory cells that are released from the crest of the neural folds in vertebrates. The NC cells give rise to a plethora of cells and tissues in the developing embryo and adult. The migratory behaviour of individual NC cells is said to be facilitated by actin filaments. Using an *in vitro* model, avian (quail) trunk neural tubes were cultured to obtain NC cells, in which the migration of individual NC cells could be studied. To determine the role of actin in the migration of NC cells, cytochalasin D was added to some of the cultures in order to block actin polymerisation. Cytochalasin D treated and untreated (control) neural crest cells were imaged over time. An anti-HNK antibody was used to specially detect NC cells in fixed cultures while Phalloidin-Atto590 was used to stain actin. Under control conditions, NC cells exhibited their typical stellate shape and displayed dynamic responses to signals from their external environment (i.e. cell-cell contact) which influenced the morphology of their projections and directed migration. In the cytochalasin D treated cells, NC cell morphology was altered, and the migratory capacity of the cells was significantly reduced. However, cytochalasin D treated cells, retained their ability to respond to environmental cues such as cell-cell contact. Thus, even when actin is disrupted, NC cell migration and their response to their environment appears to be somewhat maintained. These insights highlight the need to explore the molecular basis of NC cell migration especially under disrupted conditions, to further our understanding of neurocristopathies that arise as a result of abnormal NC cell migration.

ACKNOWLEDGEMENTS

I would like to express my deepest gratitude to all those who have supported me throughout the journey of completing this dissertation.

First and foremost, I would like to thank my supervisors, Emeritus Prof Beverley Kramer and Dr Aurelie Deroubaix, for their invaluable guidance, constant support, and insightful feedback. Their expertise and encouragement have been pivotal in shaping this work, and I feel incredibly fortunate to have had the opportunity to learn from them.

I would also like to extend my appreciation to the members of my proposal committee, Prof Tanya Augustine, Dr Kutlwano Xulu, Dr Jaclyn Johnson, Dr Sylvester Omoruyi and Dr Thabiso Tshabalala for their time, thoughtful comments, and constructive suggestions that greatly enhanced the quality of this research. Additionally, I would like to acknowledge Dr Thabiso Tshabalala for generously providing the anti-HNK antibody which was used.

I am immensely grateful to my family, whose unwavering support, love, and patience have been my strength throughout this endeavour. To my parents, thank you for believing in me and providing me with the foundation that made this possible.

A special thanks to my friends, Nastassia Altrich and Giselle Govender, for their camaraderie, and for being there during both the challenging and rewarding moments of this journey. Additionally, I would like to acknowledge Ms. Altrich for her work in testing the neutral red technique.

Finally, my heartfelt thanks to Ms. Hasiena Ali whose contributions were invaluable. I am grateful to Mr Mashudu Madauhu and Ms. Kagiso Matjila from the University of the Witwatersrand Central Animal Service Unit for their invaluable assistance.

This dissertation would not have been possible without the support of these wonderful people, and I am truly grateful to each of them.

DECLARATION ii

ABSTRACT iii

ACKNOWLEDGEMENTS iv

LIST OF FIGURES vii

LIST OF TABLES viii

NOMENCLATURE viii

Chapter 1 : Introduction/background 1
HISTORY OF NEURAL CREST CELLS AND THEIR RELEVANCE IN VERTERBRATES: 1
NEURULATION: 1
EPITHELIAL-MESENCHYMAL TRANSITION AND DELAMINATION 4
NC CELL MIGRATION 6
Permissive and restrictive signalling from ECM and surrounding tissue 6
Pathways of migration of trunk NC cells 6
Chemotaxis 7
Cell-cell contact 8
ACTIN FILAMENT FORMATION AND REMODELLING 9
A MODEL OF CELL MIGRATION FOCUSING ON ACTIN 12
INFLUENCE OF SIGNALS FROM THE ENVIRONMENT AND BETWEEN NC CELLS ON THE ACTIN REMODELLING. 14
THE MODELS OF STUDYING NC CELLS 15
CYTOCHALASIN D (MECHANISM OF ACTION) 16
Aim 17
Objectives 17
Chapter 2 : Materials and methods 17
Sterilization and equipment preparation 17
Chick Embryo Extract 17
Coating of the Nunc glass bottom dishes with fibronectin. 18
Neural crest assays 18
Cytochalasin D optimisation 21
Cytochalasin D treatment 24
Live cell imaging 24
Immunocytochemistry (ICC) 25
NCC visualization 26
Image analysis conducted using phase contrast and fluorescence NCC images. 27
Statistical analysis: 30

Chapter 3 CHAPTER THREE: Results..... 31
The number of quail eggs utilized, and NC cultures obtained: 31
Characterization of trunk neural crest cultures..... 32
Morphology of putative neural crest cells after 24 hours of incubation. 34
Morphological comparisons of putative and immunolocalised NC cells in the control and treated groups (after 48hr and 54 hrs of incubation): Cell projections and actin arrangement. 36
Migration dynamics (i.e. the patterns and velocity) of putative NC in the control and treated groups. 44
Chapter 4 CHAPTER FOUR: Discussion 54
Limitations 60
Chapter 5 CHAPTER FIVE: Conclusion. 60

List of Figures

CHAPTER ONE-Introduction

Figure 1.1 The process of neurulation 2
Figure 1.2 An illustration of an avian embryo between stages 14-15 (Hamberg and Hamilton, 1951), showing regions and categories of NC cells 4

Figure 1.3 Pathways of trunk NC cell migration and environmental signals present. 8
Figure 1.4 The dynamics of actin regulated by actin binding proteins. 11
Figure 1.5 Illustration of the cell migration model. 13

CHAPTER TWO-Materials and Methods

Figure 2.1 Illustration of the process of setting up an *in vitro* neural crest culture. 19
Figure 2.2 A diagram illustrating the three types of culture groups and the number of cultures in each group. 21
Figure 2.3 Calculating the viability ratio of cultures. 24
Figure 2.4 Measuring the positional changes of the migratory front using the linear tool Image J. 28
Figure 2.5 Determining the mean of fluorescence of phalloidin using ImageJ. 30

CHAPTER THREE-Results

Figure 3.1. Phase contrast images of neural tubes and the surrounding outgrowth of cells. 33
Figure 3.2 The difference in the position of the migratory front between 24 and 48 hours of incubation 34
Figure 3.3 Outgrowth of putative NC cells after 24hrs of incubation in DMEM 35
Figure 3.4. Putative NC cells after 48 hrs (t=0) in DMEM (Fig. A), DMSO (Fig. B), and cytochalasin D (Fig. C) and after 54 hours of incubation (t=6) in DMEM (Fig. D), DMSO (Fig. E) and cytochalasin D (Fig. F). 37
Figure 3.5. DMEM, DMSO and a cytochalasin D treated cultures that were fixed, immunolabelled with anti-HNK (green) and stained with phalloidin (red) and DAPI (blue). Images are reconstructed of Z-stacks. 39
Figure 3.6. Reconstructions of Z-stacks that were captured for individual cells from the DMEM control, DMSO control and treated group. Cells with immunolabelled with anti-HNK (green), phalloidin (red) and DAPI (blue). 41
Figure 3.7 The mean fluorescence of phalloidin of cells (n=30 for each group) in the DMEM, DMSO and treated groups (with standard deviation). 43
Figure 3.8. The migratory plots of putative NC cells were tracked in the DMEM controls, DMSO controls and the cytochalasin D treated group. 45
Figure 3.9. An analysis of putative NC cells in a DMEM control culture over 6 hours.. 47
Figure 3.10. Time lapse images of a DMEM control culture, where cell contact produced a chain-like structure. 48
Figure 3.11. An analysis of cells in a DMSO control culture over 6 hours.. 50
Figure 3.12. An analysis of putative NC cells treated with cytochalasin D for 6 hours. 52
Figure 3.13. The mean velocity of cells from all three groups (DMEM control, DMSO control and treated with cytochalasin D group, 27 cells from each group were recorded.. 54

List of Tables

Table 1. Summary of the number of eggs that were used and cultures that were obtained during this experiment. 31
Table 2. The mean minimum position of the migratory front and the mean maximum position of the migratory front (and standard deviation) measured at 24 hours and again at 48 hrs in 10 different neural tube explants that were cultured in DMEM. 33

Table 3. Results of the Dunn's test conducted between the three groups (DMEM, DMSO, TREATED) 44
Table 4. Results of Dunn's Comparisons Test- results comparing the groups in pairs (DMEM, DMSO and treated). 54

Nomenclature

NC- neural crest

ECM- extracellular matrix

EMT-epithelial mesenchymal transition

WNT pathway- wingless-related integration site pathway

BMP- bone morphogenetic protein pathway

NT- neural tube

MMP- matrix metalloproteinase

ADAM- a disintegrin and metalloproteinase

Eph-erythropoietin-producing hepatoma

Sema- semaphorin

ABPs- actin binding proteins

1. CHAPTER ONE: Introduction

HISTORY OF NEURAL CREST CELLS AND THEIR RELEVANCE IN VERTERBRATES:

Neural crest (NC) cells were initially discovered in chick embryos in 1868 by the German scientist Wilhelm His. At first glance these cells were thought to form the spinal ganglia and hence were termed ‘ganglion crest’ cells (Dupin et al., 2006). However, further observation revealed these cells to be highly motile, multipotent cells that formed a plethora of different cell types that have since been found to play an important role in the developing embryo and adult (Duband et al., 2020).

NC cells are specific to vertebrates and contribute to their complex body plan (Hall, 2008; York and Mc Cauley, 2020), as the derivatives of NC cells give rise to structures that increase the complexity of the central nervous system, the development of the peripheral nervous system, the craniofacial skeleton and elements of the cardiovascular system (Martik and Bronner, 2021). At a cellular level, the NC cells in vertebrates evolved and developed key features which not only make this group of cells significant but also distinguish the cells from “neural crest” -like cells that were noted in invertebrate chordates (York and Mc Cauley, 2020). These “neural crest” like cells in tunicates migrated short distances and were noted to be unipotent giving rise to a small group of neurons and pigment cells (Stolfi et al., 2015). The NC cells of vertebrates developed multipotency, the capability of long-range migration and a complex cellular communication system to facilitate directed migration (York and Mc Cauley, 2020).

NEURULATION:

NC cells arise in the crests of the neural folds, which are formed during neurulation (Selleck and Bronner-Fraser, 1996). During neurulation the ectoderm is differentiated into two regions, the epidermal ectoderm and the neural ectoderm (Gilbert, 2000; Steventon et al., 2009) (Fig. 1A). The epidermal ectoderm will give rise to the epidermis in the embryo while the neural ectoderm will become the neural plate (Steventon et al., 2009).

The neural plate undergoes apicobasal thickening such that it can be distinguished and isolated from the epidermis (Gilbert, 2000). The borders of the neural plate are located at the boundary between the neural plate and the epidermal ectoderm (Fig. 1.1A). As the neural plate thickens, invagination of the plate occurs (Fig. 1.1B). The boarders of the neural plate rise and form the neural folds (Schoenwolf and Smith, 1990). In avian embryos, the neural plate invagination occurs at the site of the future mesencephalon and progresses rostrally and caudally (Van Straaten et al., 1996). As the neural folds rise, they move towards the dorsal midline until they fuse. This process is also known as convergence (Fig. 1.1B). The fusion of the neural folds forms the neural tube and separates the tube from the epidermal ectoderm (Gilbert, 2000; Steventon et al., 2009) (Fig. 1.1C). The epidermal ectoderm will cover the roof of the neural tube to become the epidermis. Cells from the crest of the neural tube delaminate as neural crest cells (Van Straaten et al., 1996).

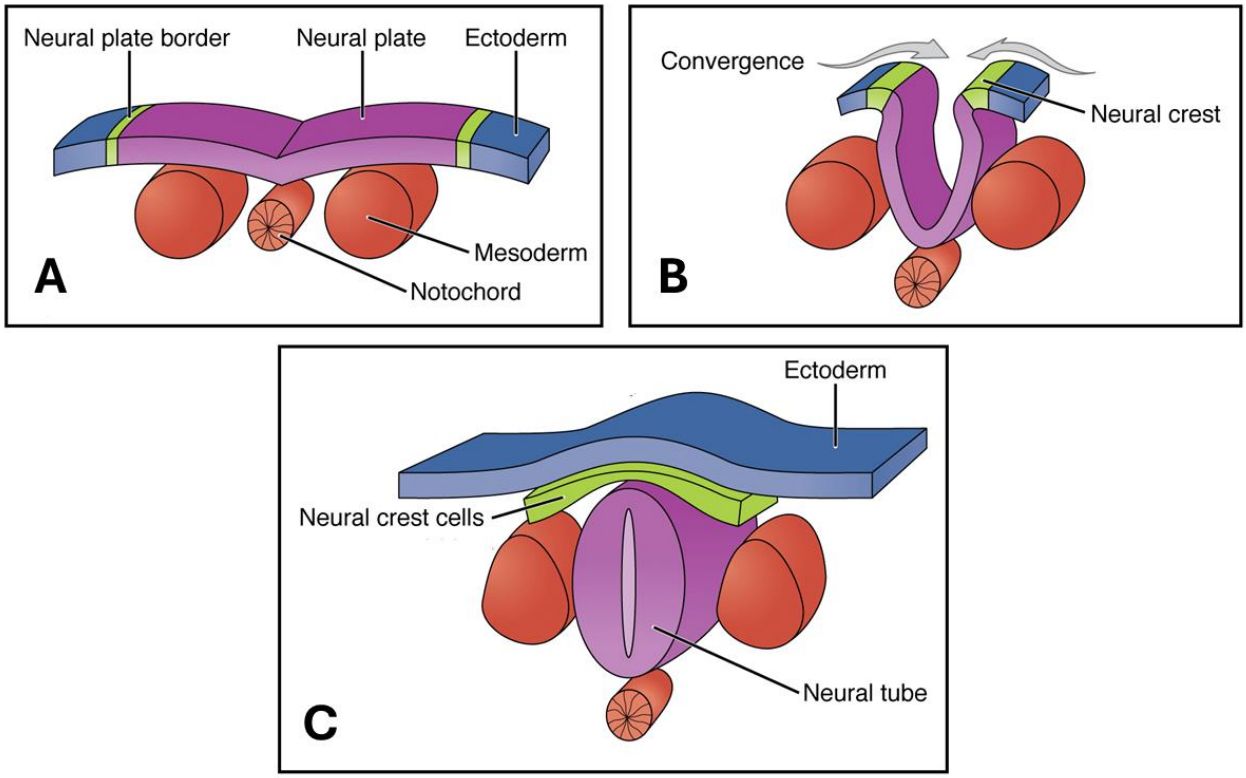


Figure 1.1 The process of neurulation. Fig. A: The differentiated ectoderm is noted, neural plate (purple) and the region of the epidermis (blue). The neural plate border (green) found on either side of the neural plate (purple). The surrounding structures including the mesoderm and notochord are also noted (red). Fig. B: Invagination of the

neural plate also known as convergence. In avian embryos the trunk NC cells are released following the closure of the tube. Fig. C: Neural tube (purple), the ectoderm (blue) and the released NC cells (green) can be seen in the region between the neural tube (purple) and ectoderm (blue). (https://biologydictionary.net/ectoderm/)

Once formed the neural tube extends along the rostro-caudal axis of the embryo, and NC cells are released along this axis (Selleck et al., 1993; Bronner and LeDouarin, 2012). The NC cells that are released are categorised into groups depending on the level from which they arise (Fig. 1.2). The levels include the cranial, vagal, trunk and sacral levels of NC cells (Bronner and LeDouarin, 2012). The cells are released from the neuroepithelium (epithelium of the neural folds) after undergoing epithelial-mesenchymal transition (EMT) and delamination. The NC cells then migrate in the extracellular matrix (ECM) of the embryo and their migration is directed by many signals such that the cells reach their target sites and eventually differentiate into a variety of cell types (Duband et al., 2020). The derivatives of NC cells include: the neurons and glial cells of the peripheral nervous system, Schwann cells, melanocytes and other cell types dispersed throughout the body (Bronner and LeDouarin, 2012). NC cells arising from the trunk levels of the embryo give rise to the sensory and sympathetic ganglia of the peripheral nervous system, the adrenal chromaffin cells as well as melanocytes (Fig. 1.2).

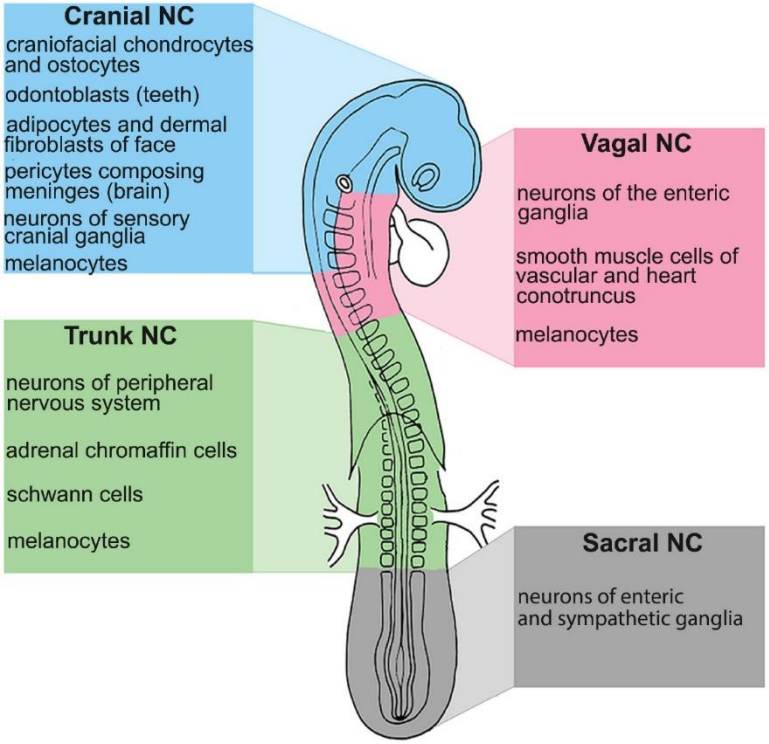


Figure 1.2 An illustration of an avian embryo between stages 14-15 (Hamberg and Hamilton, 1951), showing the neural tube along the rostro-caudal axis. The different regions and the groups of NC cells (cranial, trunk, vagal and sacral) are highlighted, and the derivatives of each group is listed (Rodrigues-Da-Silva et al., 2022).

EPITHELIAL-MESENCHYMAL TRANSITION AND DELAMINATION

The putative NC cells in the neural fold are specified through a combination of signals (Ahlstrom and Erickson, 2009; Schille and Schambony, 2017). When these specified NC cells are triggered by appropriate signals, they undergo an epithelio-mesenchymal transition (EMT) which allows the cells to delaminate (i.e. separate from the epithelium of the neural fold and assume a mesenchymal phenotype) and migrate away from the neural tube (Stuhlmiller and García-Castro, 2012; Mayanil, 2013). In avian embryos the signalling pathways that are activated following somite maturation, in a rostro-caudal direction, are responsible for activating EMT and delamination of NC cells (Sela-Donenfeld and Kalcheim, 2002; Kerouso and Bronner-Fraser, 2012; Kalcheim, 2015)

The physical changes that transform cells from an epithelial phenotype to a mesenchymal phenotype, include reduced cell-cell contact, decreased attachment to the basement membrane, the loss/modification of cell polarity and cytoskeletal rearrangements to facilitate cell motility (Leathers & Rogers, 2022).

Cell-cell contacts are mediated by tight junctions, gap junctions and adherens junctions in epithelial cells (Le Bras et al., 2012). Adherens junctions are facilitated by cadherins and catenins and during the EMT of pre-migratory NC cells in avians, high affinity cadherins i.e. E cadherins are switched to low adhesion N-cadherins (Monier-Gavelle and Duband, 1995). These N-cadherins are later cleaved causing the loss of cell-cell attachment which begins the separation of NC cells from the neuroepithelium (Park and Gumbiner, 2010). The NC cells complete their separation from the neuroepithelium once their attachment to the basement membrane of the neuroepithelium is also lost (Kerosuo and Bronner-Fraser, 2012). This occurs through the secretion of matrix metalloproteases, MMP2, and ADAM13 proteins which degrade and remodel the ECM in avian NC cells (Alfandari, et al., 2009; Kerosuo and Bronner-Fraser, 2012; Cabral-Pacheco et al., 2020).

Cell polarity in epithelial cells is maintained by tight junctions, adherens junctions and by the spatiotemporal activity of actin filaments (Pásti and Labouesse, 2018). The loss of tight junctions in NC cells (Kerouso and Bronner-Fraser, 2012) is accompanied by a change in the spatiotemporal activity of actin. When the E-cadherins are replaced, it also alters the actin arrangement, since cadherins also have a role in regulating the actin arrangement in the cell (Derycke and Bracke, 2004). Additionally, in trunk NC cells the upregulation of cadherin- cad6B, which occurs during EMT, also influences the actin filaments (Kerosuo and Bronner-Fraser, 2012; Kalcheim, 2015). Ultimately, the alterations to the cytoskeleton not only influence the cells' polarity but it also prepares the cell for migration (Schaks et al., 2019).

NC CELL MIGRATION

Permissive and restrictive signalling from ECM and surrounding tissue

NC cells migrate in the ECM, to reach their target sites by attaching to molecules that make up the ECM (Szabó and Mayor, 2018). During the initial migration of NC cells, fibronectin, laminin-1 and laminin-8, and some collagen isoforms (*in vivo*) promote cell migration (Perris, 1997). Other components of the ECM, like hyaluronan, various collagen types (Perris and Johansson, 1990; Perris, 1997), proteoglycan aggrecan and chondroitin sulfate have been shown (*in vivo*) to inhibit the migration of NC cells.

The migration of the NC cells in the ECM is directed by the adhesion affinity between NC cells and the different components of the ECM (Perris and Perssinatto, 2000). Strong adhesion of NC cells to the components of the ECM promotes migration, weak attachments inhibit migration and if NC cell adhesion to the ECM is too strong migration will also not occur (Perris and Perssinatto, 2000). Hence, when studying NC cells *in vitro*, fibronectin or laminin substrates can be used. However, fibronectin was shown by Rovasio and colleagues (1983) to be the preferred substrate for NC cell migration *in vitro* and it was thus used in the current study.

Pathways of migration of trunk NC cells

As the NC cells migrate in the ECM and respond to the components therein (*in vivo*), the NC cells also encounter other surrounding and external signals which mediate their migration (Perris and Perssinatto, 2000). These cues include interactions with the surrounding tissue/structures (such as somites, notochord, and ectoderm), cell-cell contact and the response to soluble factors in the migratory environment (Theveneau and Mayor, 2012; Szabó and Mayor, 2018). The external signals act as attractant or repellent cues that direct migration. Repellent cues from the ECM and the surrounding tissues establish compartments for cells to migrate in pathways of migration. The attraction cues (chemotaxis) assist in homing in of cells towards the target site/tissue (Vega-Lopez et al., 2017; Szabó and Mayor, 2018).

The pathways of migration (*in vivo*) that trunk NC cells are known to migrate along, include the ventromedial pathway, the ventrolateral pathway and finally the dorsolateral pathway (Vega-Lopez et al., 2017). Along the ventromedial pathway, NC cells fill the

space between the somites and blood vessels (Fig. 1.3). The NC cells that invade the space between the sclerotome and dermomyotome (in the mature somite) migrate along the ventrolateral pathway (Fig. 1.3). Finally, the dorsolateral pathway, includes the NC cells that migrate in the space between the dermomyotome and the epidermis (Fig. 1.3) (Vega-Lopez et al., 2017). These pathways of migration compartmentalise NC cells and when these cells are exposed to attractive signals the cells are directed towards their target sites.

Chemotaxis

The attractive signals arise from soluble factors that are released into the microenvironment and result in NC cells, which have been compartmentalised into their pathways, becoming positively biased and thus migrating towards the source (Szabó and Mayor, 2018). This process is known as chemotaxis (Shellard and Mayor, 2016; Szabó and Mayor, 2018). In chicks, the newly delaminated trunk NC cells respond to the chemokine CXCL12 which attracts NC cells that express the CXCR4 receptor along the ventral (ventromedial) pathway (Fig. 1.3) (Delloye-Bourgeois and Castellani, 2019).

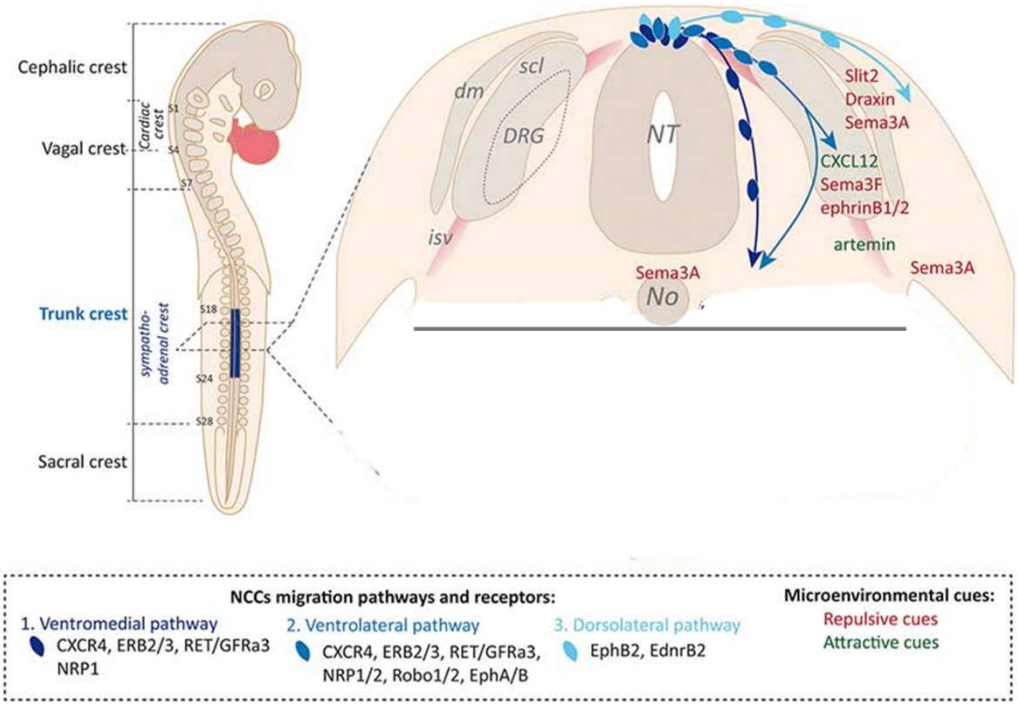


Figure 1.3 A schematic diagram of an avian embryo at stage 16 (Hamburger and Hamilton, 1951) where the different groups of NC cells are noted at the region from which they are released. In the cross section of the embryo, the neural tube (NT), the notochord (NO), the dermomyotome (dm), sclerotome (scl) and the dorsal root ganglia (DRG) are noted. The pathways of trunk NC cells are lined in different shades of blue in the diagram (ventromedial, ventrolateral and dorsolateral) and the cues (color coded as repulsive or attractive) regulating migration are noted alongside the pathway. (Delloye-Bourgeois and Castellani, 2019).

Cell-cell contact

The limiting of migration of NC cells, due to the pathways of migration, and the localisation of cells induced as a result of chemotaxis promotes high cell density migration which in turn promotes cell-cell contact between the migrating NC cells (Scarpa and Mayor, 2016). The NC cells with their outwardly extending cellular processes (namely filopodia) encounter the filopodia or the cell body of their

neighbouring cells. *In vivo* these contacts are extensive and mediated by N-cadherin proteins on the cell surface (Carmona-Fontaine et al., 2008).

Cell-cell contact influences the migration of the cells that come into contact, either by promoting cell dispersion or by inducing attractive signals that allow collective migration (Li et a., 2019). Cell dispersion is induced when contact inhibition locomotion (CIL) occurs. When NC cells contact an adjacent cell, they stop migrating and begin migrating in the opposite direction from the initial site of contact (Carmona-Fontaine et al., 2008). Cell contacts have also been shown to promote collective migration which is termed contact attraction (CoA). CoA occurs when the actin, in the individual cells that come into contact, is repolarised in the same direction allowing cells to migrate together for a short period of time (Li et al., 2019).

The signals from the aforementioned factors (ECM, surrounding tissue, chemotaxis and cell contact) converge, and influence the actin arrangement within the NC cells, since actin is essential in cell migration (Schaks et al., 2019).

ACTIN FILAMENT FORMATION AND REMODELLING

Actin filaments in the cytoskeleton are essential in maintaining cell shape, providing mechanical support, enabling mitosis and for cell motility (Pollard and Cooper, 2009). Actin filaments are formed in three phases, first the nucleation phase occurs where actin subunits are assembled from monomers, G-actin units (Cooper, 2000). Monomer units combine to form trimers which combine to form F-actin filaments. The G-actin monomers are polar molecules; hence they produce polar filaments (Cooper, 2000). The second phase, also known as the elongation phase, occurs as subunits are added to lengthen the filaments. Subunits are added at the barbed end of the filaments and subunits can be removed from the barbed and pointed ends (opposite the barbed end) (Cooper, 2000; Lambert et al., 2023). The final stage, i.e. the stationary phase occurs when the assembly (polymerisation) and disassembly (depolymerisation) of the actin filaments occur at the same rate (Cooper, 2000; Lambert et al., 2023). The continuous turnover of actin within the cell facilitates migration.

Migration occurs due to the actin turnover in the cell body and within projections (Schaks et al., 2019). F-actin filaments are arranged at the plasma membrane to form projections, and within the cell body to form stress fibres (Schaks et al., 2019). One projection involved in migration is the lamellipodium, which is broad fan shaped projections, formed from actin filaments that are arranged in dendritic/branched structures beneath the cell membrane (Parsons et al., 2010; Vinzenz et al., 2012). Another projection involved in migration is the finger-shaped filopodium, which is formed from parallel actin filament arrangement at the membrane (Wood and Martin, 2002). Within the cell body, the F-actin filaments are arranged in thick bundles which are known as stress fibres. These stress fibres interact with actin-associated motor proteins such as myosin and tropomyosin to induce contraction (Parsons et al., 2010).

Actin within the NC cells attaches to the ECM through integrins, and these sites are known as focal adhesions (Schaks et al., 2019). Signals from the ECM and environment will activate the following signalling pathways which are relevant to actin remodelling, Rho GTPases (Ridley, 2001), PI3K/Akt pathway (Xue and Hemmings, 2013), MAPK/ERK pathway (Tanimura and Takeda, 2017), Integrin signalling (Harburger and Calderwood, 2009) and the Wnt/β-catenin pathway (Akiyama and Kawasaki, 2006). It is the Rho-GTPase pathways which are important in migration (Ridley, 2001) and proteins part of the Rho-GTPase family include RhoA which is responsible for actin-myosin contraction and the formation of stress fibres (Höltje et al., 2011). Rac activates actin-binding proteins which give rise to lamellipodia and Cdc42 is responsible for the formation of filopodia (Song et al., 2015). The Rho-GTPase proteins interact with actin-associated proteins, also called actin binding proteins (ABPs), to facilitate polymerisation and depolymerisation of actin within the cell (Higgs, 2013).

Each phase of actin remodelling, beginning with the elongation phase, is facilitated by ABPs. Prior to the elongation phase, the protein profilin binds to actin monomer units that will be used later (Fig. 1.4) (Witke, 2004; Schaks et al., 2019). During the elongation phase proteins like the Arp2/3 complex facilitate the formation of branched/dendritic actin structure. The Arp2/3 complex proteins act as a nucleus for daughter filaments to form on pre-existing filaments thus creating branches (for the formation of lamellipodia) (Blanchoin et al., 2000). Formin and VASP proteins are also examples of ABPs that

facilitate elongation (Fig. 1.4) (Schaks et al., 2019). Elongation can be inhibited through the action of capping proteins which bind to the barbed end of the filaments thus preventing the addition of subunits (Fig. 1.4). Depolymerisation is facilitated by proteins such as cofilin and twifilin which disassemble the actin filaments at the barbed ends or both ends (barbed and pointed end), respectively (Fig. 1.4) (Blanchoin et al., 2000; Schaks et al., 2019).

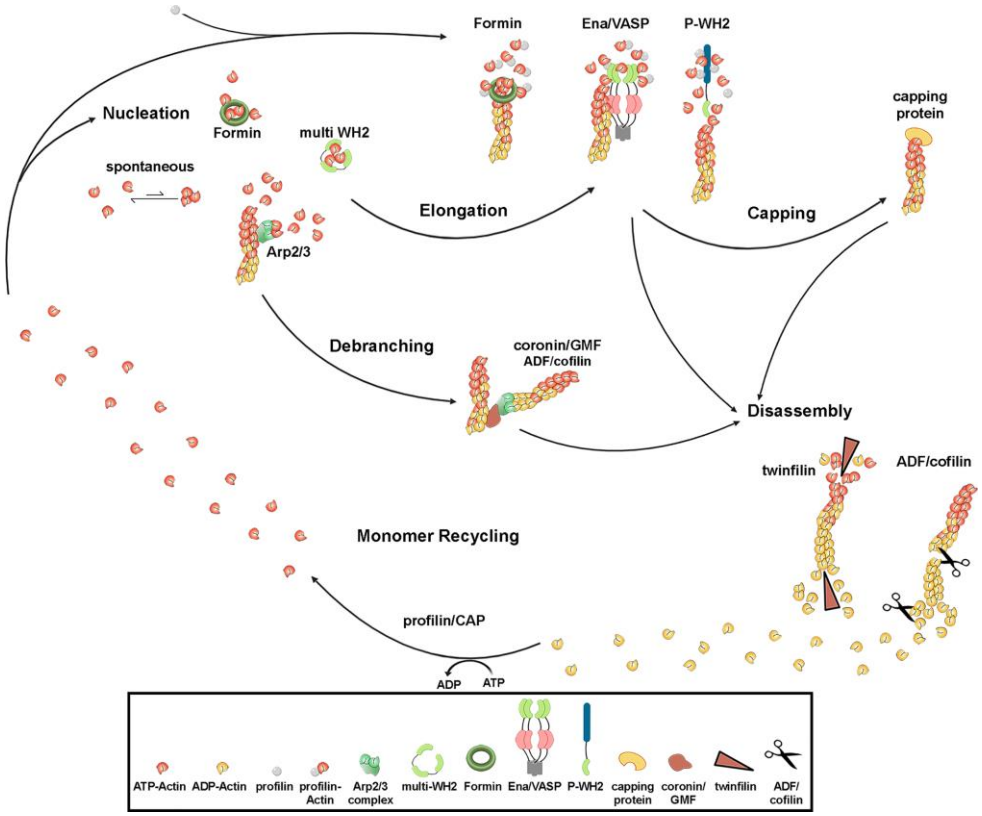


Figure 1.4 The dynamics of actin regulated by actin binding proteins. Proteins promoting nucleation include, Arp2/3 complex, formin and VASP/Ena. Capping proteins prevent elongation, coronin/GMF preventing actin branching and proteins facilitating disassembly include twifilin and ADP/cofilin. The protein profilin is responsible for monomer recycling that will prepare monomers for nucleation (Schaks et al., 2019).

MODEL OF CELL MIGRATION FOCUSING ON ACTIN

Cell migration, focusing on actin filaments in a two-dimensional model (where cultured cells migrate on a substrate), involves the following processes: extension, adhesion, translocation and de-adhesion (Fig. 1.5.1) (Tschumperlin, 2013). A leading lamellipodial projection is formed in the direction of migration (Fig. 1.5.1). The leading projection extends forward and forms attachments to the ECM ahead (Fig. 1.5.2). This activates the stress fibres in the cell body and in the rear end of the cell to contract and this contraction generates enough tractive forces to push the cell forward (Fig. 1.5.3) (Tschumperlin, 2013). Finally, the focal adhesions at the rear end are lost when the cell contracts and the cell is propelled in the direction of migration (Fig. 1.5.4) (Tschumperlin, 2013).

In this migration model, lamellipodia can be seen leading migration, as they extend ahead onto the substrate (Krause and Gautreau, 2014). However, the extensions are directed by the signals that filopodia receive, as filopodia are responsible for probing the environment for the appropriate signals (Heckman and Plummer, 2013).

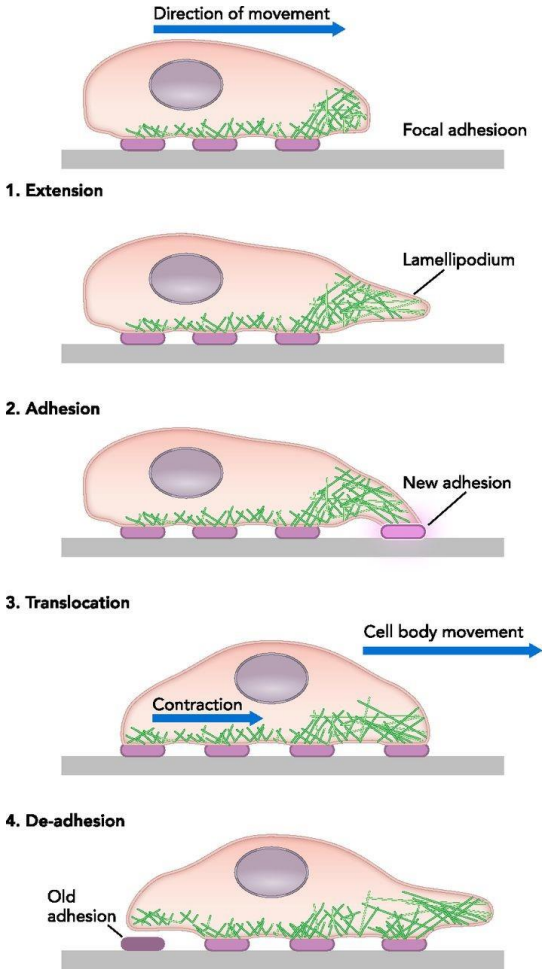


Figure 1.5 Illustration of the cell migration model. Focal adhesions attach the cell to the substrate. Signals from the environment determine the direction of the leading projection and hence the direction of migration. The leading projection then extends ahead and attaches to the substrate. The attachment stimulates the activation of stress fibres and associated motor proteins to cause the contraction of the cell body and the rear end of the cell. Adhesions located at the rear end of the cells disassemble, as new projections at the leading edge form (Tschumperlin, 2013).

INFLUENCE OF SIGNALS FROM THE ENVIRONMENT AND BETWEEN NC CELLS ON THE ACTIN REMODELLING.

The complex signals from the environment (ECM, surrounding structures, soluble factors and cell-cell contacts) all converge on the actin filaments by influencing the signalling pathways and proteins that mediate actin remodelling. Permissive signalling from the ECM (i.e. fibronectin) (Shi et al., 2012), surrounding tissue (e.g. Slit2-Nrp signalling) (Giovannone et al., 2012) and chemokines like Cxcl1 (Singleton, 2013) all have downstream signalling effects that act on the proteins of the Rho-GTPase family to promote polymerisation. The non permissive signals from the ECM, such as chondroitin sulfate (Galindo et al., 2018), and the effect of CIL (Carmona-Fontaine et al., 2008) also influence the actin cytoskeleton, through the activation of RhoA, to inhibit migration. Environmental cues and actin go hand in hand in facilitating the migration of NC cells (Szabó and Mayor, 2018). While this complex relationship maintains the long-range migration of the cells (York and Mc Cauley, 2020), errors in this process can have significant consequences

Given the plethora of cells and tissues that NC cells give rise to, abnormalities that occur in one or more of the steps in the cells lifetime [i.e. well-coordinated release of NC cells (Mayanil, 2013), signals directing migration (Szabó and Mayor, 2018), and differentiation (Hovland et al., 2020)] will have consequences in the development of the embryos, resulting in the formation of neurocristopathies (Pilon, 2021).

Neurocristopathies includes an extensive list of congenital abnormalities, which can be categorised into three groups: dysgenic malformation (abnormal brain or spinal cord during development), neoplasms (tumors) and the combination of dysgenic malformations and neoplasms (Sato et al., 2019). Neurocristopathies involving trunk NC cells include: Waardenburg syndrome, piebaldism, occulocutaneous albinism, congenital central hypoventilation syndrome and Hirschsprung's disease (Chatzi et al., 2024).

This list of neurocristopathies involving trunk NC cells, are the result of abnormal differentiation of trunk NC cells, with the exception of Hirschsprung's disease which results from the failure of NC cells to migrate and differentiate to form the sympathetic nervous tissue at the distal portion of the colon (Chatzi et al., 2024). Hirschsprung's

disease is characterised by the occurrence of aganglionosis (congenital absence of ganglion cells) of variable lengths of the distal colon (Tang et al., 2013). Although the cause of Hirschsprung's disease is not definitively known, the disease is thought to arise due to abnormalities that may occur during migration, proliferation or differentiation of trunk and enteric NC cells (Martucciello et al., 2000). Genetic mutations on the RET gene, which codes for receptors on the NC cells, and involving the corresponding ligands (GDNF) have been linked to the formation of the disease (Martucciello et al., 2000). Numerous other genes which all contribute to the control and management of NC cell processes have also been identified (Martucciello et al., 2000). Ultimately the lack of migration of the trunk NC cells results in the absence of the sympathetic nervous tissue in the gut.

MODELS OF STUDYING NC CELLS

NC cells are a significant group of cells and abnormalities in their migration can have many consequences. Thus, studying this cell type is important and it can be achieved using *in vivo* or *in vitro* models (Ribatti and Annese, 2023). *In vivo* models are advantageous since they mirror the migration that occurs in the developing embryo (where all the environmental cues are present) (Ribatti and Annese, 2023). However, the migration of the individual cells and their contacts are difficult to discern in this model. On the other hand, *in vitro* studies isolate the cells such that the mechanisms of migration and the factors that influence migration can be studied independently and can be manipulated.

In both *in vivo* and *in vitro* models heterogenous cell populations are present and thus it is important to identify NC cells from the surrounding cells. Chick-quail chimeras were one such technique used in avian embryology to study and track NC cells (Teillet et al., 2009). However, apart from chimeras NC cells can be labelled using nonspecific techniques such as DiI dye injections (Serbedzija et al., 1991). More targeted techniques such as immunolabelling, electroporation or transfection (Dickinson et al., 2002; de Bellard & Bronner-Fraser, 2005; Li et al., 2019) can be used to identify NC cells. Immunolabelling using an anti-HNK-1 antibody which recognises a specific carbohydrate epitope found on the surface of migrating NC cells (Giovannone et al.,

2015) can label migrating NC cells specifically. Thus, this antibody could specifically identify NC cells that were actively migrating (in a fixed culture). Additionally, staining using DAPI (nuclear stain) and Phalloidin Atto-590 (fluorescent peptide that binds to F-actin) can reveal the actin arrangement within the migrating cells.

Using an *in vitro* model to study the migration of NC cells can elucidate the behaviour of NC cells and the influence of cell-cell contact. Additionally, since actin is known to be a key structure in migration, studying the migration of cells in models where actin has been disrupted can further reveal the mechanisms of abnormal NC cell migration. A model of actin disruption and hence abnormal migration, can be achieved using cytochalasin D.

CYTOCHALASIN D (MECHANISM OF ACTION)

Cytochalasin D is a metabolite produced from Zygosporium fungi, known for its effect on actin. Cytochalasin D disrupts the actin organisation within the cell (Schliwa, 1982; Goddette and Frieden, 1986). The mechanism of action suggests that cytochalasin binds to the barbed end of F-actin filaments (Schliwa, 1982), thus preventing polymerisation. Cytochalasin D also plays an interesting role in affecting the actin-binding proteins that regulate actin turnover (Lambert et al., 2023). Nevertheless, the known effects of cytochalasin D include changes to cell morphology and inhibiting actin dependent processes such as migration and cytokinesis (Goddette and Frieden, 1986). The changes to cell morphology include (1) the collapse of membrane projections, (2) decrease in cell size, (3) and the formation of transformed and arborised cell projections (Goddette and Frieden, 1986; Schliwa, 1982). Cytochalasin D has been used in previous embryological, *in vitro,* studies to investigate actin disruption and the effects on the cells in question (Bentley and Raymond, 1986; Haendal et al., 1996; Hinoue et al., 2005). In the current study, cytochalasin D was administered to quail NC cultures. DMSO (dimethyl sulfoxide) (Sigma- 472301) is the diluent used in the suspension of the cytochalasin D as per the manufacturer's preparation instructions (Sigma- C8273) (Marsh and Letourneau, 1984; Hinoue at al., 2005; Nyffeler et al., 2017b).

Aim

The aim of this study was to investigate the role of actin in the migration and behaviours of quail NC cells.

Objectives

1. To set up an *in vitro* assay of avian trunk NC cells on a fibronectin substrate.
2. To observe the live migration of NC cells.
3. To identify NC cells specifically using anti-HNK antibody and to stain the actin filaments using Phalloidin Atto-590.
4. To inhibit actin polymerization in NC cells with cytochalasin D.

2. CHAPTER TWO: Materials and methods

Ethics approval was obtained from the Animal Research Ethics Committee (AREC) of the University of the Witwatersrand (AREC 23-03-016O), for the use of 207 quail eggs (*Cortunix japonica*) and 36 chicken eggs *(Gallus gallus domesticus*).

The eggs were obtained from the University of Witwatersrand's Central Animal Service Unit. The chick embryos were used to prepare chick embryo extract (to supplement the culture medium) and the quail embryos were used to set up the *in vitro* neural crest assays.

Sterilization and equipment preparation

All glassware, equipment and solutions used are shown in Appendix 3.

All the glassware used to culture the neural tubes and for preparing the chick embryo extract was heat sterilised in a sterilising oven at 180°C for 2 hours. Solutions were prepared 24 hrs prior to the culture and autoclaved at 121°C at 100kPa for 20 minutes in a Sturdy SA-300VF autoclave. Prior to the start of each experiment the sharp, fine microdissection instruments were immersed in 70% ethanol and the blunt instruments were immersed in 90% ethanol for 30 minutes.

Chick Embryo Extract

Chick embryo extract was prepared in advance to supplement the culture medium, as it is known to provide nutrition to the NC cells (Paul, 1965). One dozen fertile chick eggs

were incubated at 37°C in a humidified incubator for nine days prior to the preparation of the chick embryo extract. Three batches (12 eggs each) of the embryo extract were prepared on three different occasions under sterile conditions. (Appendix 4). Aliquots (5ml) of chick embryo extract from all three batches were frozen at -20° until use.

Coating of the Nunc glass bottom dishes with fibronectin.

Immediately prior to the start of each experiment Nunc 27mm glass bottom dishes (Thermo Fisher: 150682) were coated with fibronectin. Fibronectin (from bovine plasma; Sigma: F-4759) was diluted in sterile chick Ringer's solution (Appendix 3). To each Nunc dish, 0.5 ml of diluted fibronectin (20 µg/ml) was added to cover the glass surface of the dish where the explant would be placed.

The dishes were incubated for one hour in a humidified incubator at 37°C. Thereafter the excess fibronectin was removed, and 1 ml of Dulbecco's Modifed Eagles Medium (DMEM-PAN BIOTECH) was added to each dish and incubated at 37°C in a humidified incubator until use (Bronner-Fraser, 1996).

Neural crest assays

Fertilised quail (*Coturnix japonica*) eggs were incubated for 48 hours in a humidified incubator at 38°C.

Under sterile conditions in a laminar flow hood, each quail eggshell was wiped down with 70% ethanol, the egg was opened, and its contents were emptied into a glass dish containing sterile chick Ringer's solution. The blastoderm was separated from the yolk and was transferred to a black wax dish that contained sterile chick Ringer's solution.

The blastoderm was pinned on to a black wax dish and the embryo was staged according to Hamburger and Hamilton (1951). Hamburger and Hamilton (1951) which is used to stage chick embryos can also be used to stage quail embryos (Ainsworth et al., 2009).

Embryos between the stages of 12-16 (Hamburger & Hamilton, 1951) were used to obtain cultures of trunk NC cells. Trunk NC cells in avian embryos are known to delaminate from the neural tube following the closure of the tube (Gammill and Roffers-Agarwal, 2010). The neural tube at trunk levels (somite 17-22) was excised from

embryos that were between stages 12-16 (Hamburger and Hamilton, 1951) as the neural tube had recently closed in this region.

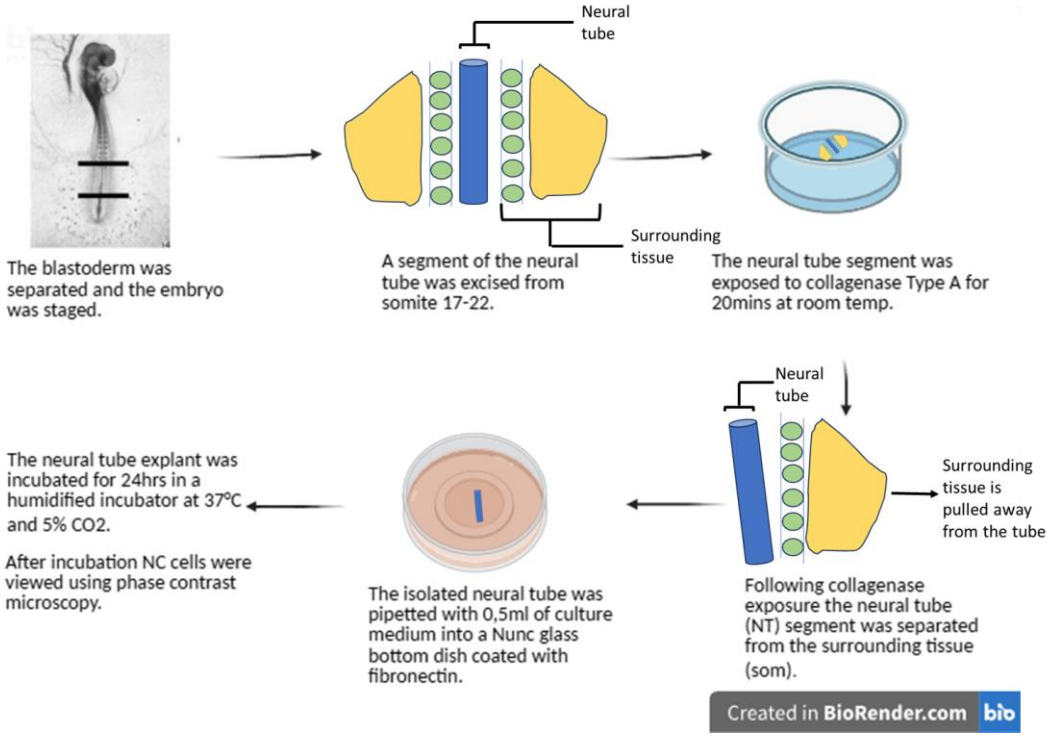


Figure 2.1 Illustration of the process of setting up an *in vitro* neural crest culture. The excised neural tube section contained the neural tube (indicated in blue), with somites lateral to it (green) and the surrounding mesoderm (yellow). (www.biorender.com)

The excised length of neural tube was then placed in a glass cavity dish containing collagenase Type A (Sigma-COLLO-RO) diluted in Tyrode's (Calcium and Magnesium-free) solution (Fig. 2.1) at a concentration of 0.0025g/ml (Appendix 3). The neural tube segment was exposed to collagenase for approximately 20 minutes at room temperature and thereafter the segment was transferred to a black wax dish containing chick Ringer's solution.

The neural tube was then separated from the surrounding tissue (overlying ectoderm, notochord and surrounding mesoderm and somites) using sterile insect pins. One pin was used to secure the tube while a second pin was used to remove the surrounding tissue (Fig. 2.1). The isolated neural tube was then rinsed in DMEM and placed in a

fibronectin-coated Nunc dish to which 0,5ml of the final medium was added (Fig. 2.1). The final culture medium consisted of 75% DMEM, 15% of the prepared chick embryo extract, 10% horse serum and penicillin/streptomycin. This final culture medium will hereafter be referred to as “DMEM” medium.

Cultures were incubated at 37°C and 5% CO_2 for 24hrs prior to observation.

After 24 hrs of incubation the cultures were viewed and imaged using phase contrast microscopy (Olympus CKX41 inverted phase contrast microscope). Those NC cultures, that showed delaminated putative NC cells, were randomly divided into three groups, a group which contained the final medium only, (“DMEM” control), a DMSO control and a treated group (cytochalasin D diluted in DMSO). The diluent control i.e. DMSO control was included as cytochalasin D was made up in 0.1% DMSO.

Each group consisted of 10 cultures. Three cultures from each group were imaged for six hours in order to track live cells, and the remaining seven were incubated in parallel for six hours. Thereafter, all the cultures were fixed, immunolabelled and stained (Fig.2.2).

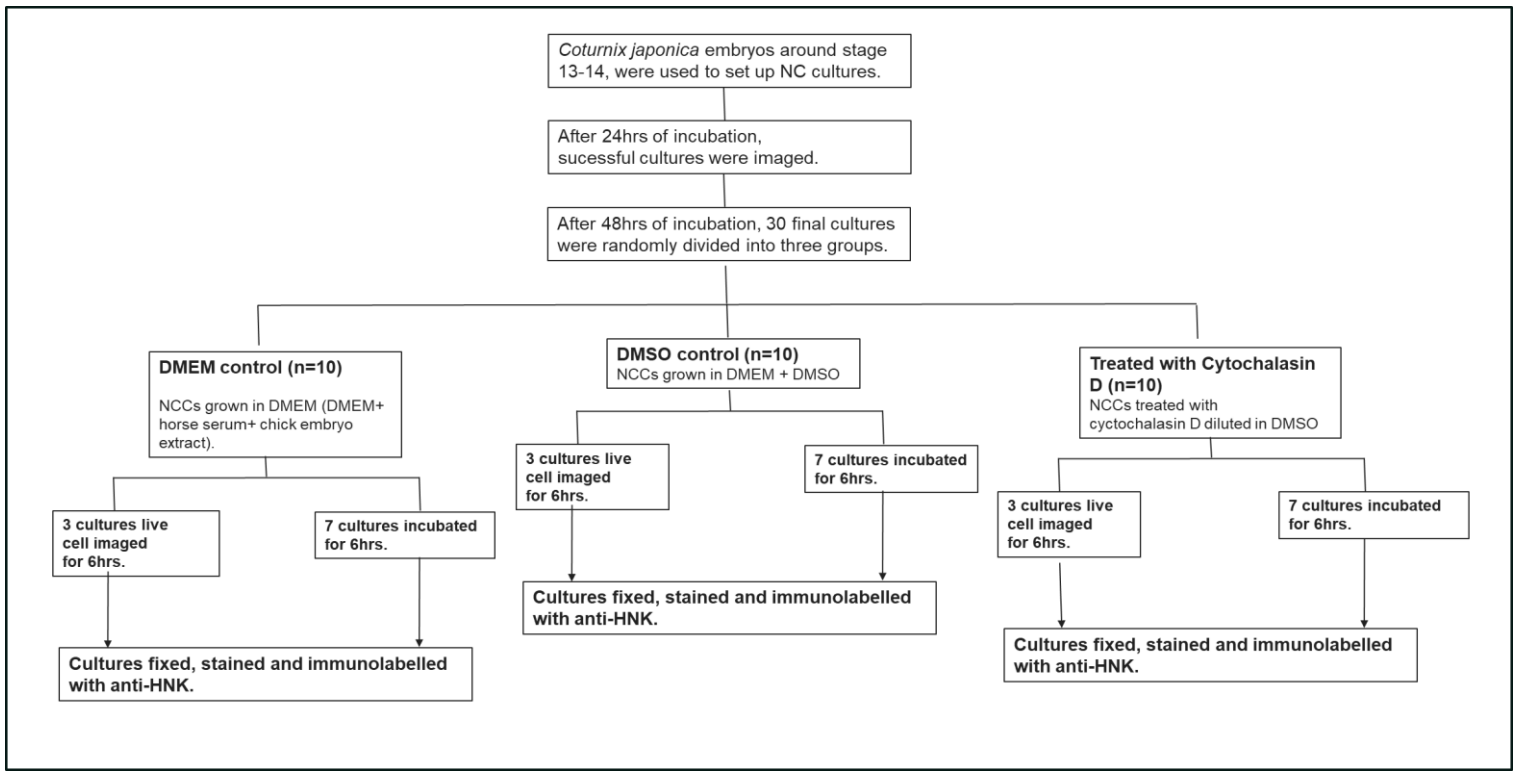


Figure 2.2 A diagram illustrating the three types of culture groups and the number of cultures in each group.

Cytochalasin D optimisation

Cytochalasin D (Sigma- C8273) in a solution of 0,1% DMSO (Sigma- 472301) was used in this study to block the polymerisation of actin (Lambert at al., 2023). A suitable concentration of cytochalasin D had to be determined for the use in this assay, as it has previously been shown to induce cell death in NC cells as cells lost adhesion to the substrate (even when cytochalasin D was used at an optimised concentration) (Hinoue et al., 2005). Thus, it was important to determine a concentration of cytochalasin D that would disrupt the actin filaments in NC cells without causing cell death.

The concentration range of cytochalasin D used in the optimisation was based on the concentrations and exposure times of cytochalasin D used in similar *in vitro* embryological studies (Bentley and Raymond, 1986; Haendal et al., 1996; Hinoue et al., 2005). Thus, the following range of concentrations of cytochalasin D were tested: 0.5, 1, 2, 3 µg/ml. Each concentration was repeated in three NC cultures and the cell viability was determined after treatment (see below). The NC cells were incubated for six hours

in the various concentrations of cytochalasin D made up in 0.1% DMSO. The treated cells were imaged prior to treatment, two hours after treatment, five hours after treatment and following fixation at six hours after treatment.

To determine cell viability, the neutral red assay (Appendix 5), a viability assay where living cells are able to take up the dye, compared to dead/dying cells that are unable to take up the dye, was initially attempted in order to obtain quantitative data. The neutral red assay was first conducted on MCF-7 cells (breast cancer cells) that were seeded at low concentrations to determine if the assay would be suitable to use on NC cultures (which have fewer cells relative to cell culture models). However, as discussed in Appendix 5, the proliferative/viability assays that are typically used in cell culture assays are not adaptable to tissue culture (NC cultures).

A method of manual cell counting to determine the cell viability was used instead. This method based on the protocol of cell counting using a haemocytometer (cells in suspension) (Absher, 1973) was adapted for use on the adherent cells in the NC cultures. The haemocytometer method counts cells using specialised glass counting chambers with grid patterns for organised counting. A grid method was thus adapted to images of the NC cultures to count cells before and after treatment (Appendix 5). Images of the cultures were taken using two different microscopes. Before treatment the images were taken using phase contrast microscopy (as these images were on live cells) and after treatment images were taken using a fluorescence microscope, since viability was assessed by the morphology of the nuclei of cells stained with DAPI.

However, there were differences in magnification between the images obtained from the phase contrast microscope (which was used to image cells before treatment) and the available fluorescence microscope (used to image fixed cells after treatment). The total magnification of the images taken from the two different microscopes were different despite the images being taken using the same objective on both microscopes indicating that an intermediary lens may have been included in one of the microscopes. The area and grid size of the images were different, and a standardised method of manually counting cells before and after treatment to determine cell viability could not be used.

Therefore, for the final assessment of viability, cells that were fixed after treatment and stained with DAPI, were counted in the DMEM cultures, DMSO cultures and in the cytochalasin D-treated cultures. From these cells a ratio of the number of viable cells to the total number of cells was determined. The ratios of cell viability were calculated for the cells in the treated group as well as for the cells in the control groups (DMEM and DMSO).

To calculate this ratio, six random equal areas (areas were equal to 211.93 x 211.93µm which was equivalent the field of view of the microscope) in a single culture which contained migrated cells were imaged using the 63x objective on a fluorescence microscope (Leica Thunder microscope). In each area the total number of cells (T^T) and the total number of viable cells (T^v) were counted. Viability was assessed on appearance of the nucleus, cells wherein nuclear condensation or fragmentation was apparent were considered to be non-viable cells (Cummings et al., 2004). The viability ratio was calculated using the following equation:

$$Viability\ Ratio = (\mathrm{T^v}) \div (\mathrm{T^T})$$

The ratio of viability for a single culture was calculated by averaging the ratios of the six areas that were counted.

Each concentration of cytochalasin D that was tested (0.5, 1, 2, 3 µg/ml) was repeated three times. An average ratio was calculated for each concentration. The ratio of viability of the treated group was compared to the ratio of viability of the control groups (DMEM and DMSO) to determine if the treatment affected the viability of the cells. Additionally, the ratio of viability for all four of the concentrations of cytochalasin D that were tested, were also compared.

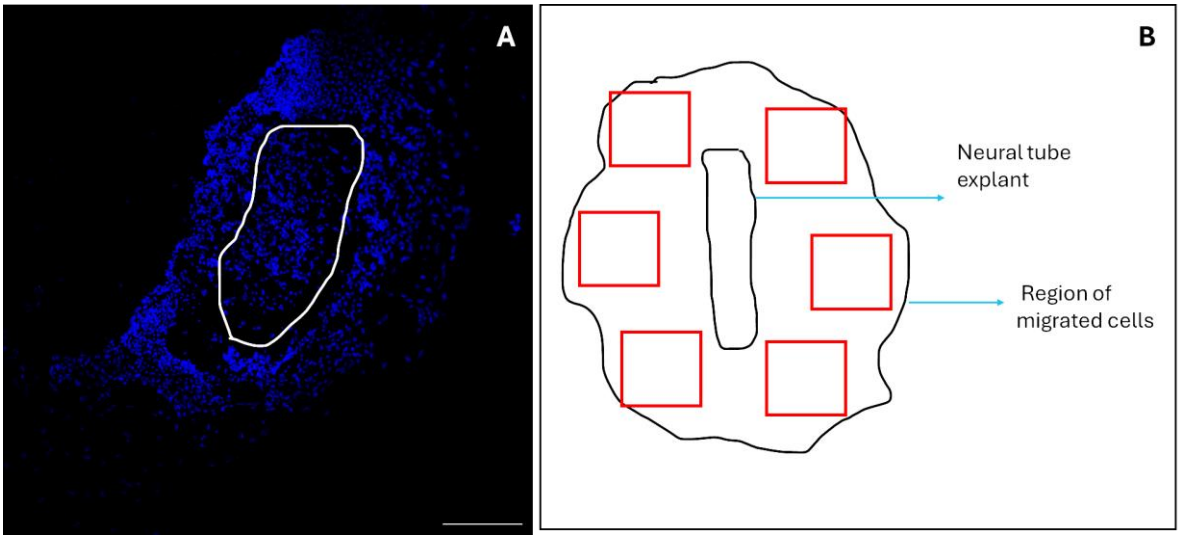


Figure 2.3 Calculating the viability ratio of cultures. Fig. A: The neural tube explant and the migrated cells DAPI (blue) stained the nuclei. The position of the neural tube explant is indicated by the white outline. Fig. B: A schematic diagram showing the six equal areas of the outgrowth that were imaged. From the images cells were counted to calculate the ratio of viability. (Figure A. Leica fluorescence microscope Thunder microscope, 10X objective, scale bar: 200µm).

Cytochalasin D treatment

The optimised concentration of cytochalasin D which was determined for use (Appendix 6) was 0.5 µg/ml of cytochalasin D (diluted in 0.1% DMSO). Following 48hrs of culture, DMEM was removed from 20 cultures and replaced with either 0,5 ml of DMEM containing 0.5 µg/ml of cytochalasin D (n=10) or DMSO (n=10) respectively but was retained in 10 cultures as the DMEM control. One image was taken of the treated, DMEM and DMSO cultures every hour for six hours. Thereafter all the cultures were fixed, immunolabelled and stained (Fig. 2.2).

As a “recovery” experiment the cytochalasin D treatment (0.5 µg/ml) was removed from three cultures after six hours and was replaced with fresh DMEM. (Appendix 6).

Live cell imaging

After 48hrs in culture, three live NC cultures of the cytochalasin D treated, DMEM and DMSO groups were imaged once every hour for six hours (Fig. 2.2). Photographs were

taken of the identical area of migrating cells in each culture over the six hours. The time-lapse photomicrographs were taken manually using brightfield microscopy on the Leica Thunder microscope which does not have automated live cell imaging settings nor an incubation facility. Thus, the Nunc glass bottom dish containing the cultures was clipped on to a removable stage to secure the position of the culture dish. Photographs were taken using the X20 and the X63 objective and the stage containing the dish was removed from the microscope and placed back in an incubator (at 37°C and CO_2) in between photographs. An hour later the stage (containing the culture dish) was again placed on the microscope for imaging. Thereafter the cultures in all three groups (10 cultures in each group) were fixed (after approximately 54 hrs of incubation), immunolabelled with the anti-HNK antibody and stained with the optimised concentrations of phalloidin-Atto 590 1:200 and DAPI 1:1000 (Appendix 7). (The anti-HNK antibody was only available for fixed cells, not live cells.)

Immunocytochemistry (ICC)

Following 54 hrs in culture, cultures from all three groups (10 in each group) were fixed with 3,6% paraformaldehyde (in PBS) for 10 minutes at room temperature. The fixed cultures were then permeabilised with 0,1% Triton X-100 (in PBS) at room temperature for 7 minutes. The cultures were then washed with PBS following which 0,5ml of 1% BSA-PBS (bovine serum albumin) was added to the dish. The blocking buffer (1% BSA-PBS) was left in the dish for 30 minutes at room temperature. The BSA solution was then removed and the primary antibody (anti HNK-1/ N-CA, (CD57), mouse monoclonal IgM- Sigma) was prepared in 1% PBS-BSA solution at a dilution of 1:500 [antibody previously optimised (Appendix 7)]. Phalloidin-Atto 590 was added to the primary antibody-PBS-BSA solution to get the Phalloidin at a final concentration of 1:200. The primary antibody-phalloidin solution was then added to the cultures and incubated for 1 hour at 37°C. After incubation the primary antibody-phalloidin solution was removed and the cultures were washed three times with PBS. The secondary antibody (goat anti-mouse IgM conjugated to Alexa-Fluor 488) at 1:1000 in 1% BSA-PBS solution was added to the cultures and incubated for 1 hour at 37°C. Thereafter the cultures were washed three times with PBS. For each immunocytochemical run an ICC control was performed, wherein the primary antibody was omitted, and the cultures were incubated in the secondary antibody only (Appendix 7).

Finally, the cells were stained with DAPI prepared in PBS at a concentration of 1:1000. DAPI was added to the cultures for 10 minutes at room temperature in the dark. The cultures were washed twice with PBS and were observed using the fluorescent module on the Leica Thunder microscope or Zeiss LSM780 confocal microscope with Airyscan module.

NC cell visualization

Living NC cells were initially observed with phase contrast microscopy (Olympus CKX41 inverted phase contrast microscope) at x10 and x20 magnification after 24 hrs of incubation. After 48 hrs in culture, the live cells from each group were imaged every hour for six hours using brightfield on the Thunder Leica microscope. The fixed, stained and immunolabelled cultures were first viewed and imaged using fluorescence microscopy on a Leica Thunder microscope with the LAX imaging software. The following filter cubes were used (on the Leica fluorescence microscope) to visualise the fluorescence: Alexa-Fluor (488nM), DAPI (405nM) and Phalloidin (546nM). Digital images were recorded using the x20 and x63 objective. The high-resolution photographs of the cells immunolabelled with anti HNK-1 antibody and stained with phalloidin and DAPI were recorded at their respective wavelengths.

The Thunder microscope uses a computational clearing method to generate high resolution images, close to the ones generated by the confocal microscope. The Thunder microscope was used as an alternative method to capture images during the period when the confocal microscope was not operational. Images taken using the Thunder microscope were used to calculate the mean fluorescence of phalloidin.

Cultures were also imaged using the Zeiss Laser Scanning Confocal Microscope (LSM) 780 and Airyscan. The following settings were first applied: bit level of 12, the appropriate laser lines were selected 488nm (for secondary antibody conjugated to Alexa Fluor 488), 590nm (Phalloidin-Atto590) and 405nm for the excitation of DAPI (blue) (fluorophore imaging setting options allows the selection of A488, A590 and DAPI: once selected the software will automatically apply the following settings laser lines, dichroic mirrors, and emission bandpass filters according to the selected fluorophore.

The emission windows were adjusted to avoid crosstalk), X63 objective and a zoom of 0.8 or 1.6 was applied to images. The gain was determined first by observing the negative control, the exposure was set to a level where no background fluorescence was apparent. This gain was then applied to the immunolabelled and stained cultures and it was maintained across all the images that were captured (from all three groups).

In addition, Z-stack images (that were taken using the Zeiss Laser Scanning Confocal Microscope) were taken to create 3D reconstructions of the cells at a zoom of 0.8 and 1.6. The number of slices and the distance of slices was determined automatically by the Zen software; however, the number of slices were kept between 8-10 slices. Three-dimensional reconstructions were created using the Zen software and were saved as an image.

Image analysis conducted using phase contrast and fluorescence NC cell images.

Cell morphology and cell behaviour were observed from the images of the live and fixed cells that were photographed using the Olympus CKX41 inverted phase contrast microscope and the Leica Thunder microscope. Quantitative analysis was undertaken from these images:

1. Position of the migratory front from the lateral border of the neural tube explant:
   Using ImageJ linear measurements were measured from the lateral side of the neural tube explant to the furthermost migrated cell at the migratory front of the DMEM group (Fig. 2.4). Measurements were taken at 24 hrs of incubation and again at 48 hrs of incubation on the same culture at the same position. The difference in the position of the migratory front was calculated by subtracting the measurements taken after 24 hrs of incubation from the measurements taken at 48 hrs of incubation. This was calculated for 10 different neural crest cultures. The measurements were only taken from DMEM cultures where the field of view of the microscope captured the border of the neural tube and the migratory front in the same image such that the linear meausrent could be taken.

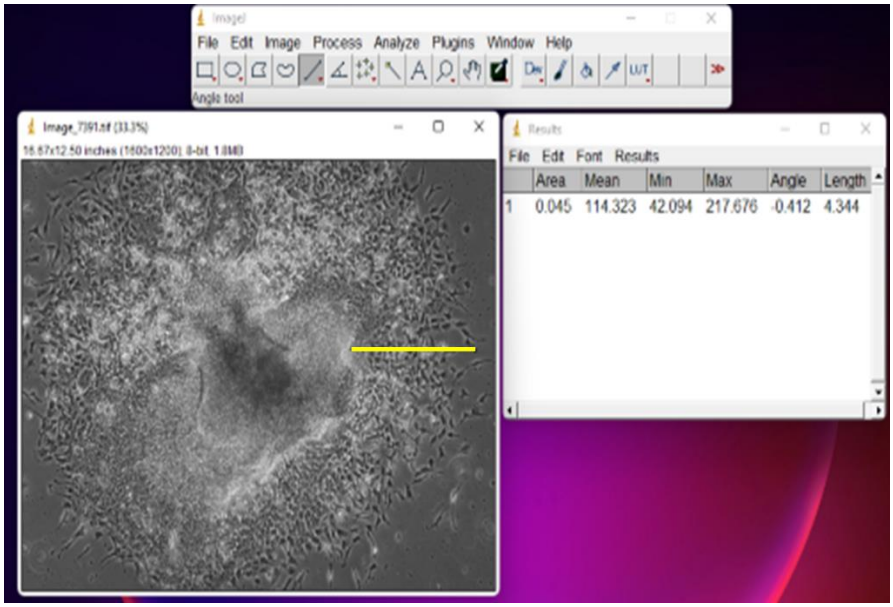


Figure 2.4 Measuring the positional changes of the migratory front of a NC culture using the linear tool ImageJ. A line was drawn from the border of the neural tube to the migratory front (yellow line) 24 hrs and 48 hrs of incubation to determine the change in position. (Olympus CKX41 inverted phase contrast microscope, 10X objective).

2. Cell viability: Cell viability of the DMEM, DMSO and cytochalasin D treated groups was measured by manually counting the fixed, DAPI stained cells from the photomicrographs that were taken with the Leica (Thunder) fluorescence microscope. The ratios of viability were calculated from these cell counts (refer to cytochalasin D optimisation section and Appendix 6).

3. Time-lapse images: Groups of cells were identified in individual cultures of the three groups. The area (211.93 x 211.93µm) containing these cells was imaged once every hour for six hours. Individual cells were identified and assigned different colours. Using ImageJ the shape of the cell was outlined and the behaviour and morphology of the cells in three cultures of each group was observed.

In addition, using ImageJ and the Manual Tracking plugin, the migration of putative NC cells (unlabelled, as the cells were live) was traced in each group (DMEM, DMSO and cytochalasin D treated). At each time interval (every hour) the position of the cell was measured with the nucleus taken as the central point. The “Chemotaxis Tool” plugin (Malagon et al., 2019) was used to plot a graph of the cells’ migration, and the velocity of each cell was calculated using the X and Y coordinates.

4. Mean fluorescence of phalloidin-Atto590: The corrected total cell fluorescence (CTCF) of cells stained with phalloidin was determined using the following formula (El-Sharkawey, 2016):

$$CTCF = Integrated\ density\ - (area\ of\ the\ selected\ cell\ \times Average\ mean\ grey\ value\ of\ the\ backgroud)$$

To use the formula above, an outline of the cell of interest was drawn using ImageJ. Thereafter the following measurements were selected and measured: Integrated density, area, mean grey value, and the minimum and maximum grey values of the region of interest (Fig. 2.5).

To calculate the average grey value of the background, three regions devoid of fluorescence, in cultures which were stained with phalloidin, were selected and three measurements of the grey value were calculated. Thereafter the measurements were averaged.

The mean fluorescence of phalloidin was calculated by averaging the CTCF of phalloidin from the individual cells (n=30 for each group).

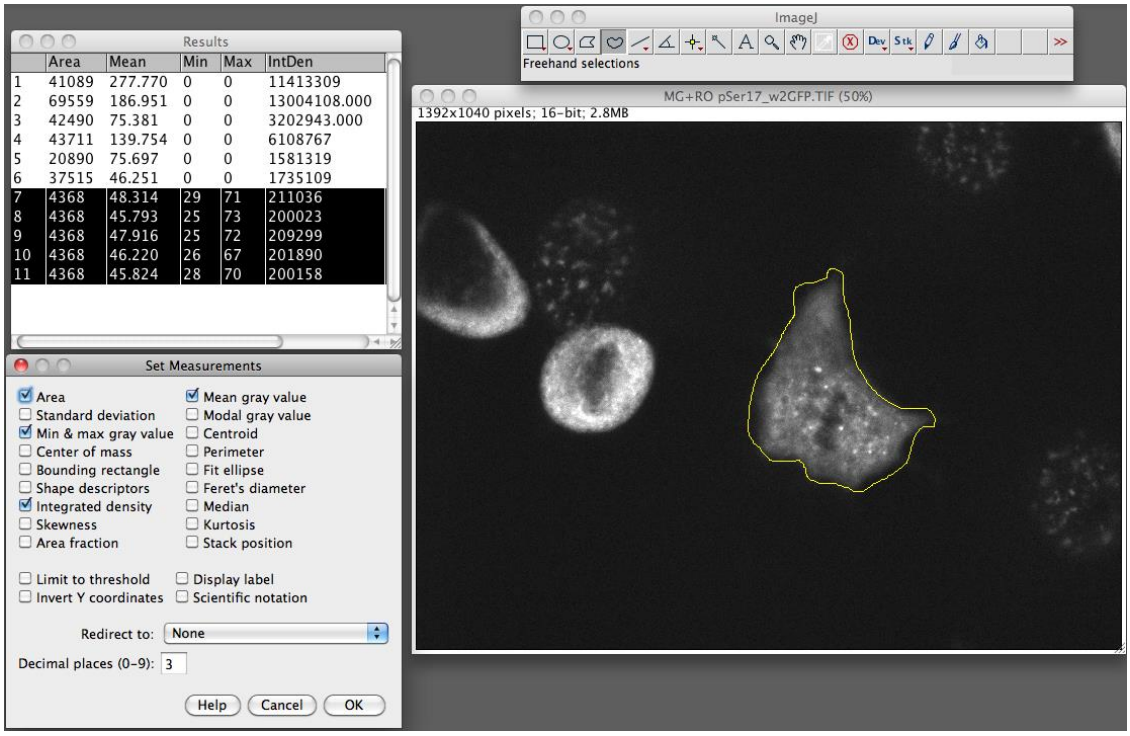


Figure 2.5 Determining the mean of fluorescence of phalloidin using ImageJ. In the example above the region of interest includes the entire cell (yellow outline of cell). The measurements that were taken can be seen in the box on the bottom left corner of the figure. Measurements include the area, integrated density and the mean grey value.

Statistical analysis:

Velocity of cells:

The velocity of 27 cells from each group was measured. The velocity was measured from live putative (unlabelled) NC cells that were tracked “Individual” cells at the migratory front were tracked as it was easy to follow their positional changes manually. Therefore, nine cells were tracked in each culture, and three cultures (from each group) were time lapse imaged (Fig. 2.3).

The data was analysed using the JASP statistic software (jasp-stats.org). The Shapiro-Wilk test was performed on the data to determine the distribution of the data. To compare the fluorescence of cells from the three groups, a Kruskal-Wallis test was conducted, followed by a Dunn’s comparative test.

The results of the Dunn's test include the Z test statistics (z-value) and a p-value. The z-value indicates how many standard deviations a data point is from the mean value of the data. The rank biserial correlation coefficient (rrb) was also calculated using the JASP software, the rrb is a measure of the strength and direction of the relationship between two variables.

Mean fluorescence:

The fluorescence of phalloidin was measured in 30 cells from each group. The data was analysed using the JASP statistic software. The Shapiro-Wilk test was performed on the data to determine the distribution of the data. To compare the fluorescence of cells from the three groups, a Kruskal-Wallis test was conducted, followed by a Dunn's test. Similarly, the results of the Dunns test included the z-value and p-value and the rank biserial correlation coefficient (rrb) was also determined.

3. CHAPTER THREE: Results

The number of quail eggs utilized, and NC cultures obtained:

A total of 207 quail eggs were used in this experiment. Embryos that were used, were between the stages of 12 to 16 (Hamburger & Hamilton, 1951).

Table 1. Summary of the number of eggs that were used and cultures that were obtained during this experiment.

Total number of eggs used	**Number of cultures**	**Cultures that were viable after 24hrs in culture**	**Total cultures that were fixed after +48hrs in culture**
207	127	117	81

Of the 207 eggs that were obtained, 80 eggs were not used as half of these eggs were infertile and the remaining eggs were not at the appropriate stage of development.

Ten of the 127 cultures did not show evidence of delaminating cells and were thus not used.

Thirty-six of the cultures that were viable after 24 hrs were lost due to fungal contamination that persisted in the shared lab space. Hence 81 cultures were used and finally fixed after 54 hrs in culture. The total number of fixed cultures (n=81) included the cultures that were used for the immunocytochemistry optimisation and phalloidin staining (n=21) and the optimisation of the cytochalasin D (n=30). The remaining cultures (n=30) were divided into one of the three groups (DMEM control, DMSO control and treated group).

For the immunocytochemistry optimisation 21 of the 81 fixed cultures were used. Different concentrations of the primary antibody were tested in nine cultures, eight cultures were used as “negative” controls for the immunocytochemistry, and four cultures were used in the optimisation of DAPI staining (Appendix 7).

Thirty cultures (included in the 81 fixed cultures) were used in the cytochalasin D optimisation. The concentrations of cytochalasin D were tested in 16 cultures, while a further seven cultures each were used for the DMEM and DMSO controls (Appendix 6).

The balance (n=30) of the 81 fixed cultures included cultures that were divided into one of the final three groups; DMEM control (n=10), DMSO control (n=10) or treated with cytochalasin D (n=10). Within each group, three cultures were live cell imaged for six hours while the remaining seven were allowed to continue undisrupted for six hours within their respective media.

Characterization of trunk neural crest cultures

Following 24 hours of incubation neural tube explants, incubated in DMEM, were seen to be attached to the fibronectin-coated dishes. Cells were noted surrounding the borders of the tube as an outgrowth (Fig. 3.1A). The region at the periphery of the outgrowth is henceforth referred to as the migratory front (Fig. 3.1B and Fig. 3.1C). In this region, individual cells were noted (Fig. 3.1B and Fig. 3.1C).

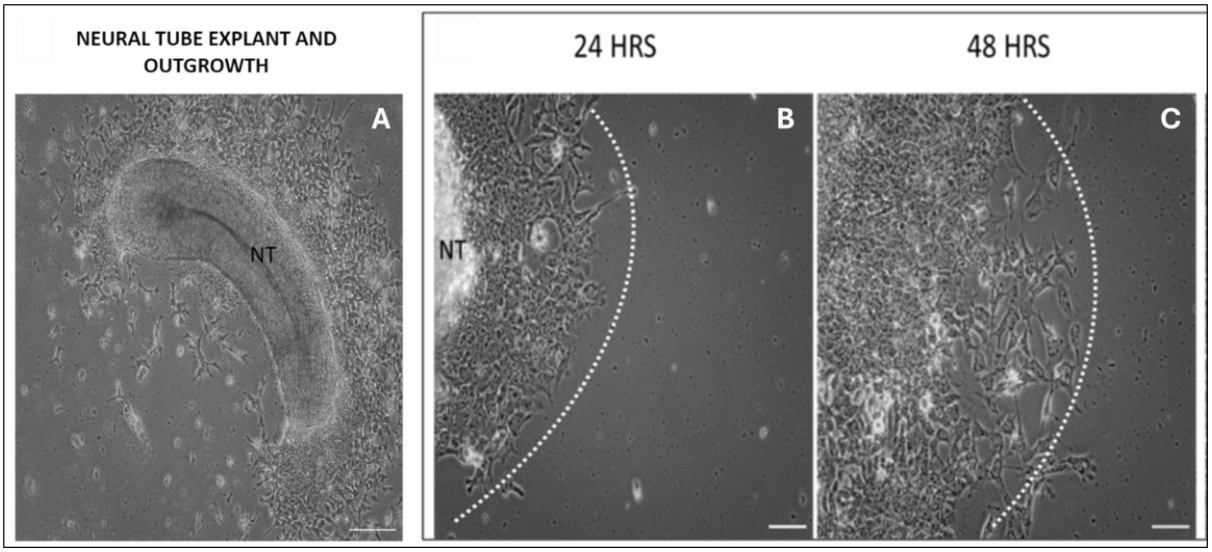


Figure 3.1. Phase contrast images of neural tubes and the surrounding outgrowth of cells. Fig A: A neural tube (NT) explant showing the outgrowth of cells (X10). Fig. B and C: The outgrowth of culture imaged 24 and at 48 hours and the position of the migratory front is indicated by the white dashed line. The migratory front extended further into the cell free space and away from the NT explant (X20). NT explant is not shown in Fig. C. (Phase contrast microscopy, scale bar: 200 µm and 100 µm).

The positions of the migratory front in 10 DMEM cultures were recorded at 24 hours and again at 48 hours of incubation. The minimum and maximum positions of the migratory front (at 24 hours and 48 hours) was averaged and presented in Table. 2. The minimum positions at 24 hours and the maximum positions at 48 hours had a high variability as shown by the high standard deviation (Table. 2).

Table 2. The mean minimum and maximum positions of the migratory front from the border of the neural tube (and standard deviation) measured at 24 hours and again at 48 hrs in 10 different neural tube explants that were cultured in DMEM. ***** the high standard deviations.

Period of incubation	**Mean minimum position (µm) ± SD**	**Mean maximum position (µm) ± SD**

24HRS	76,98± 34,15*	77,31 ±4,22
48HRS	201,35± 2,46	205,77± 31,60*

The difference in the position of the migratory front between 48 hrs and 24 hrs of incubation was also calculated. The position of the migratory front was seen to have increased over the period of incubation (Fig. 3.2).

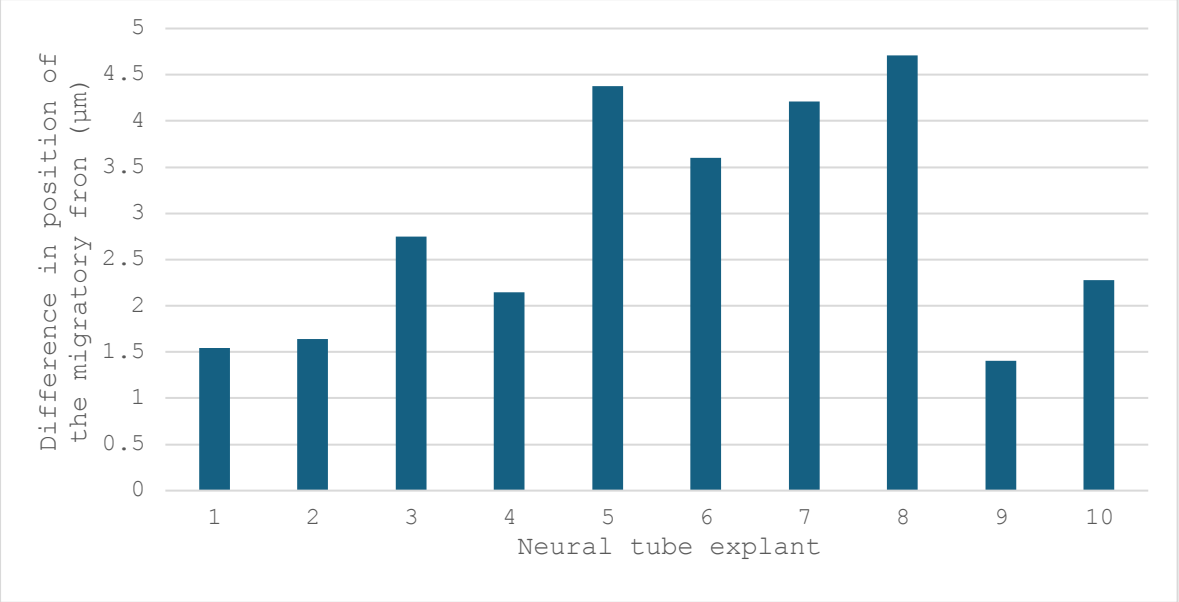


Figure 3.2 The difference in the position of the migratory front between 24 and 48 hours of incubation (on the y axis), measured in 10 different NC cultures (on the x axis) that were incubated in DMEM.

Morphology of putative (unlabelled) neural crest cells after 24 hours of incubation.

Within the outgrowths of explants cultured in DMEM, the cells situated closer to the explant were multipolar. These cells were separated by small intercellular spaces (Fig. 3.3A). At the migratory front, multipolar cells within the outgrowth were separated by

larger intercellular spaces. These cells had projections that extended into the cell free space (Fig. 3.3B).

Individual cells were noted at the migratory front (Fig. 3.3C). These cells were stellate shaped and had broad fan shaped lamellipodia (Fig. 3.3D).

As immunocytochemical labelling of the NC cells could not be undertaken on living cultures, cells were presumed to be neural crest cells, based on their well described stellate shape (Fig. 3.3).

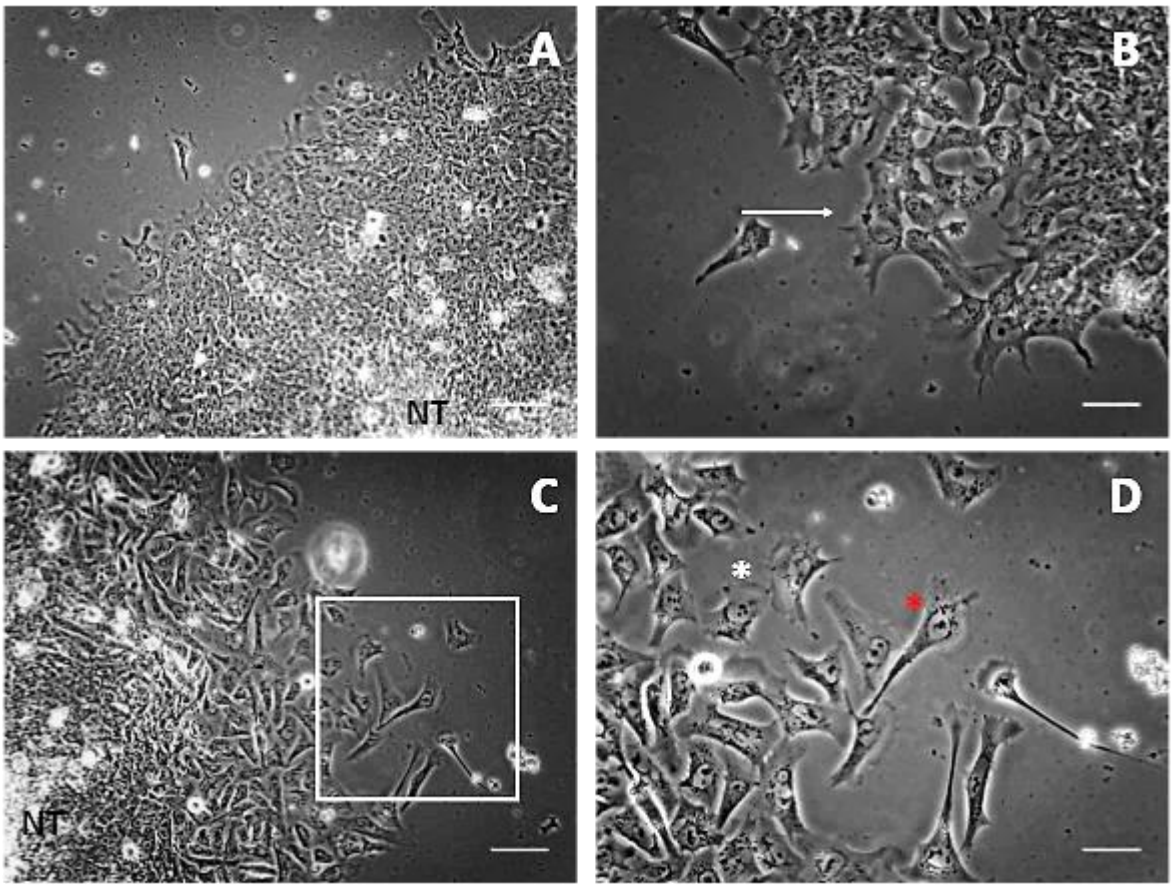


Figure 3.3 Outgrowth of putative NC cells after 24hrs of incubation in DMEM. Fig. A: Part of the neural tube (NT) explant and a region of the outgrowth of migratory cells (X10). Fig. B: The multipolar cells at the migratory front with projections (white arrow) extending towards the cell free space (X40). Fig. C: A group of individual cells at the migratory front was identified (white box) (X20), these cells were observed at a higher magnification in the Fig. D. Fig. D: A higher magnification of the cells in Fig. C (white

box) showed a cell with broad lamellipodia (red asterisk) (X40). (Phase contrast, scale bar A- 200 µm; C- 100 µm; B and D- 50 µm).

Morphological comparisons of putative and immunolabelled NC cells in the DMEM and DMSO controls and the treated group (after 48 hr and 54 hrs of incubation): Cell projections and actin arrangement.

After 48 hours of incubation (t=0), putative NC cells in the DMEM control group exhibited a stellate shape (Fig. 3.4A), characterized by broad lamellipodia and filopodia. In those assays cultured in either, DMSO (Fig. 3.4B) or cytochalasin D (Fig. 3.4C) membrane blebbing was noted within 15 minutes of administration (t=0). However, in the cytochalasin D-treated group, membrane blebbing was also accompanied by cell rounding (Fig. 3.4C).

Following a further 6 hours of incubation (t=6 or 54 hours of culture), an increased number of cells was observed at the migratory front in the DMEM control group and cells maintained their stellate shape (Fig. 3.4D). However, at the same time point (t=6) cells in the DMSO control displayed a mix of rounded and stellate shapes (Fig. 3.4E). The projections of the stellate shaped DMSO control cells appeared narrower relative to the broader projections observed in the DMEM control (Fig. 3.4D). Similarly, cells treated with cytochalasin D also showed a mix of rounded cells and cells with an altered morphology. However, the altered cells exhibited the most pronounced morphological changes, with rounded cell bodies and thin, branching projections (Fig. 3.4F). This altered morphology gave the previously stellate cells a “spidery” appearance.

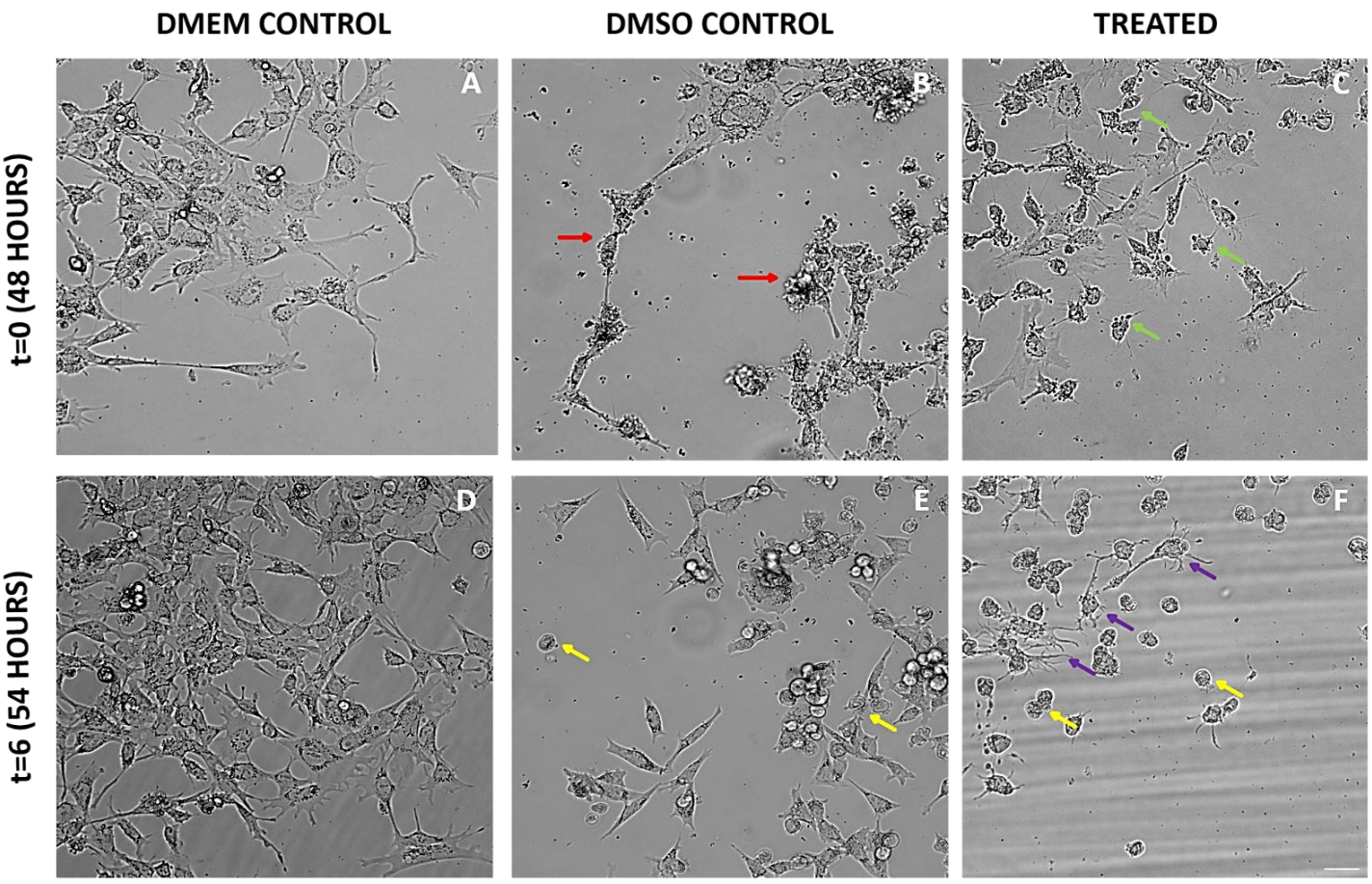


Figure 3.4. Putative NC cells after 48 hrs (t=0) in DMEM (Fig. A), DMSO (Fig. B), and cytochalasin D (Fig. C) and after 54 hours of incubation (t=6) in DMEM (Fig. D), DMSO (Fig. E) and cytochalasin D (Fig. F). Fig. A: Putative stellate shaped NC cells (DMEM). Fig. B: Membrane blebbing (red arrows) on cells (DMSO). Fig. C: Membrane blebbing with cell rounding (green arrows) in cells (cytochalasin D treated). Fig. D: Cells (DMEM) retained their stellate shape cells after 54 hours of incubation (t=6). Fig. E: Rounded cells (yellow arrows) after 6 hrs and stellate shape cells with narrow projections (DMSO). Fig. F: Rounded cells (yellow arrows) and cells with an altered morphology (purple arrows) after 6 hrs (cytochalasin D treated). (Brightfield Thunder microscope, Objective X20, zoom by 33%, scale bar= 100µm).

In those cultures, fixed for immunocytochemistry, the identified NC cells (immunolabelled with anti-HNK antibody) were interspersed with surrounding non-NC cells (stained with only phalloidin and DAPI) (Figure. 3.5D, H and L). Generally, in the DMEM and DMSO control groups a dense network of cells (NC and non-NC cells) was

noted (Fig. 3.5D and H), relative to the treated group where cells were sparsely organised (Fig. 3.5L).

The immunolocalization (of the primary antibody) was confirmed by the “negative” controls that were included, which showed no specific labelling when only the secondary antibody was added to some cultures (Fig. 3.5M). Additionally, the cells showed little to no autofluorescence or background fluorescence when the phalloidin stain was omitted (Fig. 3.5N).

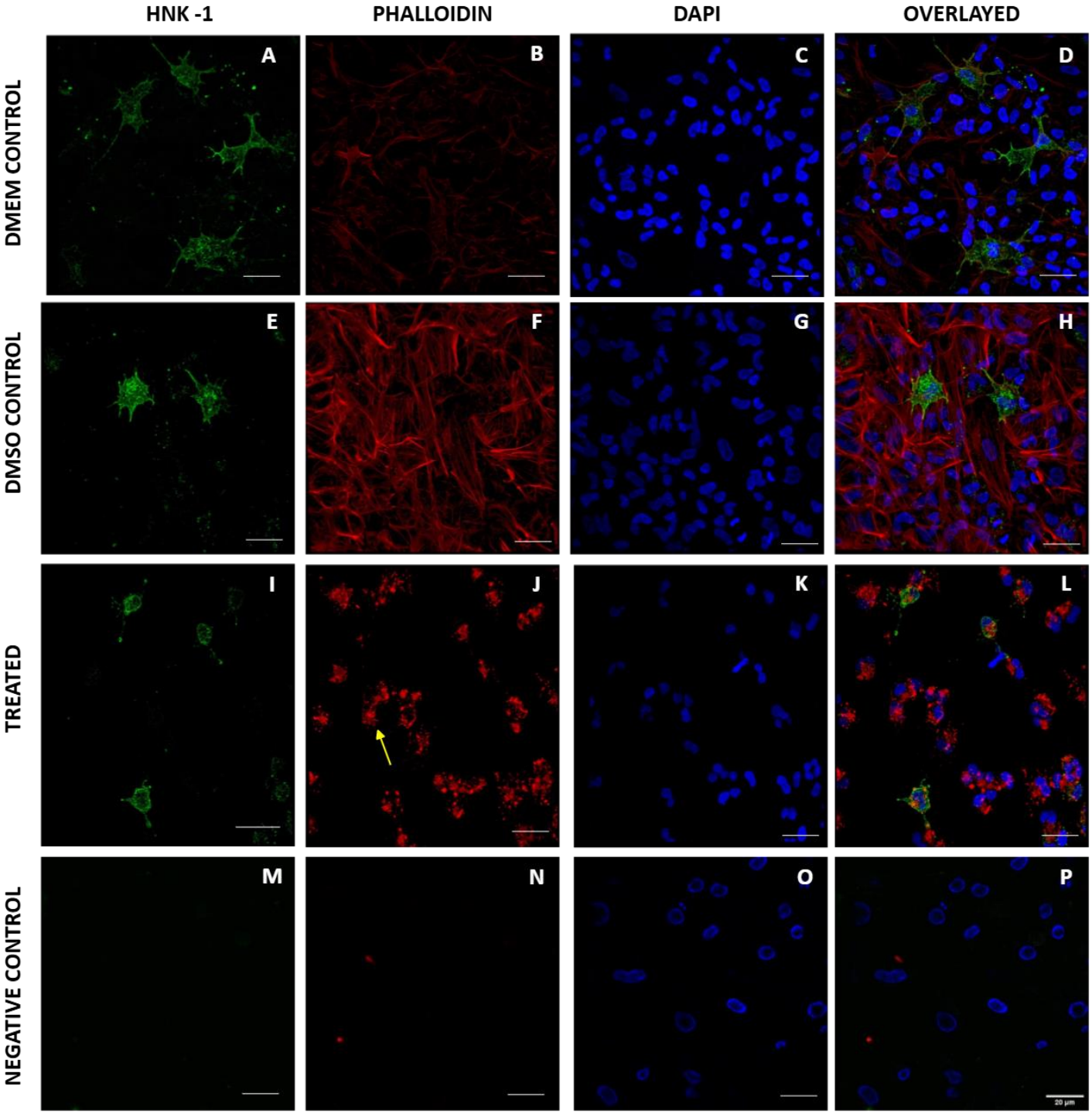


Figure 3.5. DMEM, DMSO and a cytochalasin D treated cultures that were fixed, immunolabelled with anti-HNK (green) and stained with phalloidin (red) and DAPI (blue). Images are reconstructed from Z-stacks. Fig. A: Stellate shaped NC cells (green)(DMEM). Fig. B: Organised actin filaments (red) of NC cells and non-NC cells stained with phalloidin. Fig. C: DAPI stained nuclei (blue) of cells (DMEM). Fig. D:

Overlayed images showing the dense network of cells as well as the interspersed NC cells (green)(DMEM). Fig. E: Two stellate shaped NC cells (green) (DMSO). Fig. F: Actin filaments (red) in NC cells and non-NC cells (DMSO). Fig. G: DAPI stained nuclei (blue) of cells (DMSO). Fig. H: Overlayed image showing a dense network of cells (DMSO). Fig. I: Cytochalasin D treated NC cells (green). Fig. J: The disrupted actin (red) arrangement of cells (cytochalasin D treated), actin appeared in aggregated clumps (yellow arrow). Fig. K: DAPI stained nuclei (blue) of cells (cytochalasin D treated). Fig. L: Overlayed images showed the sparse organisation of cells (cytochalasin D treated). Fig. M: Negative control, containing secondary antibody only (DMEM). Fig. N: Autofluorescence of cells that were not stained with phalloidin. Fig. O: DAPI stained nuclei (blue) cells (DMEM). Fig. P: Overlayed images of cells in negative control (DMEM). (Confocal microscopy -Fluorescence, HNK-1: GREEN, Phalloidin-Atto 590: RED, DAPI: BLUE, Objective: X63, zoom 0.7, scale bar= 20 μm).

The HNK- antibody was immunolocalised to the cell membrane and cell projections. The anti- HNK antibody also attached to granular structures in the cell body and these granules were noted in the cytoplasm of the cells (of all three groups) (Fig. 3.6A, E and I). The actin, stained with phalloidin, in the cells of the DMEM (Fig. 3.6B) and DMSO (Fig. 3.6F) groups was organised in long filaments which lined the membrane and the cell projections. In contrast, actin in the cytochalasin D treated cells was drastically altered, with clumps of actin visible in the cell body surrounding the nucleus (Fig. 3.6J).

Due to the dense network of cells in the DMEM (Fig. 3.5D) and DMSO (Fig. 3.5H) groups, the individual non-NC cells was not easily distinguishable. However, thin filaments of actin which extended from the non-NC cells (projections) was noted (Fig. 3.6B and Fig. 3.6F). In the cytochalasin D treated group, although the cells are sparsely arranged (Fig. 3.5L), due the disruption of actin it is difficult to distinguish the cell borders from the phalloidin stained cells (Fig. 3.6J). Thus, the morphology of the treated non-NC cells cannot be defined from the fluorescence images.

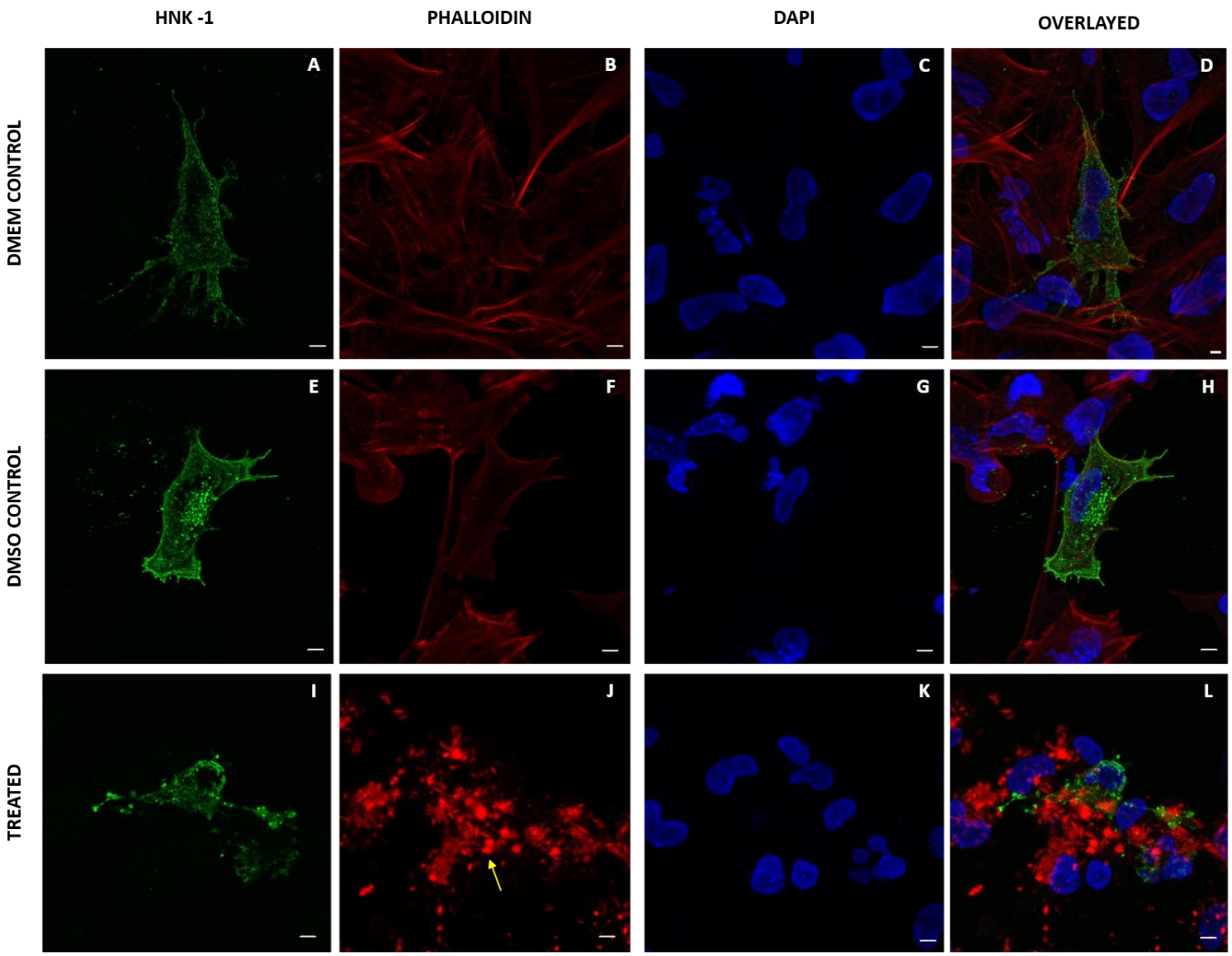


Figure 3.6. Reconstructions of Z-stacks that were captured for individual cells from the DMEM control, DMSO control and treated group. Cells with immunolabelled with anti-HNK (green), phalloidin (red) and DAPI (blue). Fig. A: NC cell (green) with numerous filopodia extending from the cell (DMEM). Fig. B: The long-organised actin filaments (red) within the NC cell and the surrounding cells (DMEM). Fig. C: DAPI stained nuclei (blue) of cells (DMEM). Fig. D: Overlayed images of a cell (DMEM) showing the projections of the NC cell that extended outwards and spread between the neighbouring non-NC cells. Fig. E: A stellate shaped NC cell (green) (DMSO). Fig. F: Long organised actin filaments (red) noted in the cells (DMSO). Fig. G: DAPI stained nuclei (blue) of cells (DMSO). Fig. H: Overlayed images of the cells (DMSO), showing the NC cell

(green) in relation to its neighbouring non-NC cells. Fig. I: A treated NC cell (green) showing an altered morphology. Fig. J: Disrupted actin (red) which appear as aggregates concentrated in the cell body (yellow arrow) (cytochalasin D treated). Fig. K: DAPI stained nuclei (blue) of cells (cytochalasin D treated). Fig. L: Overlayed image where the positions of the NC cell (green) in relation to the surrounding non-NC cells is obscured due to the disrupted actin (red). (Confocal microscope -Fluorescence, HNK-1: GREEN, Phalloidin-Atto 590: RED, DAPI: BLUE, Objective: X63, zoom 0.7, scale bar= 50 µm).

The fluorescence of phalloidin in cells from the DMEM, DMSO and treated groups (n=30 per group) was measured to quantify actin in individual cells. When the mean fluorescence of phalloidin was compared between the three groups, the results of the Kruskal-Wallis test indicated a significant difference ($p < 0.001$) between the groups.

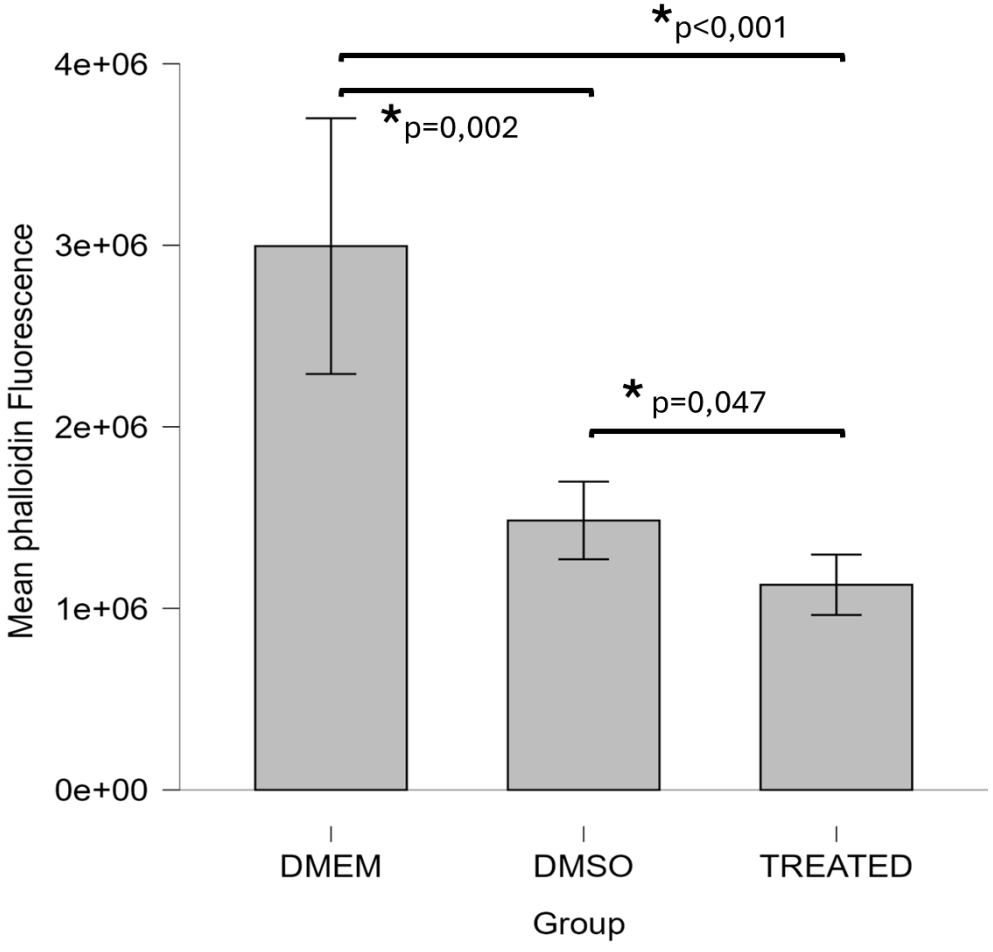


Figure 3.7 The mean fluorescence of phalloidin of cells (n=30 for each group) in the DMEM, DMSO and treated groups (with standard deviation). When the groups were compared in pairs, there was a significant difference (indicated by the asterisks) between all the groups.

The images showed a higher fluorescence of phalloidin in the DMSO control (Fig. 3.6F) and treated cells (Fig. 3.6J) compared to the DMEM control (Fig. 3.6B). However, when qualitative measurements of the mean fluorescence of phalloidin were calculated, the DMEM control had a significantly higher mean fluorescence of phalloidin compared to the DMSO control and cytochalasin D-treated group. Overall, the treated group had the lowest mean fluorescence of phalloidin of the three groups (Fig. 3.7). The groups were compared in pairs, using Dunn's test, (Table. 3).

The mean fluorescence of phalloidin decreased in the DMSO control and cytochalasin D treated groups compared to the DMEM control (Table. 3). However, the Dunn's test showed that the decrease in the mean fluorescence between the treated group and the DMEM control was more significantly. This is indicated by the p-value<0.001, z-value of 5.102 and a rank-biserial correlation (effect size) of 0.718. The decrease mean fluorescence of the DMSO control when compared to the DMEM control was moderately significant since the p=0.002, z-value = 3.069 and the effect size = 0.513. There was also a significant decrease(p=0.047) in the mean fluorescence of phalloidin between the DMSO control and the cytochalasin D group. However, this difference was the lowest since this pair had the lowest z-value of 1.989 and the lowest effect size of 0.349 (Table 3).

Table 3. Results of the Dunn's test conducted between the three groups (DMEM, DMSO, TREATED) showing the z-value, rank biserial correlation and the p-value**.** * Indicates the pairs that were significantly different.

Comparison	Z value	Rank-biserial correlation (effect size)	P value
DMEM – DMSO*	3.069	0.513	0.002
DMEM – TREATED*	5.102	0.718	<0 .001
DMSO - TREATED*	1.989	0.349	0.047

Migration dynamics (i.e. the patterns and velocity) of putative NC cells in the control and treated groups.

As live cells could not be immunolabelled with anti- HNK, the migration of putative live NC cells in all three groups was tracked and imaged using brightfield microscopy (Thunder microscope). Using these images and Image J software the positional changes of the cells was tracked and visualised in migratory plots (Fig. 3.8). Three cultures from each group were observed, and nine cells were tracked in each culture.

In the migratory plot each cell is assigned the same starting point (0;0), cells have an end point (black dot) and the path of migration is shown from the starting point to the end point. The position of the end point (block dot) shows the direction in which the cell moved, relative to its starting point.

Cells in the DMSO control exhibited the most random migration. the randomness of the migration was indicated by their paths and the end points of the individual cells that were scattered across three or all four quadrants of the migratory plot (Fig.3.8B, E and H), with cells having appeared to move in different directions relative to the starting point. Although cells in the DMEM control had random migratory paths, the end points of individual cells could be noted in one or two quadrants of the plots (Fig. 3.8A, D and G) and cells appeared to move in a common direction relative to the starting point. The treated group displayed the most restricted migration since the individual cells exhibited

linear migration paths and similar to the DMEM migratory plots, cells appeared to move in the same direction since the end points were concentrated in one or two quadrants of the plot (Fig. 3.8C, F and I).

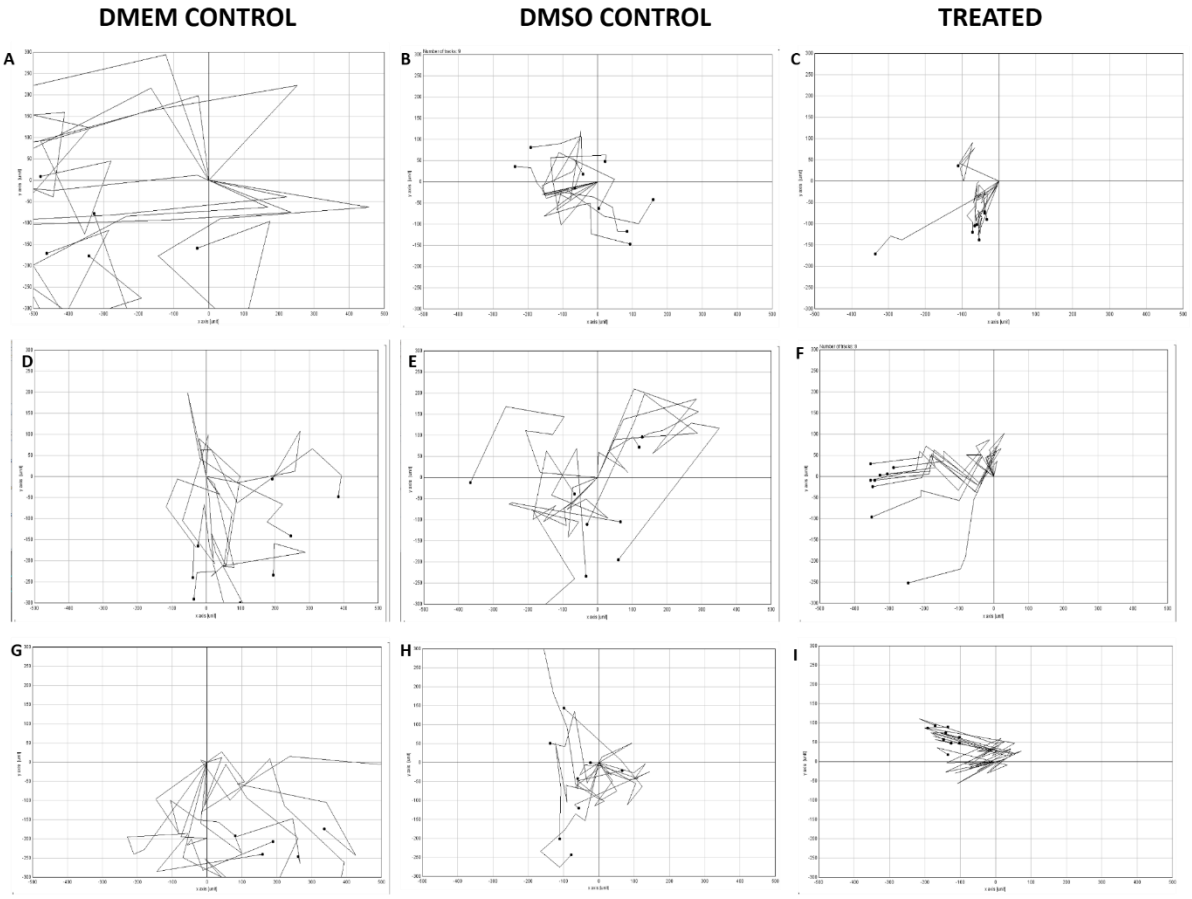


Figure 3.8. The migratory plots of putative NC cells were tracked in the DMEM controls, DMSO controls and the cytochalasin D treated group. A plot was created using the Chemotaxis Tool on Image J software for each culture that was observed. The plot demonstrates positional changes of cells from the common starting point (0;0), the axes indicate the direction of movement. Although migration paths of cells in the DMEM control were random, the end points of the cells were noted in two quadrants i.e. the top and bottom left quadrants (Fig. A), the bottom left and right quadrants (Fig. D) or in one quadrant i.e. the bottom right quadrant (Fig. G). In DMSO, the end points were scattered

across three (Fig. B) or four quadrants (Fig. E and H). In the treated group end points were localised in two quadrants (Fig. C and F) or in one quadrant (Fig. I).

The brightfield, time-lapse images of cells in Figure. 3.8A (DMEM control) are shown below (Fig. 3.9A). Cell -cell contact occurred between the cells and morphological and positional changes were noted after contact occurred (Fig. 3.9). The cyan-marked putative NC cell which was in contact with its neighbouring cells (the white-marked cell and the pink-marked cell) at t=0, had “retracted” projections. However, at t=3 the cyan marked cell had projections which appeared “stretched” (Fig. 3.9A). From the migratory data (Fig. 3.9B-migratory plots) the velocity was calculated and the velocities ranged between 110 – 156 units/sec. The highest velocity observed of a cell in the DMEM group was 156.24 units/sec (magenta marked cell), and the lowest velocity was 117.57 units/sec, the red-marked cell (Fig. 3.9C).

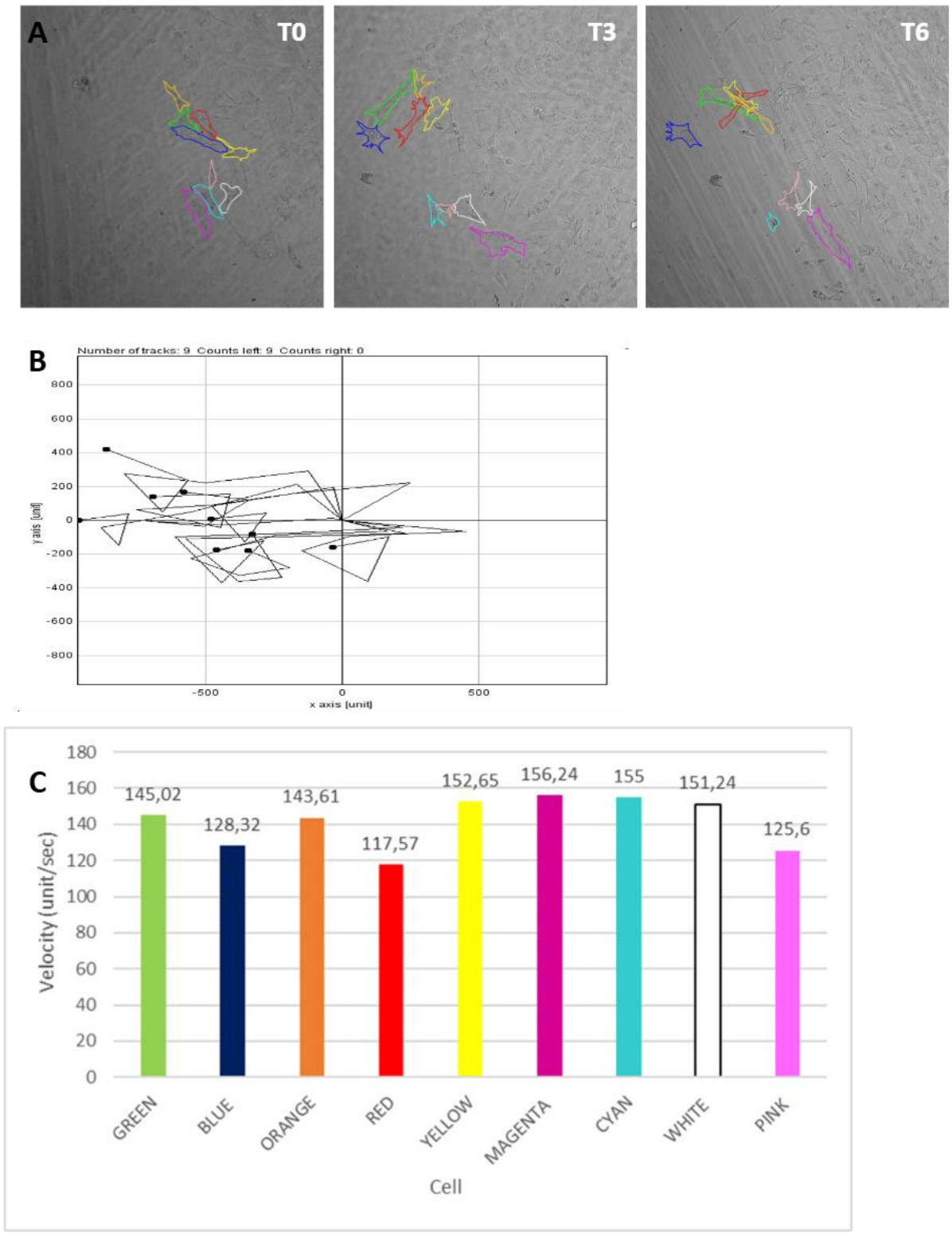


Figure 3.9. An analysis of putative NC cells in a DMEM control culture over 6 hours. Fig. A: A group of nine cells at the migratory front were identified and outlined in different colours, showing the morphology of each cell. The images were taken at t=0, t=3 and

t=6 hrs, where t=0 was at 48 hours of incubation. Morphological changes of all the identified cells were seen at t=3 and t=6. Fig. B: The migratory plot demonstrated the disorganised paths of movement of the cells (both axes represent distance). Fig. C: The velocity of each of the nine putative NCCs, categorised by colour showed varying cell velocities (Brightfield- Thunder microscope, objective: X20, scale bar- 100µm).

The brightfield images of the DMEM culture in Figure 3.8D, demonstrate putative NC cells forming a chain (Fig. 3.10A). The chain was composed of a “leading” cell i.e. the cyan-marked cell (cell furthermost in the cell free space) (Fig. 3.10A) and the trailing cells. Within the chain, cells appeared to enter, leave or re-enter the chain. As an example, the orange-marked cell at t=2 left the chain and later returned at t=3 and the leading cell separated from the chain and eventually moved towards cells in a neighbouring cluster at t=4 to t=6. The green marked cells which originated from a cluster of cells neighbouring the chain, became part of the chain at t=6 (Fig. 3.10A).

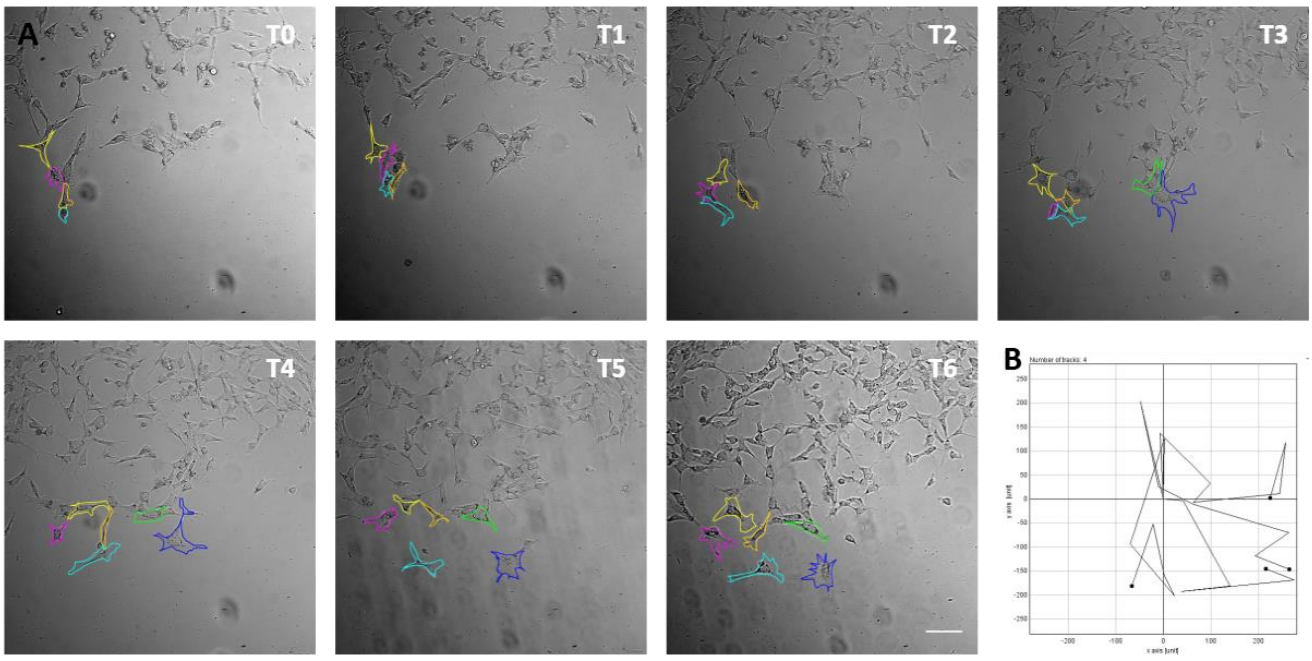


Figure 3.10. Time lapse images of a DMEM control culture, where cell contact produced a chain-like structure. The cells that were in contact at t=0, were outlined and contact between the cells formed a chain structure. The leading cell (cyan marked) located at the periphery of the chain (furthermost in the cell free space) separated from the chain

at t=5. The orange-marked cell can be seen in the chain at t=1, the cell left the chain at t=2 and returned at t=3. The green marked cell identified at t=3 joined the chain at t=6. Fig. B: The migratory plot visualised the movements of the cells that formed the chain structure. (Brightfield-Thunder microscope, objective: X20, scale bar: 100μm).

Similar cell contacts and morphological changes proceeding cell contact were observed in the putative NC cells of the DMSO control group to that of the DMEM control group. The red marked cell and the green marked cell in the DMSO control (Fig. 3.11A), which were in contact with each at t=0, both the green marked and red marked cells displayed a different morphology at t=3 (Fig. 3.11A). The migration paths of the cells were random (Fig. 3.11B) and the recorded velocities of the cells in the DMSO control (Fig. 3.11) ranged from 34 units/sec to 47 units/sec (Fig. 3.11C) which were lower than the cell velocities noted in the DMEM control (Fig. 3.9).

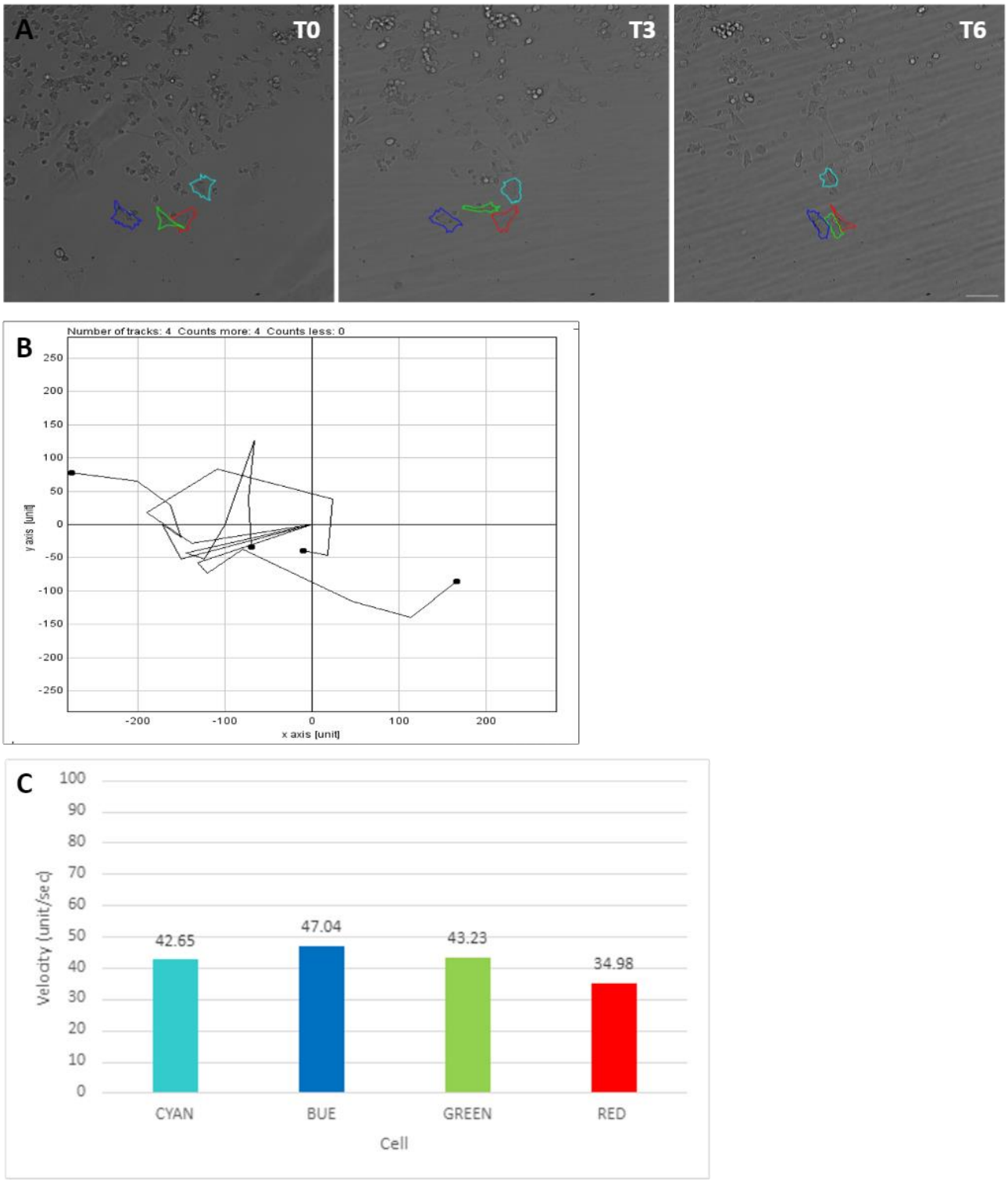


Figure 3.11. An analysis of cells in a DMSO control culture over 6 hours. Fig. A: Time lapse images were taken at t=0, t=3 and t=6 (t=0 is at 48 hours of incubation). Four individual cells were identified and outlined in different colours to highlight the

morphological changes that proceeded cell contact. The red-marked cell and the green marked cell were in contact and at t=0 and the morphology of both cells were altered at t=3. Fig. B: The migratory plot showed the random movement of the cells. Fig. C: A graph showing the velocity of each identified cell. Cell velocities ranged between 34 units/sec to 47 units per second. (Brightfield- Thunder microscope, objective: X20, scale bar- 100µm).

In the cytochalasin D treated group, while cell-cell contact occurred, cell projections appeared to be affected following contact (as in the DMEM and DMSO control groups). The cells that encountered a neighbouring cell developed thin projections (Fig. 3.12A), while cells that remained in contact with the same neighbouring cell maintained their projections throughout the period of exposure (Fig. 3.12A).

Contrary to the cell contact observed in the DMEM and DMSO control, the lack of cell contacts in a few of the cells in the treated group, resulted in cells (which had projections) losing their projections completely (Fig. 3.12A).

The recorded cell velocities of the cells in the treated group were the lowest relative to the DMEM and DMSO control (Fig. 3.12C). The velocity of the cells ranged between 43 units/sec to 47 units/sec (Fig. 3.12C).

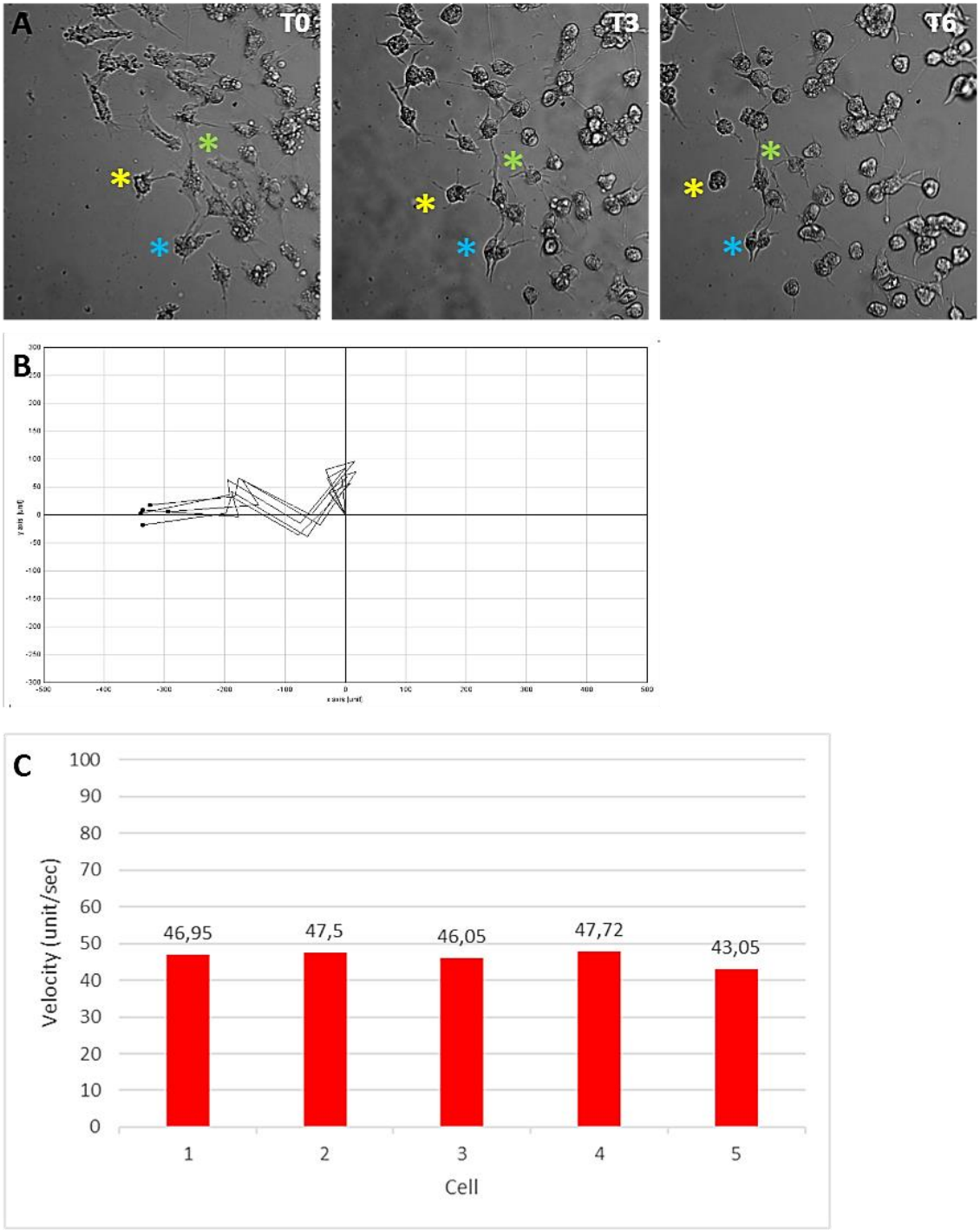


Figure 3.12. An analysis of putative NC cells treated with cytochalasin D for 6 hours. Fig. A: Time lapse images were taken at t=0, t=3 and t=6. The cell that formed contacts with surrounding cells formed projections (projections marked by a green asterisk). The cell that lost contact with surrounding cells lost its projections (projections marked by a yellow asterisk). Cells that maintained contact with each other maintained their

projections (projections of both cells marked by a blue asterisk). Fig. B: The migratory plot shows the restricted movement of treated cells. Fig. C: The velocities of the identified cells which ranged between 40 units/sec to 50 units/sec. (Brightfield- Thunder microscope, objective: X20, zoom by 43%, scale bar- 50µm)

The mean velocity of cells (27 cells for each group were tracked) was calculated and compared (Fig. 3.13), and the difference in the velocities between the groups was determined to be significant ($p < 0.001$). The mean cell velocity of cells in the DMSO and treated groups was significantly lower than the DMEM and the treated group showed the lowest mean velocity of the three groups. (Fig. 3.13).

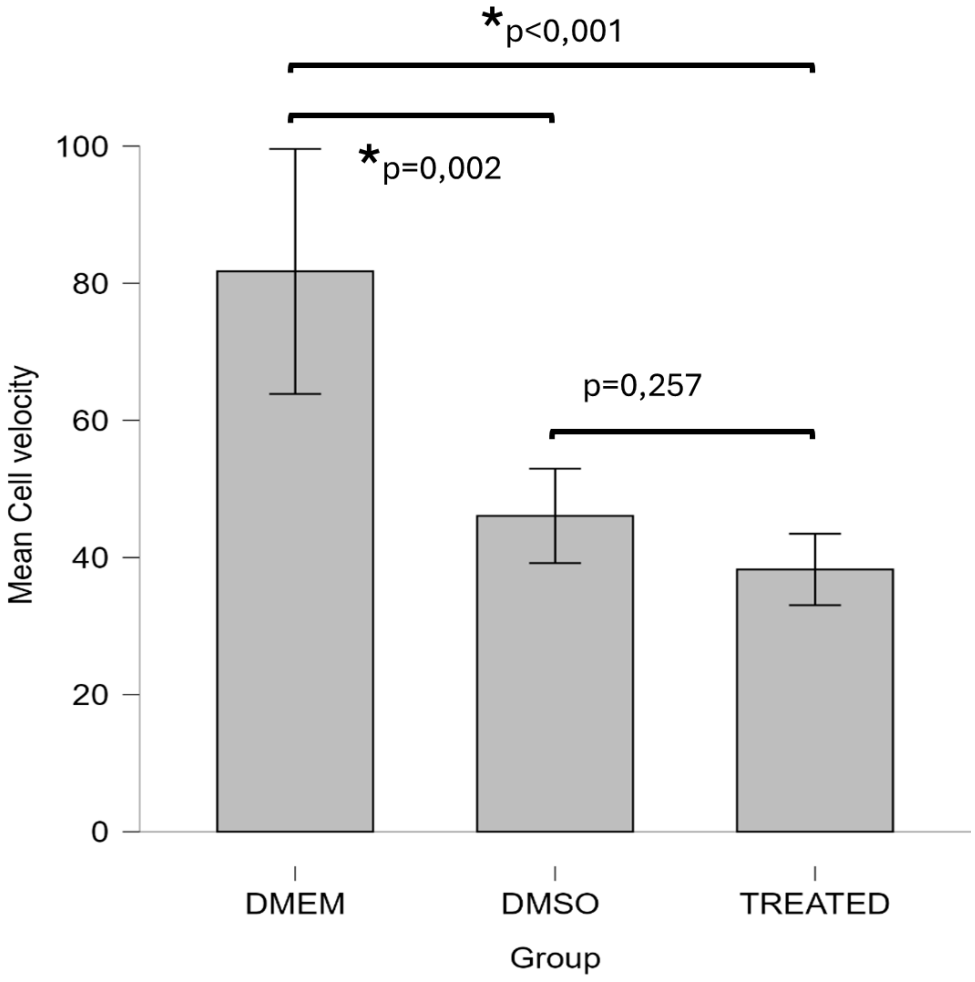


Figure 3.13. The mean velocity of cells from all three groups (DMEM control, DMSO control and treated with cytochalasin D group, 27 cells from each group were recorded. The treated cells had the lowest mean velocity, and it was significantly lower than the DMEM ($p < 0.001$). The mean velocity of the cells in the DMSO was significantly lower than the mean velocity of cells in DMEM ($p = 0.002$).

Table 4. Results of Dunn's Comparisons Test- results comparing the groups in pairs (DMEM, DMSO and treated). Results included the z-value, rank biserial correlation and the p-value. *Indicates the pairs that were significant.

Comparison	Z-value	Rank-biserial correlation (effect size)	p-value
DMEM – DMSO*	3.129	0.514	0.002
DMEM – TREATED*	4.263	0.654	< 0.001
DMSO - TREATED	1.134	0.199	0.257

When the Dunn's test was done to compare the groups in pairs, there was a significant difference between the DMEM and the treated group, and between the DMEM and the DMSO control (p-value <0.05) (Table.4). Additionally, the difference between the velocity of the cells in the DMEM and the treated group was more pronounced, as indicated by the higher z- value of 4.263 and the greater rank biserial correlation of 0.654. However, the difference between the DMEM and the DMSO was moderate, indicated by the z-value of 3.129 and effect size of 0.514 while difference between the treated and the DMSO control was not significant (Table. 4).

4. CHAPTER FOUR: Discussion

NC cells (in the DMEM and DMSO controls) displayed their typical stellate shape and high migratory capacity (Bronner and LeDouarin, 2012; Duband et al., 2020). Both the morphology and migratory capacity have been attributed to actin filaments within the cell (Kuriyama and Mayor, 2008) and in the current study this role of actin has been confirmed. Following, treatment with cytochalasin D, both the cell shape and migratory capacity of (putative) NC cells in the culture were markedly changed. The treatment altered the characteristic stellate shape and treated cells transformed “spidery”-like cells with rounded cell bodies and thin, branching projections. Additionally, the high migratory capacity of these cells was severely limited, as the velocity of the migrating cytochalasin D treated-putative NC cells was significantly reduced. However, despite the actin disruption induced by the cytochalasin D, the treated cells retained their ability to sense and respond to their environment.

The mechanism of action of cytochalasin D, which blocks actin polymerization (Brown and Spudich, 1981), explains the altered morphology observed in the cells in this experiment and it is consistent with previous research involving cytochalasin D where the toxin resulted in the cell body shrinking and affected the morphology of projections (Haendel at al., 1996; Hinoue et al., 2005; Lambert et al., 2023; Schliwa, 1986). The disruption of actin in cell projections likely contributed to altered projections that were noted on the treated cells. Additionally, the possible breakdown of stress fibres in the cell body may have resulted in the rounded appearance of the cell bodies in the cytochalasin D treated cells. Overall, the disruption of actin resulted in the loss of organized actin structures that typically maintain the stellate shape of NC cells. It should, however, be noted that the alterations observed cannot be solely attributed to the cytochalasin D, as the diluent DMSO, in which the cytochalasin D was reconstituted, caused some effect.

Contrary to the findings of Hinoue et al., (2005), where NC cells underwent apoptosis due to the loss of adhesion to the substrate following treatment with cytochalasin D, the cytochalasin D-treated cells remained attached to the fibronectin substrate and were

viable, as confirmed by a recovery experiment where the effects of cytochalasin D were shown to be reversible upon removal of the treatment. Additionally, the velocity of the cytochalasin D treated cells was significantly reduced, likely because the transformed morphology could not sustain normal migration. Contrary to the broad lamellipodia in normal NC cells (DMEM control) which maintain stable attachments to the substrates for migration (Duband et al., 2020; Heck et al., 2020), it is possible that the thinner projections of the cytochalasin D treated cells were not able to form stable attachments thereby limiting adhesion to the substrate. Also, the stress fibres in the cells which would under normal conditions facilitate cell contraction to move the cell forward (Heck et al., 2020), were possibly disrupted. Hence contraction of the cell could not occur, thus reducing migration.

Despite the altered morphology and reduced velocity, the cytochalasin D treated cells maintained their characteristic responsiveness (to signals such as cell contact), which is a hallmark of NC cells (Duband et al., 2020). The highly responsive nature of NC cells involves signal detection and eliciting responses to ultimately direct and control migration both *in vivo* and *in vitro* (Perris and Perissinotto, 2000; Carmona-Fontaine et al., 2008; Shellard and Mayor, 2016). However, in *in vitro* models, cell contact would become the primary signal directing migration (Carmona-Fontaine et al., 2008; Barriga and Mayor, 2015). Cell-cell contact was observed in both controls, and it was followed by changes in cell projections, suggesting the initiation of contact inhibition locomotion (CIL) and contact attraction (CoA) (Li et al., 2019).

In NC cells the process of CIL involves the cessation of migration, the collapse the existing projections and the repolarization of the actin filaments away from site of contact. New projections are formed in the opposite direction and as a result, cells separate, and the direction of migration is changed (Carmona-Fontaine et al., 2008; Li et al., 2019). The occurrence of CIL was suggested in the DMEM and DMSO control cultures, as some cells which came into contact with each other showed retracted projections and the formation of new projections in the opposite direction (to the site of contact). Although the actin remodelling could not be captured in the live cells as they underwent CIL, the retracted projections and the migration of the cells away from each other, supports the occurrence of CIL.

The process of contact attraction (CoA), which involves the remodelling of actin to form new projections in the direction of contact (Li et al., 2019), was also thought to occur between the migrating cells. In the cells where projections appeared to be outstretched towards a neighbouring cell, CoA may have been occurring. The cell contacts and the resultant effects on the projections was most likely responsible for the migration pathways that were noted in the DMEM control giving rise to chain like migration as well. The other external factors (i.e. signals from the surrounding tissue and chemotaxis) that would guide cell migration *in vivo*, were absent *in vitro*, which likely led to the random migratory paths of putative NC cells in the DMEM control which were observed. However, despite the random migration pathways the signals from cell contact may have allowed somewhat directed migration since cells appeared to migrate in a common direction.

The cell contacts observed are said to be mediated by N-cadherins (Carmona-Fontaine et al., 2008) and the downstream signalling influences actin-regulating proteins, including members of the Rho-GTPase family (Rac1, RhoA, and Cdc42) (Carmona-Fontaine et al., 2008) which regulate actin dynamics in projections, to produce the observed responses (CIL and CoA). Interestingly, in cytochalasin D-treated cells, despite the disrupted arrangement of actin within the cells, the cells retained their ability to receive signals from their environment and the actin within the cell was also able to respond to these signals by forming projections. This finding suggests that despite the inhibition of polymerisation, actin through the complexities involved in its remodelling, was still able to retain its function.

The complexities involved in actin remodelling include proteins of the Rho-GTPase family, actin binding proteins (ABPs) and microtubules. Previous studies have shown the increased activation of proteins RhoA and Rac by cytochalasin D (Ren et al., 1999; Betson et al., 2002). ABPs that facilitate polymerisation (VASP, Arp2/3 complex, formins) and depolymerisation (capping proteins) were also shown to be affected by cytochalasin D (Lambert et al., 2023). The full extent of this effect is still unclear. However, studies have shown that, VASP was observed to be delocalized from the cell membrane. The concentration and location of the Arp2/3 complex appeared unchanged (Scott et al., 2006), and only the elongation function of formins was impaired by cytochalasin D

(Pruyne et al., 2002). ABPs that cap barbed ends of actins i.e. capping proteins, such as those described by Akin et al. (2008) and Funk et al. (2021), as well as Lpd (lamellipodin protein) (Dimchev et al., 2020), which stabilize actin filaments by binding to the barbed ends, are said not to be significantly affected by cytochalasin D (Schafer et al., 1996; Krause et al., 2004). Finally, microtubules, which should not be affected by cytochalasin D, have been shown to influence actin since microtubules anchor F-actin filaments within the cortex and filopodia (Dogterom and Koenderink, 2019).

The effects of cytochalasin D on the Rho-GTPase proteins and ABPs as well as the supportive function of microtubules suggests that actin inhibition in the cytochalasin D treated cells is not complete and that the potential for actin polymerisation remains. Therefore, it is possible that the Rho-GTPase proteins, their accompanying ABPs that facilitate actin polymerisation such as the Arp2/3 complex and the support of microtubules could have allowed the formation of projections. When the cytochalasin D treated cells came into contact with one another, the stimulus (i.e. cell-cell contact) may have triggered the formation of new projections or may have allowed projections to remain on the treated cells. Despite the actin disruption, the role of actin in facilitating responses to cell contacts and its role in the migration of cells was maintained. However, the migration was significantly reduced relative to the control cells. The limited migration of the cytochalasin D treated cells resulted in the simple and linear migratory pathways that were noted.

Although not reported in other studies, it should be noted that in the current study the low concentrations of DMSO (0.1%) appeared to affect the morphology and velocity of NC cells. DMSO is frequently used as a diluent for cytochalasin D, (Hinoue et al., 2005; Nyffeler et al., 2017a and Nyffeler et al., 2017b) *in vitro* and *in vivo* (Fantel et al., 1981), since DMSO has been shown to maintain cell viability. In the current study, DMSO maintained cell viability, but it also appeared to decrease the velocity of migrating cells and induce slight alterations to their morphology. Since the arrangement of actin, which has a major role in cell morphology (Salbreux et al., 2012), appeared unchanged the observed morphological effects may have been the result of an increase in membrane fluidity, which has been shown to be an effect of DMSO (Gurtovenko et al., 2008; Kirsch and Böckmann, 2016). In addition to the altered morphology the increased membrane

fluidity may have also (indirectly) decreased actin polymerisation (Betorz et al., 2023) resulting in the decreased levels of actin that were noted in the DMSO control. Thus, it appears that DMSO may have affected actin in the cells. However, since no obvious morphological affects were noted in the arrangement of actin in the DMSO cells in this study, this affect may have been slight. The slight effect on the actin appears to have maintained random cell migration. However, it may have also resulted in the loss of directional migration as indicated by the randomly scattered endpoints of the cells in the DMSO control. Overall, the effect of DMSO has implications for the results observed in the cytochalasin D treated groups in this study.

Actin and migration were the focus of this study, and the findings point to the inherent nature of NC cells to migrate and remain responsive to external signals (i.e. cell contact) under control and cytochalasin D treated conditions. Additionally, the results highlight the advantage of the highly complex and regulated processes that remodel actin since actin was able to maintain its role in migration and in responding to external stimuli. Factors that regulate actin and hence migration such as Rho-GTPase proteins, actin-binding proteins and microtubules, which all appear to be interrelated, may have compensated the disruption of actin. In the study current, although these factors that regulate actin were not the focus of the study, the findings are suggestive that these factors may have been present. The question thus arises as to how abnormal migration, that leads to disease such as Hirschsprung's, occurs since actin appears to be well compensated for within the cell.

Future research could expand on the findings of this work by focusing on the actin dynamics as well the external signals during migration of NC cells. Isolating the factors (using different substrates or 3D matrix gels, culturing somites or notochord samples with the neural tube, or administering soluble factors to regulate chemotaxis) that affect migration could elucidate the role of each of these factors in guiding migration. Thus, investigations could determine which of these factors could result in the lack of migration or abnormal migration that results in the formation of neurocristopathies. Additionally, actin and microtubule inhibiting agents may also be applied to all the models, where a factor of migration has been isolated, to study the relationship between the factors that influence migration and the cells' cytoskeleton that enables cell migration.

Finally, a model of live cell migration where microtubules and actin can be visualised, to track the actin dynamics when cells are triggered by the different factors that guide migration, would reveal how actin in the NC cells is remodelled during migration, this can be achieved using methods of transfection. Transfection of a protein conjugated to a fluorophore which binds to actin can be conducted on live cells and using live cell imaging actin remodelling can be visualised.

a. Limitations

The manual capture of time-lapse images and the small sample size are both limitations to this study. The manual repositioning of the stage on the microscope introduced slight positional discrepancies, which may have affected the observed cell positions in the time-lapse images. Consequently, the calculated cell velocities, derived from manual tracking measurements, were influenced by these positional variations. This should be considered when interpreting the migratory plots of the live cells. However, this discrepancy was consistent across all the conditions (i.e. DMEM control, DMSO control and the treated group). Additionally, the small sample size means that the behaviour observed may have been specific to the cultures studied.

5. CHAPTER FIVE: Conclusion.

This study investigated the migration, cell-cell contact and actin arrangement in avian trunk NC cells. The study demonstrated the characteristic nature of NC cells *in vitro*, their stellate shape, lamellipodia and filopodia used in migration and demonstrated the cell contacts that directed migration. It also confirmed the crucial role of actin in NC cells in maintaining cell projections and facilitating migration, and revealed that NC cells are capable of responding to their environment even when actin disruption occurs. Further research using models of actin disruption in NC cell migration should be explored and microtubule inhibiting agents may reveal deeper insights into the observed responses (to cell contact) that were noted in the putative NC cells in this *in vitro* model. Findings of this study and future studies will enhance our understanding of cell migration and neurocristopathies resulting from the abnormal migration of NC cells.

References

Absher, M. (1973). Tissue culture: Methods and applications. *Massachusetts, MA: Elsevier Inc. [Google Scholar]*.

Ahlstrom, J.D. and Erickson, C.A. (2009). The neural crest epithelial-mesenchymal transition in 4D: A tail of multiple non-obligatory cellular mechanisms, *Development*, 136 (11), 1801–1812.

Ainsworth, S.J., Stanley, R.L. and Evans, D.J. (2010). Developmental stages of the Japanese quail. *Journal of Anatomy*, *216*(1), 3-15.

Akin, O. and Mullins, R.D. (2008). Capping protein increases the rate of actin-based motility by promoting filament nucleation by the Arp2/3 complex. *Cell*, *133*(5), pp.841-851.

Akiyama, T. and Kawasaki, Y. (2006). Wnt signalling and the actin cytoskeleton. *Oncogene*, *25*(57), 7538-7544.

Alfandari, D., McCusker, C. and Cousin, H. (2009). ADAM function in embryogenesis. In *Seminars in cell & developmental biology,* Academic Press, 20 (2), 153-163.

Ates, G., Vanhaecke, T., Rogiers, V. and Rodrigues, R.M. (2017). Assaying cellular viability using the neutral red uptake assay. *Cell Viability Assays: Methods and Protocols*,19-26.

Bard, J. (1974). Tissue culture, methods and applications. *Cell* 2, 120–121. doi: 10.1016/0092-8674(74)90102-0

Barriga, E.H. and Mayor, R. (2015). Embryonic cell–cell adhesion: a key player in collective neural crest migration. *Current topics in developmental biology*, *112*, 301-323.

Bentley, D. and Toroian-Raymond, A. (1986). Disoriented pathfinding by pioneer neurone growth cones deprived of filopodia by cytochalasin treatment. *Nature*, *323*(6090), 712-715.

Betorz, J., Bokil, G.R., Deshpande, S.M., Kulkarni, S., Araya, D.R., Venturini, C. and Sáez, P. (2023). A computational model for early cell spreading, migration, and competing taxis. *Journal of the Mechanics and Physics of Solids*, *179*, 105390.

Betson, M., Lozano, E., Zhang, J. and Braga, V.M. (2002). Rac activation upon cell-cell contact formation is dependent on signaling from the epidermal growth factor receptor. *Journal of Biological Chemistry*, *277*(40), pp.36962-36969.

Biology Dictionary. Ectoderm. Biology Dictionary. [No date]. Available from: https://biologydictionary.net/ectoderm/

Blanchoin, L., Pollard, T.D. and Mullins, R.D. (2000). Interactions of ADF/cofilin, Arp2/3 complex, capping protein and profilin in remodeling of branched actin filament networks. *Current Biology*, *10*(20), 1273-1282.

Bronner, M.E. and LeDouarin, N.M. (2012). Development and evolution of the neural crest: an overview. *Developmental biology*, *366*(1), 2-9.

Bronner-Fraser, M. (1996). Manipulations of neural crest cells or their migratory pathways. *Methods in cell biology*, *51*, 61-79.

Brown, S.S. and Spudich, J.A. (1981). Mechanism of action of cytochalasin: evidence that it binds to actin filament ends. *The Journal of cell biology*, *88*(3), 487-491.

Cabral-Pacheco, G.A., Garza-Veloz, I., Castruita-De la Rosa, C., Ramirez-Acuña, J.M., Perez-Romero, B.A., Guerrero-Rodriguez, J.F., Martinez-Avila, N. and Martinez-Fierro, M.L. (2020). The roles of matrix metalloproteinases and their inhibitors in human diseases. *International journal of molecular sciences*, *21*(24), 9739.

Carmona-Fontaine, C., Matthews, H.K., Kuriyama, S., Moreno, M., Dunn, G.A., Parsons, M., Stern, C.D. and Mayor, R. (2008). Contact inhibition of locomotion in vivo controls neural crest directional migration. *Nature*, *456*(7224), 957-961.

Chatzi, D., Kyriakoudi, S.A., Dermitzakis, I., Manthou, M.E., Meditskou, S. and Theotokis, P. (2024). Clinical and Genetic Correlation in Neurocristopathies: Bridging a Precision Medicine Gap. *Journal of Clinical Medicine*, *13*(8), 2223.

Cooper, G.M. (2000). Structure and organization of actin filaments. *The cell: a molecular approach*, *2*.

Copp, A.J. and Greene, N.D. (2013). Neural tube defects—disorders of neurulation and related embryonic processes. *Wiley Interdisciplinary Reviews: Developmental Biology*, *2*(2), 213-227.

Cummings, B.S. and Schnellmann, R.G. (2004). Measurement of cell death in mammalian cells. *Current protocols in pharmacology*, *25*(1), 12-8.

de Bellard, M.E. and Bronner-Fraser, M. (2005). Neural crest migration methods in the chicken embryo. *Cell Migration: Developmental Methods and Protocols*, 247-267.

Delloye-Bourgeois, C. and Castellani, V. (2019). Hijacking of embryonic programs by neural crest-derived neuroblastoma: from physiological migration to metastatic dissemination. *Frontiers in molecular neuroscience*, *12*, 52.

Deroubaix, A., Busakwe, K. and Kramer, B. (2021). Tracking the movement of individual avian neural crest cells in vitro. *In Vitro Cellular & Developmental Biology-Animal*, *57*, 53-65.

Derycke, L.D. and Bracke, M.E. (2004). N-cadherin in the spotlight of cell-cell adhesion, differentiation, embryogenesis, invasion and signalling. *International Journal of Developmental Biology*, *48*(5-6), 463-476.

Dickinson, M.E., Murray, B.A., Waters, C.W., Haynes, S.M. and Longmuir, K.J. (2002). Using electroporation and lipid-mediated transfection of GFP-expressing plasmids to label embryonic avian cells for vital confocal and two-photon microscopy. *Differentiation*, *70*(4-5), 172-180.

Dimchev, G., Amiri, B., Humphries, A.C., Schaks, M., Dimchev, V., Stradal, T.E., Faix, J., Krause, M., Way, M., Falcke, M. and Rottner, K. (2020). Lamellipodin tunes cell migration by stabilizing protrusions and promoting adhesion formation. Journal of cell science, 133(7), 239020.

Dogterom, M. and Koenderink, G.H. (2019). Actin–microtubule crosstalk in cell biology. *Nature reviews Molecular cell biology*, *20*(1), 38-54.

Duband, J.L., Nekooie-Marnany, N. and Dufour, S. (2020). Establishing primary cultures of trunk neural crest cells. *Current Protocols in Cell Biology*, *88*(1), 109.

Dupin, E., Creuzet, S. and Le Douarin, N.M. (2006). The contribution of the neural crest to the vertebrate body. *Neural crest induction and differentiation*, 96-119.

El-Sharkawey, A. (2016). Calculate the Corrected Total Cell Fluorescence (CTCF). *Calculate the Corrected Total Cell Fluorescence (CTCF)*.

Fantel, A.G., Greenaway, J.C., Shepard, T.H., Juchau, M.R. and Selleck, S.B. (1981). The teratogenicity of cytochalasin D and its inhibition by drug metabolism. *Teratology*, *23*(2), 223-231.

Funk, J., Merino, F., Schaks, M., Rottner, K., Raunser, S. and Bieling, P. (2021). A barbed end interference mechanism reveals how capping protein promotes nucleation in branched actin networks. Nature communications, 12(1), 5329.

Galindo, L.T., Mundim, M.T., Pinto, A.S., Chiarantin, G.M., Almeida, M.E., Lamers, M.L., Horwitz, A.R., Santos, M.F. and Porcionatto, M. (2018). Chondroitin sulfate impairs neural stem cell migration through ROCK activation. *Molecular neurobiology*, *55*(4), 3185-3195.

Gammill, L.S. and Roffers-Agarwal, J. (2010). Division of labor during trunk neural crest development. *Developmental biology*, *344*(2), 555-565.

Gilbert, S.F. (2000). An introduction to early developmental processes. In *Developmental Biology. 6th edition*. Sinauer Associates.

Giovannone, D., Ortega, B., Reyes, M., El-Ghali, N., Rabadi, M., Sao, S. and de Bellard, M.E. (2015). Chicken trunk neural crest migration visualized with HNK1. Acta histochemica, 117(3), 255-266.

Giovannone, D., Reyes, M., Reyes, R., Correa, L., Martinez, D., Ra, H., Gomez, G., Kaiser, J., Ma, L., Stein, M.P. and De Bellard, M.E. (2012). Slits affect the timely migration of neural crest cells via Robo receptor. *Developmental dynamics*, *241*(8), 1274-1288.

Goddette, D.W. and Frieden, C. (1986). Actin polymerization. The mechanism of action of cytochalasin D. *Journal of Biological Chemistry*, *261*(34), 15974-15980.

Gurtovenko, A.A., Onike, O.I. and Anwar, J. (2008). Chemically induced phospholipid translocation across biological membranes. Langmuir, 24(17), 9656-9660.

Haendel, M.A., Bollinger, K.E. and Baas, P.W. (1996). Cytoskeletal changes during neurogenesis in cultures of avian neural crest cells. *Journal of neurocytology*, *25*, 289-301.

Hall, B.K. (2008). *The neural crest and neural crest cells in vertebrate development and evolution*, 11. Springer Science & Business Media.

Hamburger, V. and Hamilton, H.L. (1951). A series of normal stages in the development of the chick embryo. Journal of morphology, 88(1), 49-92.

Harburger, D.S. and Calderwood, D.A. (2009). Integrin signalling at a glance. *Journal of cell science*, *122*(2), 159-163.

Heck, T., Vargas, D.A., Smeets, B., Ramon, H., Van Liedekerke, P. and Van Oosterwyck, H. (2020). The role of actin protrusion dynamics in cell migration through a degradable viscoelastic extracellular matrix: Insights from a computational model. *PLoS computational biology*, *16*(1), p.e1007250.

Heckman, C.A. and Plummer III, H.K. (2013). Filopodia as sensors. *Cellular signalling*, *25*(11), 2298-2311.

Higgs, H.N. (2013). Actin Assembly/Disassembly.

Hinoue, A., Takigawa, T., Miura, T., Nishimura, Y., Suzuki, S. and Shiota, K. (2005). Disruption of actin cytoskeleton and anchorage-dependent cell spreading induces apoptotic death of mouse neural crest cells cultured in vitro. The Anatomical Record Part A: Discoveries in Molecular, Cellular, and Evolutionary Biology: An Official Publication of the American Association of Anatomists, 282(2), 130-137.

Höltje, M., Just, I. and Ahnert-Hilger, G. (2011). Clostridial C3 proteins: recent approaches to improve neuronal growth and regeneration. *Annals of Anatomy-Anatomischer Anzeiger*, *193*(4), 314-320.

Hovland, A.S., Rothstein, M. and Simoes-Costa, M. (2020). Network architecture and regulatory logic in neural crest development. *Wiley Interdisciplinary Reviews: Systems Biology and Medicine*, *12*(2), pp.e1468.

Juarez, M., Reyes, M., Coleman, T., Rotenstein, L., Sao, S., Martinez, D., ... and De Bellard, M. E. (2013). Characterization of the trunk neural crest in the bamboo shark, Chiloscyllium punctatum. *Journal of Comparative Neurology*, *521*(14), 3303-3320

Kalcheim, C. (2015). Epithelial–mesenchymal transitions during neural crest and somite development. *Journal of clinical medicine*, *5*(1), 1.

Kerosuo, L. and Bronner-Fraser, M. (2012). What is bad in cancer is good in the embryo: importance of EMT in neural crest development. In *Seminars in cell & developmental biology*. Academic Press, 23(3), 320-332.

Kerosuo, L., and Bronner, M. E. (2014). Biphasic influence of Miz1 on neural crest development by regulating cell survival and apical adhesion complex formation in the developing neural tube. *Molecular biology of the cell*, *25*(3), 347-355.

Kirsch, S.A. and Böckmann, R.A. (2016). Membrane pore formation in atomistic and coarse-grained simulations. Biochimica et Biophysica Acta (BBA)-Biomembranes, 1858(10), 2266-2277.

Krause, M. and Gautreau, A. (2014). Steering cell migration: lamellipodium dynamics and the regulation of directional persistence. *Nature reviews Molecular cell biology*, *15*(9), 577-590.

Krause, M., Leslie, J.D., Stewart, M., Lafuente, E.M., Valderrama, F., Jagannathan, R., Strasser, G.A., Rubinson, D.A., Liu, H., Way, M. and Yaffe, M.B. (2004). Lamellipodin, an Ena/VASP ligand, is implicated in the regulation of lamellipodial dynamics. Developmental cell, 7(4), 571-583.

Kuriyama, S. and Mayor, R. (2008). Molecular analysis of neural crest migration. *Philosophical Transactions of the Royal Society B: Biological Sciences*, *363*(1495), 1349-1362.

Lambert, C., Schmidt, K., Karger, M., Stadler, M., Stradal, T.E. and Rottner, K. (2023). Cytochalasans and their impact on actin filament remodeling. *Biomolecules*, *13*(8), 1247.

Le Bras, G.F., Taubenslag, K.J. and Andl, C.D. (2012). The regulation of cell-cell adhesion during epithelial-mesenchymal transition, motility and tumor progression. *Cell adhesion & migration*, *6*(4), 365-373.

Le Douarin, N.M. and Dupin, E. (2018). The “beginnings” of the neural crest. *Developmental biology*, *444*, pp.S3-S13.

Leathers, T.A. and Rogers, C.D. (2022). Time to go: neural crest cell epithelial-to-mesenchymal transition. *Development*, *149*(15), p.dev200712.

Li, Y., Vieceli, F.M., Gonzalez, W.G., Li, A., Tang, W., Lois, C. and Bronner, M.E. (2019). In vivo quantitative imaging provides insights into trunk neural crest migration. *Cell reports*, *26*(6), 1489-1500.

Malagon, S.G.G., Dobson, L., Muñoz, A.M.L., Dawson, M., Barrell, W., Marangos, P., Krause, M. and Liu, K.J. (2019). Dissection, culture and analysis of primary cranial neural crest cells from mouse for the study of neural crest cell delamination and migration. *Journal of visualized experiments: JoVE*, (152), 10-3791.

Marsh, L. and Letourneau, P.C. (1984). Growth of neurites without filopodial or lamellipodial activity in the presence of cytochalasin B. *The Journal of cell biology*, *99*(6), 2041-2047.

Martik, M.L. and Bronner, M.E. (2021). Riding the crest to get a head: neural crest evolution in vertebrates. *Nature Reviews Neuroscience*, *22*(10), 616-626.

Martucciello, G., Ceccherini, I., Lerone, M. and Jasonni, V. (2000). Special basic science review: Pathogenesis of Hirschsprung's disease. *Journal of pediatric surgery*, *35*(7), 1017-1025.

Mayanil, C.S. (2013). Transcriptional and epigenetic regulation of neural crest induction during neurulation. *Developmental neuroscience*, *35*(5), 361-372.

Monier-Gavelle, F. and Duband, J.L. (1995). Control of N-cadherin-mediated intercellular adhesion in migrating neural crest cells in vitro. *Journal of cell science*, *108*(12), 3839-3853.

Nyffeler, J., Dolde, X., Krebs, A., Pinto-Gil, K., Pastor, M., Behl, M., Waldmann, T. and Leist, M. (2017a). Combination of multiple neural crest migration assays to identify environmental toxicants from a proof-of-concept chemical library. *Archives of toxicology*, *91*, 3613-3632.

Nyffeler, J., Karreman, C., Leisner, H., Kim, Y.J., Lee, G., Waldmann, T. and Leist, M. (2017b). Design of a high-throughput human neural crest cell migration assay to indicate potential developmental toxicants. Alternatives to Animal Experimentation, 34(1), 75-94.

Park, K.S. and Gumbiner, B.M. (2010). Cadherin 6B induces BMP signaling and de-epithelialization during the epithelial mesenchymal transition of the neural crest. *Development*, *137*(16), 2691-2701.

Parsons, J.T., Horwitz, A.R. and Schwartz, M.A. (2010). Cell adhesion: integrating cytoskeletal dynamics and cellular tension. *Nature reviews Molecular cell biology*, *11*(9), 633-643.

Pásti, G. and Labouesse, M. (2018). Epithelial junctions, cytoskeleton, and polarity. *WormBook: The Online Review of C. elegans Biology [Internet]*.

Paul, J. (1965). Cell and tissue culture.

Perris, R. (1997). The extracellular matrix in neural crest-cell migration. *Trends in neurosciences*, *20*(1), 23-31.

Perris, R. and Johansson, S. (1990). Inhibition of neural crest cell migration by aggregating chondroitin sulfate proteoglycans is mediated by their hyaluronan-binding region. *Developmental biology*, *137*(1), 1-12.

Perris, R. and Perissinotto, D. (2000). Role of the extracellular matrix during neural crest cell migration. *Mechanisms of development*, *95*(1-2), 3-21.

Pilon, N. (2021). Treatment and prevention of neurocristopathies. *Trends in molecular medicine*, *27*(5), 451-468.

Pollard, T.D. and Cooper, J.A. (2009). Actin, a central player in cell shape and movement. *science*, *326*(5957), 1208-1212.

Pruyne, D., Evangelista, M., Yang, C., Bi, E., Zigmond, S., Bretscher, A. and Boone, C. (2002). Role of formins in actin assembly: nucleation and barbed-end association. *Science*, *297*(5581), 612-615.

Ren, X.D., Kiosses, W.B. and Schwartz, M.A. (1999). Regulation of the small GTP-binding protein Rho by cell adhesion and the cytoskeleton. *The EMBO journal*.

Ribatti, D. and Annese, T. (2023). Chick embryo in experimental embryology and more. *Pathology-Research and Practice*, *245*, p.154478.

Ridley, A.J. (2001). Rho GTPases and cell migration. *Journal of cell science*, *114*(15), 2713-2722.

Rodrigues-Da-Silva, M.A., de Espindola da Silveira, G., Taufer, C.R. and Calloni, G.W. (2022). The mesenchymal potential of trunk neural crest cells. *The International Journal of Developmental Biology*, *66*(4-5-6), 317-331.

Rogers, C. D., Phillips, J. L., and Bronner, M. E. (2013). Elk3 is essential for the progression from progenitor to definitive neural crest cell. *Developmental biology*, *374*(2), 255-263.

Rovasio, R.A., Delouvee, A., Yamada, K.M., Timpl, R. and Thiery, J.P. (1983). Neural crest cell migration: requirements for exogenous fibronectin and high cell density. *The Journal of cell biology*, *96*(2), 462-473.

Salbreux, G., Charras, G., and Paluch, E. (2012). Actin cortex mechanics and cellular morphogenesis. *Trends in cell biology*, *22*(10), 536-545.

Sato, T.S., Handa, A., Priya, S., Watal, P., Becker, R.M. and Sato, Y. (2019). Neurocristopathies: Enigmatic appearances of neural crest cell–derived abnormalities. *Radiographics*, *39*(7), 2085-2102.

Scarpa, E., and Mayor, R. (2016). Collective cell migration in development. *Journal of cell Biology*, *212*(2), 143-155.

Schafer, D.A., Jennings, P.B. and Cooper, J.A.(1996). Dynamics of capping protein and actin assembly in vitro: uncapping barbed ends by polyphosphoinositides. *The Journal of cell biology*, *135*(1), pp.169-179.

Schaks, M., Giannone, G. and Rottner, K. (2019). Actin dynamics in cell migration. *Essays in biochemistry*, *63*(5), 483-495.

Schille, C. and Schambony, A. (2017). Signaling pathways and tissue interactions in neural plate border formation. *Neurogenesis*, *4*(1), p.e1292783.

Schliwa, M. (1982). Action of cytochalasin D on cytoskeletal networks. *The Journal of cell biology*, *92*(1), 79-91.

Schoenwolf, G.C. and Smith, J.L. (1990). Mechanisms of neurulation: traditional viewpoint and recent advances. *Development*, *109*(2), 243-270.

Scott, J.A., Shewan, A.M., den Elzen, N.R., Loureiro, J.J., Gertler, F.B. and Yap, A.S. (2006). Ena/VASP proteins can regulate distinct modes of actin organization at cadherin-adhesive contacts. *Molecular biology of the cell*, *17*(3), 1085-1095.

Sela-Donenfeld, D. and Kalcheim, C. (2002). Localized BMP4–noggin interactions generate the dynamic patterning of noggin expression in somites. *Developmental biology*, *246*(2), 311-328.

Selleck, M.A. and Bronner-Fraser, M. (1996). The genesis of avian neural crest cells: a classic embryonic induction. *Proceedings of the National Academy of Sciences*, *93*(18), 9352-9357.

Selleck, M.A., Scherson, T.Y. and Bronner-Fraser, M. (1993). Origins of neural crest cell diversity. *Developmental biology*, *159*(1), 1-11.

Serbedzija, G.N., Burgan, S., Fraser, S.E. and Bronner-Fraser, M. (1991). Vital dye labelling demonstrates a sacral neural crest contribution to the enteric nervous system of chick and mouse embryos. *Development*, *111*(4), 857-866.

Shellard, A. and Mayor, R. (2016). Chemotaxis during neural crest migration. In *Seminars in cell & developmental biology*, Academic Press, 55, 111-118.

Shi, L., Li, J.R., Shih, Y.P., Lo, S.H. and Liu, G.Y. (2012). Nanogratings of fibronectin provide an effective biochemical cue for regulating focal adhesion and cellular structure. *Nano Research*, *5*, 565-575.

Singleton Escofet, R. (2013). *Role of CXCR4 dynamics and activity in neural crest migration* (Doctoral dissertation, UCL (University College London)).

Song, H.P., Li, R.L., Zhou, C., Cai, X. and Huang, H.Y. (2015). Atractylodes macrocephala Koidz stimulates intestinal epithelial cell migration through a polyamine dependent mechanism. Journal of Ethnopharmacology, 159, 23-35.

Steventon, B., Araya, C., Linker, C., Kuriyama, S. and Mayor, R. (2009). Differential requirements of BMP and Wnt signalling during gastrulation and neurulation define two steps in neural crest induction. *Development*, 136 (5), 771–779.

Stolfi, A., Ryan, K., Meinertzhagen, I.A. and Christiaen, L. (2015). Migratory neuronal progenitors arise from the neural plate borders in tunicates. *Nature*, *527*(7578), 371-374.

Stuhlmiller, T.J. and García-Castro, M.I. (2012). Current perspectives of the signaling pathways directing neural crest induction. *Cellular and Molecular Life Sciences*, *69*, 3715-3737.

Szabó, A. and Mayor, R. (2018). Mechanisms of neural crest migration. *Annual Review of Genetics*, *52*(1), 43-63.

Tang, W., Li, Y., Li, A., and Bronner, M. E. (2021). Clonal analysis and dynamic imaging identify multipotency of individual Gallus gallus caudal hindbrain neural crest cells toward cardiac and enteric fates. *Nature Communications*, *12*(1), 1894.

Tang, W., Tang, J., Qin, J., Geng, Q., Zhou, Z., Li, B., Zhang, J., Chen, H., Xia, Y. and Wang, X. (2013). Involvement of down-regulated E2F3 in Hirschsprung's disease. *Journal of Pediatric Surgery*, *48*(4), 813-817.

Tanimura, S. and Takeda, K. (2017). ERK signalling as a regulator of cell motility. *The Journal of Biochemistry*, *162*(3), 145-154.

Teillet, M.A., Ziller, C. and Le Douarin, N.M. (2009). Quail—Chick Chimeras. *Molecular Embryology: Methods and Protocols*, 337-350.

Theveneau, E. and Mayor, R. (2012). Neural crest migration: interplay between chemorepellents, chemoattractants, contact inhibition, epithelial–mesenchymal transition, and collective cell migration. *Wiley Interdisciplinary Reviews: Developmental Biology*, *1*(3), 435-445.

Tschumperlin, D.J. (2013). Fibroblasts and the ground they walk on. *Physiology*, *28*(6), 380-390.

Van Straaten, H.W., Janssen, H.C., Peeters, M.C., Copp, A.J. and Hekking, J.W. (1996). Neural tube closure in the chick embryo is multiphasic. *Developmental dynamics*, *207*(3), 309-318.

Leathers Vega-Lopez, G.A., Cerrizuela, S. and Aybar, M.J. (2017). Trunk neural crest cells: formation, migration and beyond. *Int. J. Dev. Biol*, *61*(1-2), 5-15.

Vinzenz, M., Nemethova, M., Schur, F., Mueller, J., Narita, A., Urban, E., Winkler, C., Schmeiser, C., Koestler, S.A., Rottner, K. and Resch, G.P. (2012). Actin branching in the initiation and maintenance of lamellipodia. *Journal of cell science*, *125*(11), 2775-2785.

Witke, W. (2004). The role of profilin complexes in cell motility and other cellular processes. *Trends in cell biology*, *14*(8), 461-469.

Wood, W. and Martin, P. (2002). Structures in focus—filopodia. *The international journal of biochemistry & cell biology*, *34*(7), 26-730.

Xue, G. and Hemmings, B.A. (2013). PKB/Akt–dependent regulation of cell motility. *Journal of the National Cancer Institute*, *105*(6), 393-404.

York, J.R. and McCauley, D.W. (2020). The origin and evolution of vertebrate neural crest cells. *Open biology*, *10*(1), p.190285.0

Appendix

PLAGIARISM DECLARATION TO BE SIGNED BY ALL HIGHER DEGREE STUDENTS

SENATE PLAGIARISM POLICY: **APPENDIX ONE**

I MARIAM BIBI SAHIB _____(Student number: ____1892562_____) am a

student registered for the degree of Master of Science Medicine (by research)_____in the

academic year 2025.

I hereby declare the following:

- I am aware that plagiarism (the use of someone else's work without their permission and/or without acknowledging the original source) is wrong.
- I confirm that the work submitted for assessment for the above degree is my own unaided work except where I have explicitly indicated otherwise.
- I have followed the required conventions in referencing the thoughts and ideas of others.
- I understand that the University of the Witwatersrand may take disciplinary action against me if there is a belief that this is not my own unaided work or that I have failed to acknowledge the source of the ideas or words in my writing.
- I have included as an appendix a report from "Turnitin" (or other approved plagiarism detection) software indicating the level of plagiarism in my research document.

Signature: : Mariam Bibi Sahib _____ Date: 09/02/2025_____

APPENDIX 2- Ethical clearance

STRICTLY CONFIDENTIAL

CLEARANCE CERTIFICATE NUMBER: AREC23-03-

016O APPLICANT: Ms M Sahib

School: School of Anatomical Sciences; Department: N/A; Location: School of Anatomical Sciences

PROJECT TITLE: An analysis of avian *(Coturnix japonica)* trunk neural crest cell migration *in vitro:* Investigating the role and arrangement of actin in migrating neural crest cells.

Category: O ; Species and Numbers involved: 12X fertile eggs, Male or Female, *Gallus gallus domesticus* and 84X fertile eggs, Male or Female, *Coturnix japonica*

Approval is hereby given for the use of animals for the research project named above and described in the application reviewed by a quorate meeting of the AREC held on 30 May 2023. This approval remains valid until 4 Jul 2025 and is conditional to the following (if blank there are no special conditions):

Condition 1	Condition 2	Condition 3	Condition 4

All material changes to the approved research must be reported to the AREC before they are implemented. Failure to do so will invalidate this clearance certificate.

An annual progress report must be provided to the AREC.

The use of these animals is subject to AREC guidelines on the use and care of laboratory animals, is limited to the procedures described in the application and is subject to additional conditions listed below:

I, the Chair of the AREC (or my designated representative) am satisfied that the proposed research is ethical as judged by local law, international standards and University policy.

a. Signed: _____ _____ Date: _____05/07/2023_____

(Chairperson of the AREC)

I am satisfied that the persons listed in this application are competent to perform the procedures described in the application, in the context of Section 23 (1) (c) of the veterinary and Para-veterinary Professions Act (19 of 1982).

b. Signed: _ _____ Date: 5/07/2023_____

(Registered Veterinarian)

Appendix 3 – Equipment list and solutions for the neural crest assay

1. Equipment list for setting up neural crest assays:

Glassware:

- Egg dishes
- Oval dishes
- Glass cavity dish with lid
- 100ml beaker
- 250ml beaker
- 1l beaker
- Coarse glass pipettes
- Fine glass pipettes
- Coplin jars with lids
- Nunc glass bottom dishes (Thermo-Fisher, catalog no. 150682)

Instruments:

Blunt instruments (immersed in 90% ethanol) –

- spoon
- blunt forceps
- straight scissor

Fine instruments (immersed in 70% ethanol)-

- eye knife
- watchmaker's forceps
- indectomy scissors
- insect pins

Other materials:

- Sterile cotton wool
- Rubber teats
- Sponges
- Black wax dishes
- 20ml syringes
- Alcohol burner
- Stereomicroscope

2. Solutions:

- Chick Ringers' solution
- Tyrode solution (Mg^{2+} and Ca^{2+} free solution)
- PBS (phosphate buffer solution)

Preparing solutions:

Chick Ringer's solution: in 1000ml of distilled water

- 8.5g NaCl
- 0.42g KCl
- 0.25g $CaCl_2$
- 100µl pen-strep (penicillin-streptomycin)

Tyrode's solution (Magnesium and calcium free solution): solution is part in 3 parts labelled A,B and C. prior to experiment solutions are added to each together and 100µl of pen-strep

Tyrode's solution A: in 500ml of distilled water

- 2.0 g NaCl
- 0.05 g KCl
- 0.012 g NaH_2PO_4

Tyrode's solution B: in 480ml of distilled water

- 0.025 g $NaHCO_3$

Tyrode's solution C: in 20ml of distilled water

- 1 g glucose

To prepare Tyrode's solution, solution B was added to solution A, thereafter solution C was filtered into solution A and 100 µl of pen step was added to the final solution.

3. Collagenase:

To prepare the collagenase:

0.0025g of collagenase Type A (COLLA-RO-SIGMA) was measured in a sterile bijou bottle and 6ml of complete/final Tyrode's (Magnesium and calcium free) solution was added to the powder. The collagenase solution was refrigerated before and in between use during the experiment.

Appendix 4- Chick embryo extract equipment list and preparation

Glassware:

- Coplin jars with lids (2x)
- Egg dishes (12x)
- 250ml beakers (2x)
- Glass rods
- Glass bijou bottles

Other:

- Sterile cotton wool
- Sponges

- 50ml tubes
- 20ml syringes
- Graduated centrifuge tubes.
- Sterile pipette tips
- Alcohol burner
- 70% ethanol and 90% ethanol

Blunt instruments:

- spoon
- blunt forceps
- straight scissor

Solutions:

- Ringers' solution as prepared in Appendix 3.
- Distilled water

Method

Two dozen fertile chick eggs were placed in a humidified incubator at 37°C nine days before the chick embryo extract was made.

The outer surface of the egg was wiped with 70% ethanol and its contents was emptied into an egg dish that contained sterile chick Ringer's solution (Appendix 3). Following this, the embryo was separated from the yolk sac and decapitated. The head of the embryo was completely separated from the body. Excess yolk was removed with chick Ringer's solution. Four embryos were prepared in this way. The embryos were put in a 50 ml tube and were pulverized using a glass rod. The embryos were then transferred into a 20 ml sterile syringe and expressed from the syringe. This solute was collected in a sterile graduated centrifuge tube. Five millilitres of Chick ringer's solution with 5ml of the chick embryo extract was poured into a clean centrifuge tube. This mixture was left to stand in the laminar floor for an hour at room temperature before being centrifuged (Hettich Zentrifugen, Rotofix 32A, Germany) for 20 minutes at 2000g. The supernatant was poured into sterile 5ml bijou bottles, labelled with the date and stored at -20°C until use.

Appendix 5- Determining the cell viability for cytochalasin D optimisation

1. Neutral red assay

Method

Neutral red assays are typically used to determine the viability of cells *in vitro*. The neutral red assay was tested as a possible method to determine the cytotoxic effect of cytochalasin D on quail neural crest cultures. Cell viability is dependent on the uptake of the dye into the lysosome of viable cells after the cells are treated. Once the excess dye is removed by washing, the dye that is taken up by the lysosomes of living cells is extracted using desorb (consisting 1% of acetic acid and 50% ethanol) (Ates et al., 2017). However, this process of precipitation using desorb may be cytotoxic to the cells.

When considering the assay to determine viability, the potential cytotoxicity of desorb was considered and the assay was adapted to neural crest cultures (tissue cultures) that don't reach the same number of cells or percentages of confluency that other cell cultures reach. Hence the volume of desorb was adjusted and it was tested in wells where fewer cells were seeded. Using MCF7 cells (breast adenocarcinoma cells), cells were seeded into a 96 well microplate at a density of 10,000 cells (recommended seeding density for a 96 well plate), 100 cells and 50 cells and the neutral red assay was conducted on untreated cells.

In a sterile laminar flow hood, MCF-7 cells were trypsinised and the cells were seeded in a 96 well plate. The cells were washed twice with 100µl of PBS, thereafter 100µl of the neutral red dye was added to each well. The neutral red dye stock solution is diluted in complete media. The cells were incubated at 37°C and 5% CO_2 in the dye solution for 3 hours. After 2 and a half hours of incubation the cells were imaged. Thereafter the dye was removed from the cells and the cells were washed twice with 100µl PBS. After washing 100 µl (recommended volume) of desorb was added to 24 of the wells and the adjusted volumes of desorb i.e., 50 µl and 25 µl were added to 24 wells each. Each volume of desorb (100 µl, 50 µl and 25 µl) was added to wells that were seeded with 10000, 100 and 50 cells (Fig. 5.1).

The plate containing the cells was placed on an orbital shaker set at 1000rpm for 60 minutes and the absorbance was measured using the Glomax spectrophotometer at 560nm and a reference of 600nm.

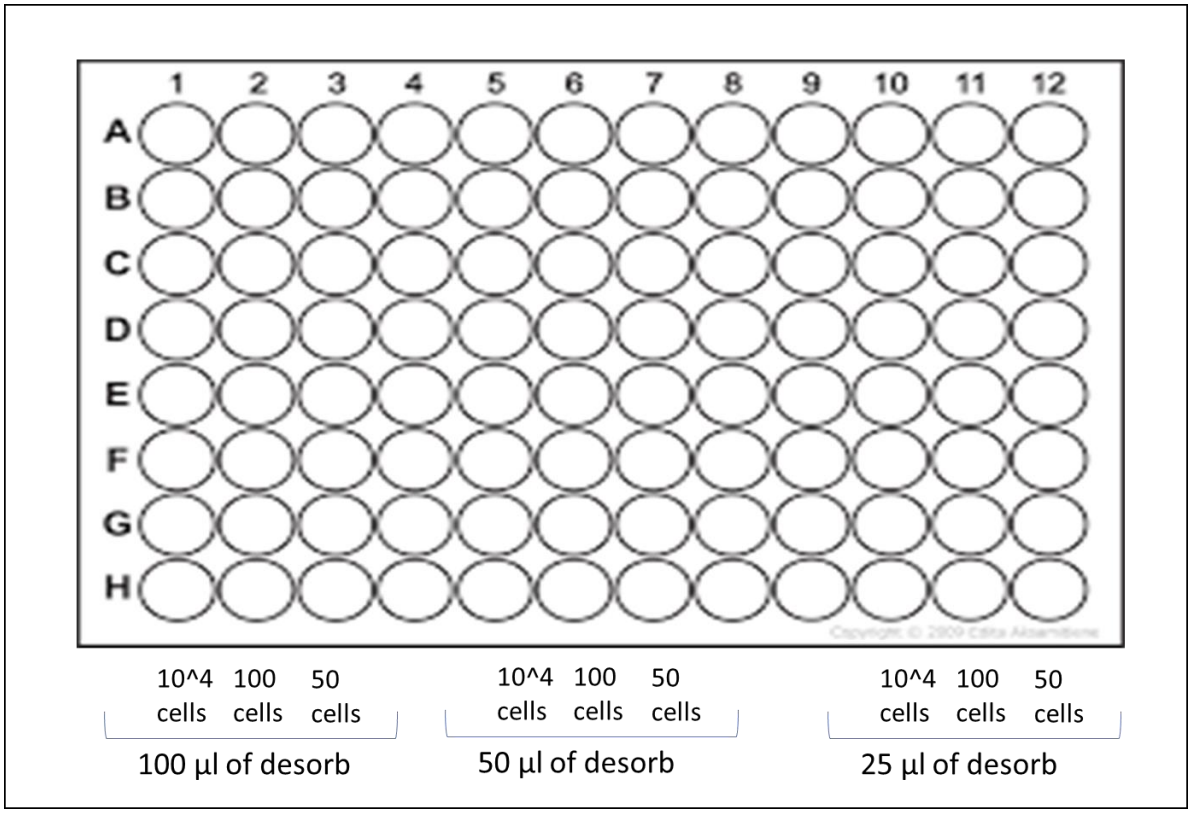


Figure 5.1 Diagram showing the plate layout for the neural red assay conducted on MCF7 cells. Three different volumes of desorb were tested on three different cell amounts. In the first three rows, 10 000, 100 and 50 cells/100 µl were seeded respectively and 100 µl of desorb was added to the wells in these rows. In the next three rows cells were seeded at the same amounts (10000, 100 and 50) in that order and 50 µl of desorb was added to each row. In the last three rows of cells were seeded at the same amounts (10000, 100 and 50) in that order and 25 µl of desorb was added to these rows.

Results.

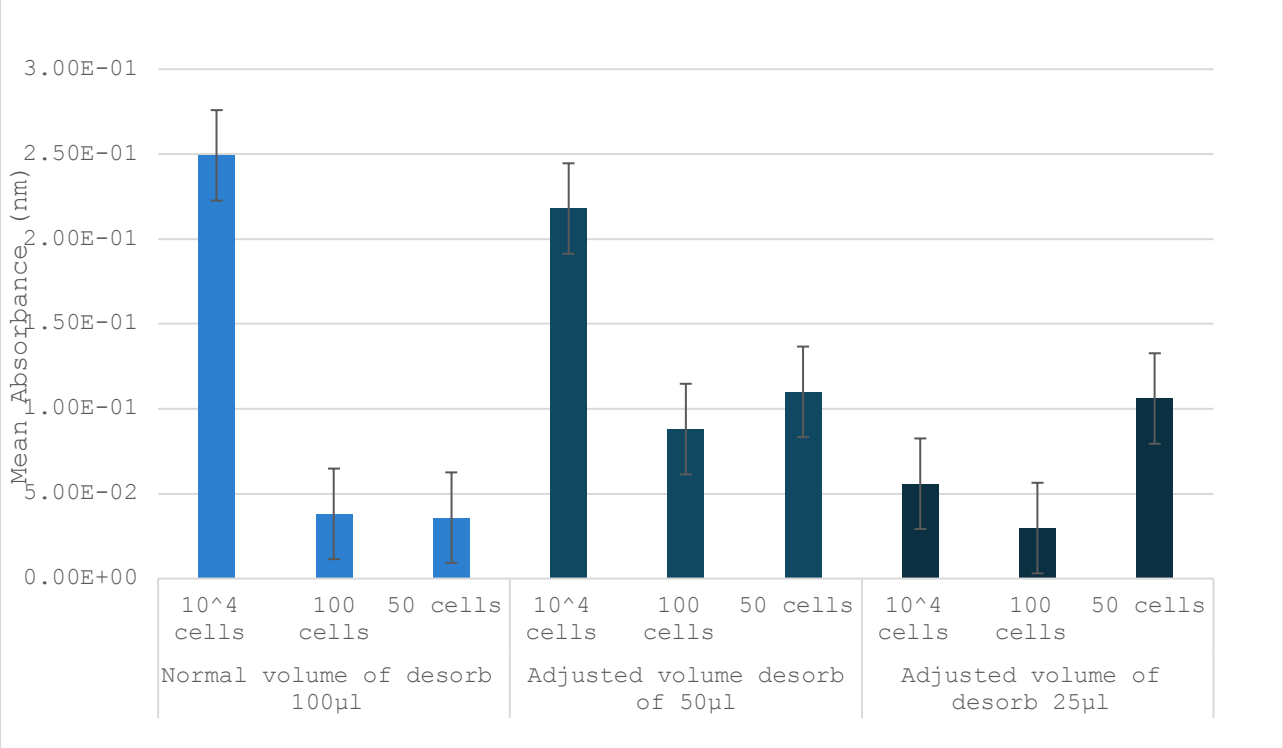


Figure 5.2 Neutral red dye absorbance measurements grouped by the volumes of desorb that were tested. Three volumes of desorb were tested on different cell amounts (x-axis) and the absorbance (y-axis) was measured for each.

The absorbance was measured, and a measurement was recorded for all the wells that were seeded with cells and for the reference wells (reference wells only contained media). At the normal/recommended volume of desorb (100µl) the mean absorbance of the wells with more cells (10^4 cells) was higher than that of the wells with fewer cells (100 and 50 cells), as expected, since there are more cells. At the adjusted volume of 50µl of desorb the wells with 10^4 cells showed a higher mean absorbance overall, but mean absorbance of wells with 100 cells was less than mean absorbance of wells with 50 cells. Finally, at the adjusted volume of 25µl of desorb the wells with 50 cells showed a higher mean absorbance than the wells with more cells (10^4 and 100 cells).

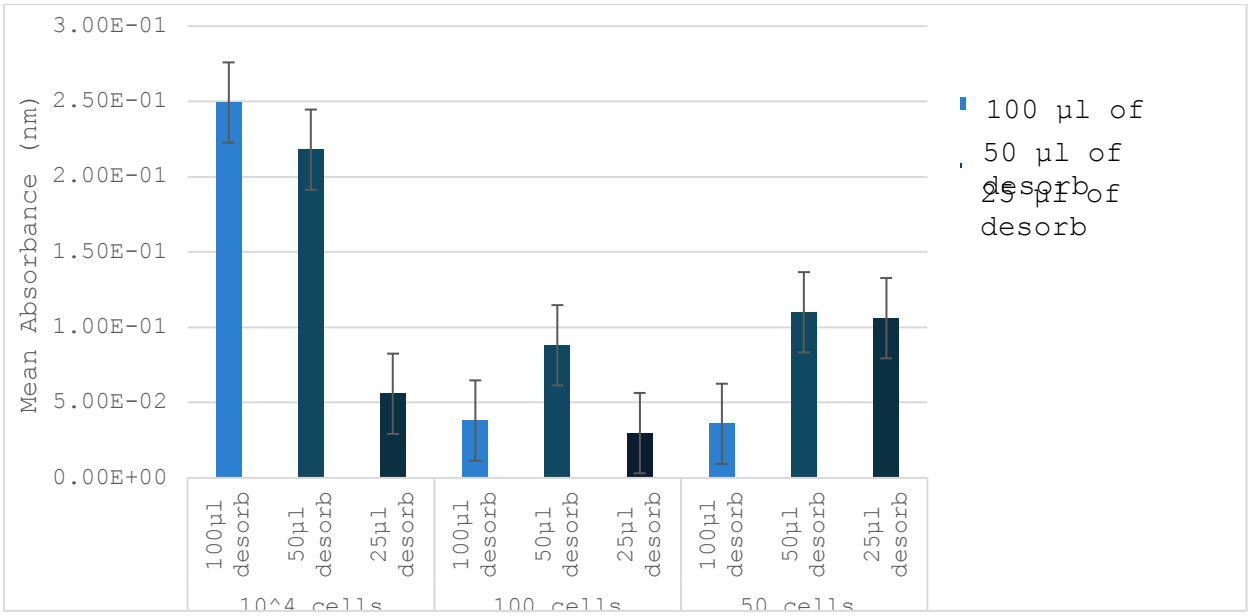


Figure 5.3 The neutral red absorbance (y-axis) at different volumes of desorb (x-axis), grouped by the number of cells that was seeded. The volume of desorb and the resultant absorbance can be seen comparatively for the different cell numbers.

It is noted that in the wells seeded with 10^4 cells, the mean absorbance decreased as the volume of desorb decreased. While for wells with 100 cells the highest mean absorbance was recorded at the adjusted volume of 50µl of desorb. Similarly in wells with 50 cells the highest mean absorbance was recorded at the adjusted volume of 50µl of desorb.

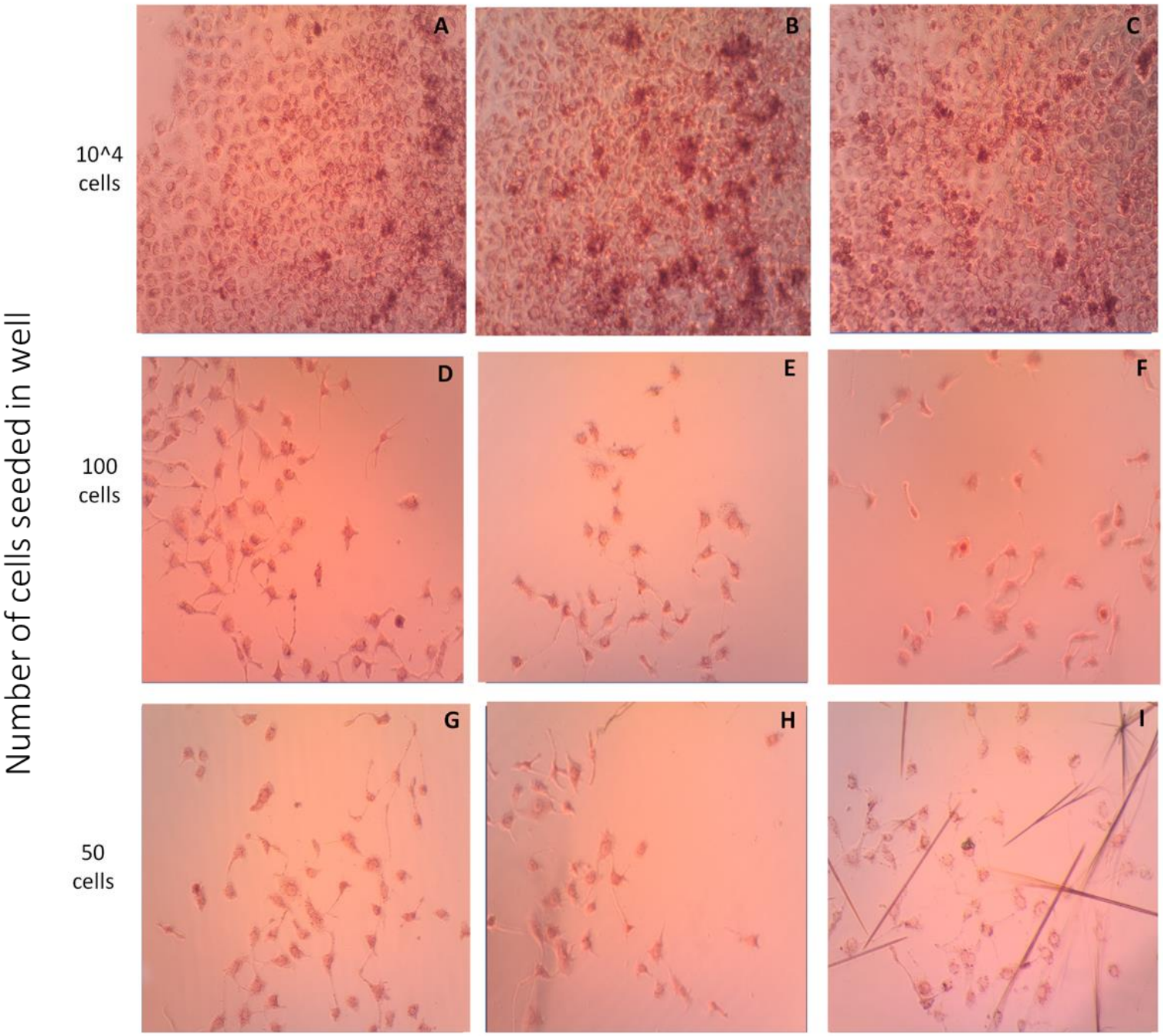


Figure 5.4 Images taken of viable cells before the neutral red dye was extracted using desorb. The images above show the cells that contain the neutral red dye for the wells seeded with different amounts of cells. Fig. A-C: The wells that were seeded with 10^4 cells and the red dye that was taken up by the viable cells. Fig. D-F: The wells that were seeded with 100 cells and the dye that was taken up by the cells. Finally, row G-I show wells seeded with 50 cells. Fig. I: The occurrence of crystals in the well.

Discussion

The neutral red assay is a viability assay that measures the number of healthy cells *in vitro* (cell culture). It can be used as a toxicity assay that measures the number of healthy cells that remain after the cells are treated with a xenobiotic substance. The neutral red assay was considered as a method to measure the cytotoxicity of cytochalasin D on neural crest cells in culture (tissue cultures). However, the cell culture assay had to be adapted to a tissue culture model and in doing so, the following concerns arose: (a.) the potential cytotoxic effects of desorb when there are fewer cells present, (b.) the lack of absorbance readings with fewer cells and (c.) finally the result that no further protocols (i.e., immunocytochemistry) could be conducted using these cells. To address the first concern the recommended volume of desorb was decreased and two additional volumes were tested. The recommended volume and adjusted volumes were then tested on MCF-7 (breast carcinoma cells) seeded at 10^4 cells, 100 cells and 50 cells.

In wells with 10^4 cells, the deceasing volumes of desorb may have resulted in a decreased level of dye extraction from the living cells and as a result the mean absorbance decreased as the volumes of desorb decreased.

In wells seeded with 100 cells the highest mean absorbance was recorded at the adjusted volume of 50µl, which could suggest that the normal volume of desorb (100µl) may have caused some cell death. The lowest mean absorbance for 100 cells was recorded at the adjusted volume of 25µl, the decreased volume of desorb would result in a decrease in the dye extraction from the living cells hence the absorbance was the lowest at this volume.

Finally, in wells seeded with 50 cells, the normal volume of desorb (100µl) may have resulted in cell death as the mean absorbance was the lowest at this volume and the highest mean absorbance, similar to the wells with 100 cells, was observed at the volume of 50 µl of desorb. In the wells seeded with few cells the highest mean absorbance was observed at the adjusted volume of 50 µl of desorb. It is therefore

possible to conclude that in wells with fewer cells the optimised volume of desorb is 50µl.

The results obtained from the neutral red assay experiment, address the first two concerns, in that it was shown that the assay may be adapted to cultures with fewer cells as the absorbance was measured for all wells and the optimised volume of desorb was found. However, after further consideration, of this assay and other cell culture viability assays (MTT, and crystal violet), there are still procedural/technical complications that arise since the nature of neural crest cultures is different from cell culture. In cell culture methods the number of cells that are seeded is known before treatment, and after treatment when the viability is measured the number of living cells is known. Thus, the extent of cell death can be calculated, and the cytotoxicity of the drug/substance can be determined. However, for neural crest cultures, there is no accurate method to determine the number of living neural crest cells before treatment. After treatment the number of cells remaining can be measured (using these assays) but the number of cells that were lost/died cannot be calculated.

Additionally procedural complications limit the application of these assays to neural crest cultures. For colorimetric viability assays (i.e. neutral red, MTT and crystal violet), measurements of cell metabolic activity are measured spectrophotometrically. Hence, neural tubes would need to be cultured in 96 well plates in order to measure the absorbance. However, this is not recommended since the structure/ the walls of the wells could disrupt/displace the cells that are released from the neural tube explant and impair migration (Duland, 2020). Additionally, no further immunolabelling (ICC) or staining (phalloidin staining) can be performed on these cells. As a result, it was determined that the neutral red assay (or any viability assay used in cell culture) while it provides a quantitative analysis of cell viability, is not suited to neural crest cultures.

2. Manual cell counting (based on haemocytometer method)

Using phase contrast microscopy and fluorescence microscopy.

As discussed above, proliferative/viability assays that are typically used in cell culture are not adaptable to NC cultures. Hence the viability of NC cells were calculated by manual cell counting before and after treatment. Cells can be manually counted (using a protocol-haemocytometer) or using automated cell counters.

Generally, manual cell counting methods for cells in suspension, calculates the number of cells in a volume of media. To count the cells, a volume of cells in media is added to the chamber of a specialised glass slide. The chambers have grid patterns on their base that facilitate organised counting (Bard, 1974). The depth and volume of the chamber can vary, and the size and pattern of the grid also varies. The chamber and grid pattern are chosen according to the sample that is being analysed and is dependent on cell size and shape of the cells in the sample.

The most used grid pattern is the improved Neubauer haemocytometer grid. The grid has 9 blocks in total, blocks in the corners contain 16 squares, and the centre block has 25 squares (Fig. 5.5). The blocks in the corner with 16 squares have a larger area for counting bigger cells (0.25 mmx0.25 mm) whereas the centre block with 25 squares is smaller and used for counting rounded small cells (0.05mm x 0.05 mm).

Generally, cells are counted in the corner blocks (with 16 squares). The cells are counted according to a system i.e. cells found only within or on the upper right-hand boundary of the blocks are counted. The system is not standard, and any system can be employed to count cells (as long as the same system is maintained throughout the sample). Cells are counted in all four corner blocks and the average number of cells is calculated and multiplied by 10,000. This is also multiplied by a dilution factor if the cells are diluted in media or trypan blue. The final volume if of viable cells per ml can be calculated.

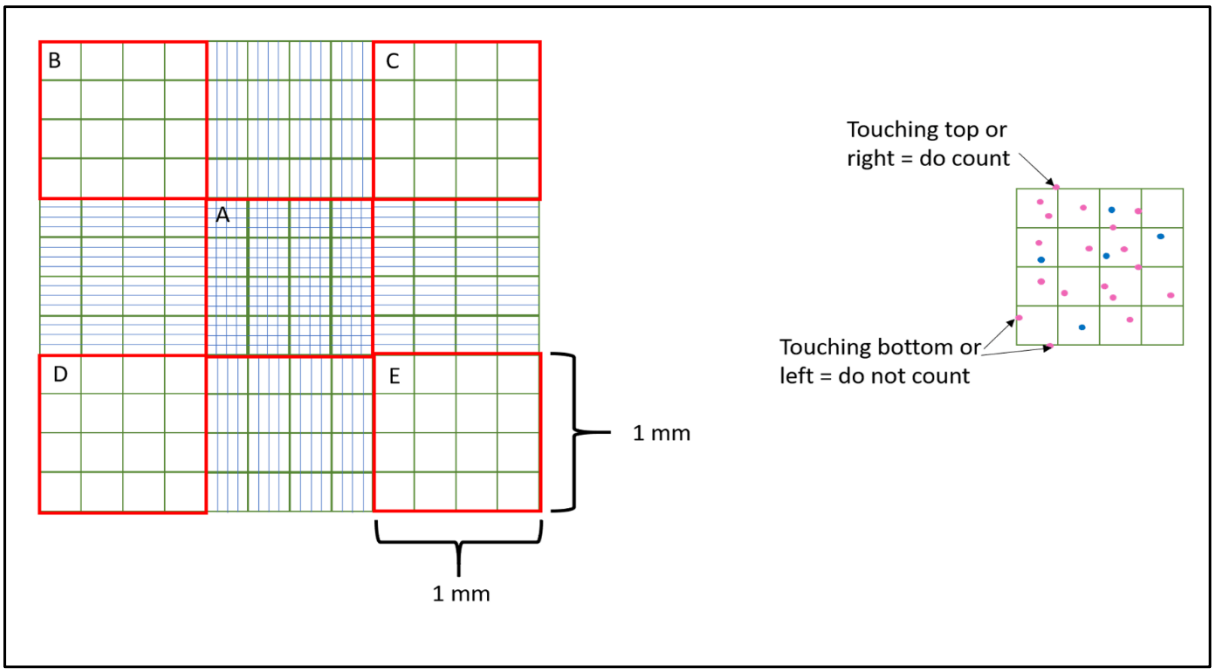


Figure 5.5 shows a Neubauer grid patterns found in the chamber. The corner blocks with 16 sqaures each labelled B-E the squares measure (0.25mm x 0.25mm). The centre block labelled A has 25 squares, each square measures (0.05mmx 0.05mm). The block diagram on the right, cell on the upper right boundary will be counted, while cells on the lower left boundry are not included. The cells in each of the four blocks will be counted and averaged. The avearge number will be multilied by 10 000 and the dilution factor to calculate the number of cells in the volume of media. (https://lab.rockefeller.edu/chen/assets/file/Hemocytometer.pdf) https://images.app.goo.gl/WTjMWMqpnoqrjWhB9

However, for NC cells, since cells are adherent to the fibronectin substrate and must remain attached to the substrate. To study the migration of cells after treatment with cytochalasin D, the adherent cells are counted. Hence, manual cell counting was used for the NC cultures. The attached explant and the migrated cells were imaged before treatment using phase contrast microscopy. The entire explant and the migrated cells were imaged with a 10X objective, to include the entire area of cells. The images were taken in sections/ quadrants (Fig. 5.6).

Each quadrant is imaged at 10X and a grid of 5x7 squares (the area of each square on the grid measured 5 inches^2) was applied to each image. Cells were counted by counting the nuclei that were contained within a square, (using the multipoint function on Image J). Nuclei overlying a grid line were excluded. The nuclei were

used to count cells, since quail cells have prominent nucleoli that can be easily identified (Le Duoarin and Dupin, 2018). Cells were counted in each of the four quadrants and the number of cells from each quadrant was totalled and an approximate number of viable cells before treatment was determined.

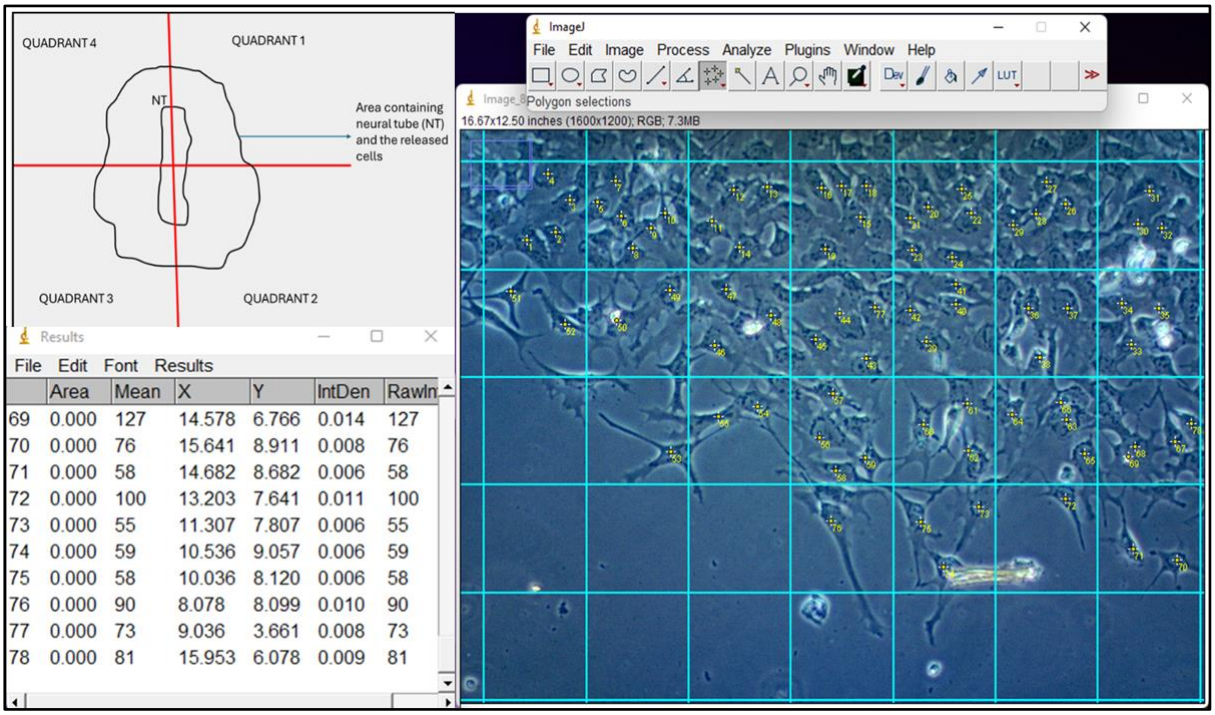


Figure 5.6 Diagram of the neural tube (NT) and the area of migrated cells and an image of counted cells in quadrant 3. The diagram in the upper left corner of the figure shows the neural tube (NT) and the region containing the migrating cells. From the centre of the tube the area covered by cells is divided into four quadrants. Each quadrant was imaged with a 10x objective, the photomicrograph above shows the cells in quadrant 3. A grid was applied to the image and using the ImageJ software, nuclei contained within a square were counted and assigned a number (marked with yellow point) while the nuclei found on the boarders the square were not included. The total number of nuclei (cells) counted for the third quadrant was 78 (shown in the table in the bottom left corner of the figure).

After 6hrs of treatment the cells were fixed, and nuclei of the cells were stained with DAPI. The explant and the area of migrated cells were imaged in the same manner, using a10x objective (fluorescence microscopy) and the neural tube and the migrated cells were divided into quadrants. Each quadrant was imaged, and the viable cells were counted. Viable and non-viable cells were distinguished by the DAPI staining. In non-viable cells DAPI revealed fragmented nuclei and the

occurrence of apoptotic bodies. The grid consisting of 5x7 squares was applied to the images and viable nuclei contained within the squares of the grid were counted (using image J) and the viability was calculated using the following equation:

$$Cell\ viability\ \% = \frac{Number\ of\ viable\ cells\ after\ treatment}{Number\ of\ viable\ cells\ before\ treatment} \times 100$$

However, when attempting this method of cell counting there was a difference between the magnification and the sizes of the images taken with the phase contrast microscope (before treatment) and the available fluorescence microscope (after treatment). The difference can be noticed (Fig. 5.7). This difference in size meant that no standardised grid could be applied to the images and hence cells could not be counted using this method.

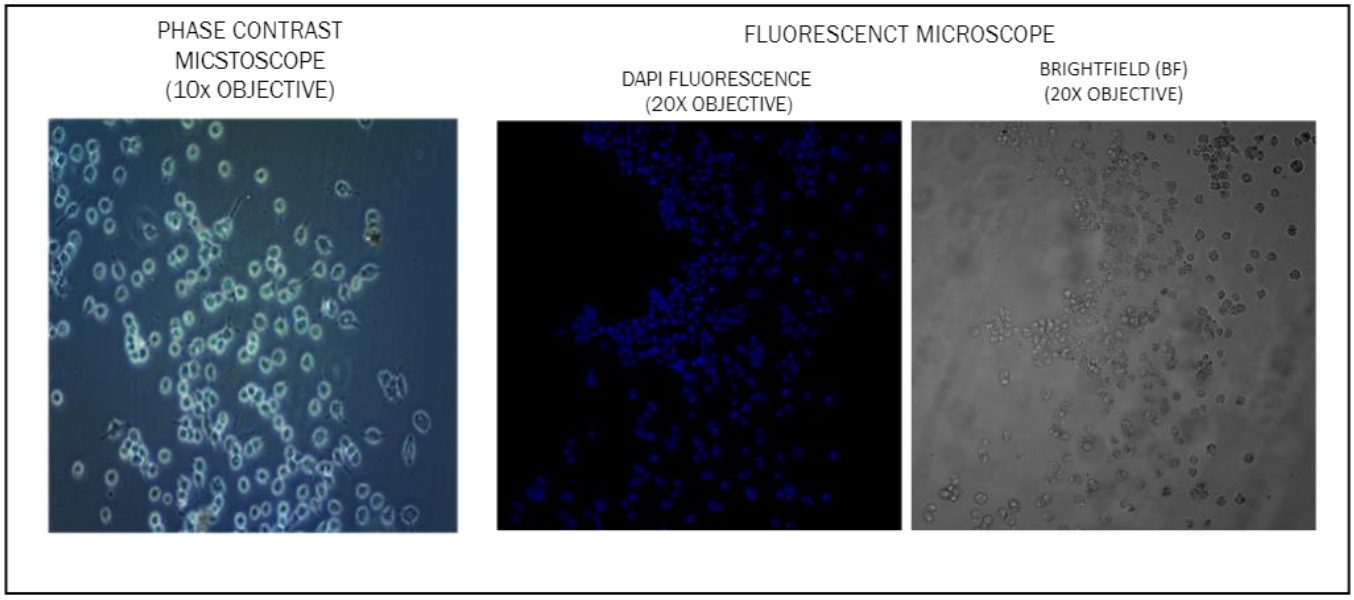


Figure 5.7 The photomicrograph taken with the phase contrast microscope using X10 objective. Two photomicrographs captured on the fluorescent microscope using a X20 objective, the first showing the DAPI stained cells and the second brightfield (BF) image. All the photomicrographs were taken of the same area in the same culture, but it is evident that the magnification of both images is different. The phase contrast image using the X10 objective has a higher magnification than the

fluorescent microscope image which was taken the X20 objective. Even at a higher objective, the magnification on the fluorescent microscope is less than the magnification of the phase contrast. This may the result of a difference between the camera magnification for each microscope.

Appendix 6- Cytochalasin D optimisation results

Results

Cytochalasin D optimisation

Cytochalasin D (diluted in DMSO) was administered to quail NC cultures in an attempt to disrupt the actin filaments and halt NC cell migration. Neural tubes were cultured for 48hrs to allow the migration of NC cells, followed by treatment with cytochalasin D at the following concentration: 0,5µg/ml, 1 µg/ml, 2µg/ml, and 3 µg/ml for 6hrs. In addition, a DMEM control and DMSO control were included in each concentration run. Live cells from all three groups were imaged at 2hrs, 4hrs and 5hrs following treatment. After 6hrs in the treatment cells were fixed with 3,6% paraformaldehyde and were stained with DAPI (1:1000) and Phalloidin- Atto 590 (1:200). The morphology and effects of the treatment were compared between the different cytochalasin D concentrations and with control cultures. The cell viability for each concentration was calculated. The optimised concentration was found to be 0,5 µg/ml of cytochalasin D. As the treatment at this concentration was able to alter the morphology of the cells (to possibly halt migration) without being cytotoxic to the cells.

Prior to treatment (at 48hrs of incubation) the cells (neural crest cells from the neural tube cultures) were stellate shaped. The cells had both broad lamellipodial and fine filopodial projections (Fig. 6.1A to 6.1C). After treatment the following sequential effects were observed: cell projections collapsed, the cell body decreased in size and rounded, transformed cell projections arose and projection arborisation occurred (Fig. 6.1G to 6.1R).

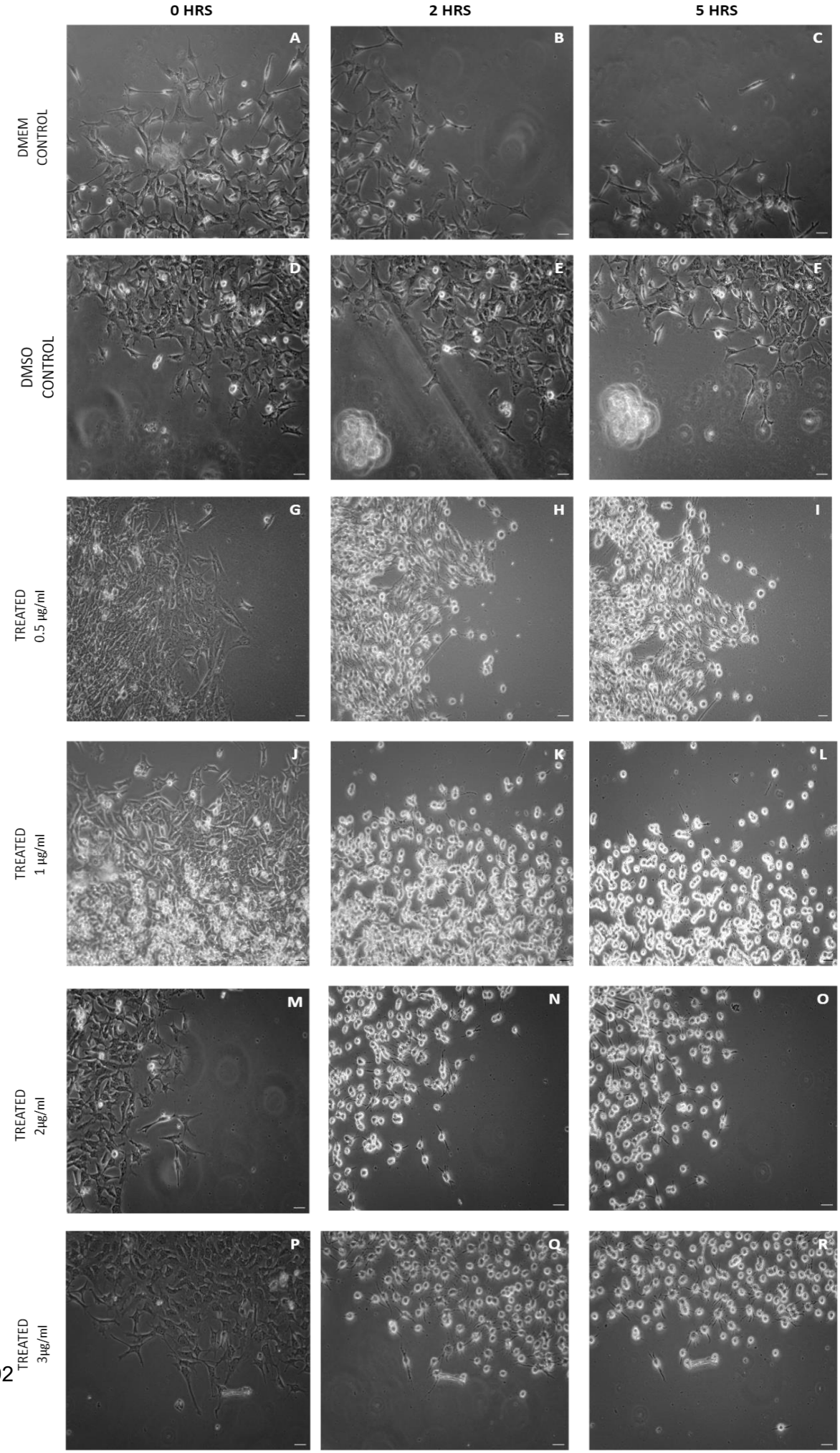

0 HRS
2 HRS
5 HRS
DMEM CONTROL
DMSO CONTROL
TREATED 0.5 µg/ml
TREATED 1 µg/ml
TREATED 2µg/ml
TREATED 3µg/ml
A
B
C
D
E
F
G
H
I
J
K
L
M
N
O
P
Q
R

Figure 6.1 Live quail neural crest cultures in the DMEM control group, DMSO control group and treated group. At T=0 (just prior to the treatment, after 48hrs of the culture), T=2 and T=5 post treatment with cytochalasin D at 0,5 µg/ml, 1µg/ml, 2µg/ml, and 3µg/ml. (Phase contrast microscopy, objective-X10, scale bar- 200µm).

The cells in both control groups (DMEM and DMSO), displayed the characteristic stellate appearance of putative neural crest cells (Fig. 6.2A to 6.2D). Following two hours of treatment with cytochalasin D the cell bodies had rounded and "transformed" projections arose (Fig 6.1H, 6.1K,6.1N, 6.1Q) this altered morphology was maintained after six hours in the treatment (Fig.6.2E to 6.2H). The transformed projections were finer relative to the lamellipodia and filopodia of the cells in the control groups. Additionally, the projections were arborised. The rounded cell bodies and fine branched projections gave the treated cells a spidery appearance (Fig.6.2E to 6.2H).

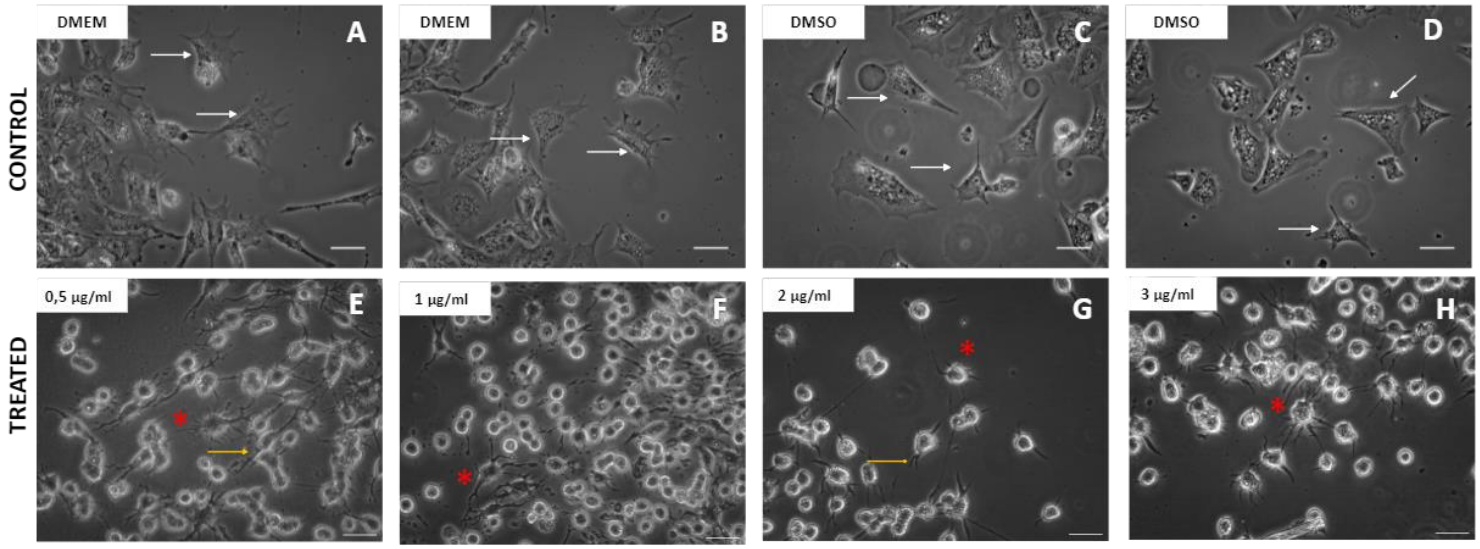


Figure 6.2 Live cells after 6hrs of treatment in their respective media. Cells in the control groups (top panel) had a characteristic stellate appearance with broad lamellipodia and fine filopodia (cells indicated by the white arrows). The treated cells had transformed projections that were fine and branched (indicated by the yellow arrows in the bottom panel). The rounded cell body of the treated cells and the transformed cell projections gave these cells a spidery appearance (cells marked by a red asterisk in the bottom panel). (Phase contrast, objective: X40, scale bar- 50µm)

After 6hrs, cells from all three groups were fixed and stained with DAPI and phalloidin. The cytochalasin D had altered the arrangement of actin in the cell projections and the cell body (Fig. 6.3E to 6.3H). In the control cells (DMEM and DMSO) the actin arrangement was organised, and long filaments of actin lined the cell body and extended within the projections (Fig. 6.3A to 6.3D). In the treated cells the actin was disrupted. The disruption resulted in the loss of long filaments of actin and caused the formation of actin aggregates that were concentrated in the cell body, surrounding the nucleus. The aggregates of actin fluoresced intensely within the cell body (Fig.6.3E to 6.3H).

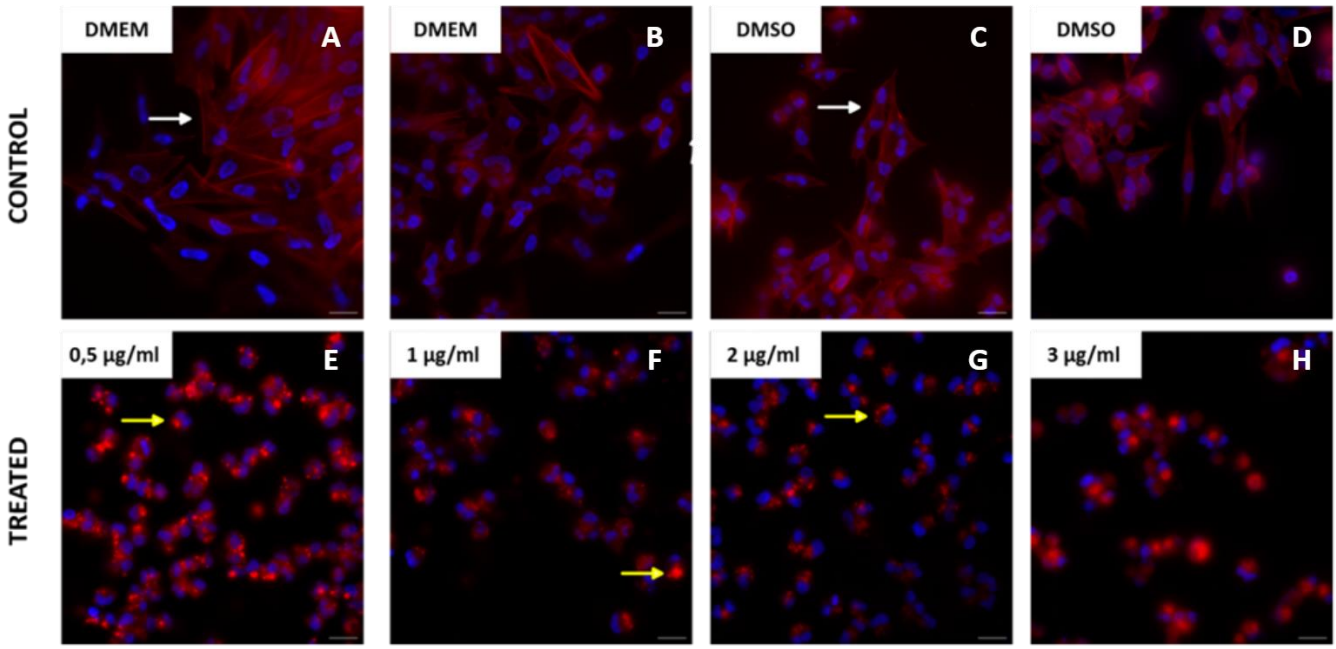


Figure 6.3 Fixed cells from the control and treated groups stained with DAPI (blue) and Phalloidin-Atto 590 (red). Fig A – D: In the control cells, DMEM and DMSO, the phalloidin stain revealed an organised arrangement of actin along the cell body and within projections (indicated by the white arrows in the top panel). Fig. E-H: Treatment with cytochalasin D disrupted the actin arrangement. In the treated cells, aggregates of actin that surrounded the nucleus were noted in the cell body (indicated by the yellow arrows in the bottom panel). (Phalloidin-Atto 590 and DAPI, Fluorescence microscopy, X63 objective, scale bar 20µm).

Cell viability was measured using DAPI for the cells in all three groups. The viability of cells was assessed by the appearance of the DAPI stained nuclei which showed apoptotic bodies in cells that were not viable. In a culture (DMEM, DMSO or treated), six equal areas were imaged, the total number of cells was counted and the proportion of viable cells in each area was determined. The average ratio of viability was calculated and is represented as percentages in Figure. 6.4. The viability of cells from all the tested concentrations did not fall below 50%. The viability of the cells in the DMEM and DMSO control groups was above 80%, indicating healthy cultures. The cells treated with 0,5 µg/ml had a high viability percentage, 85%. The group treated with 1 µg/ml had a cell viability of 72% and the lowest viability of 63% and 62% was observed in the groups treated with 2 µg/ml and 3 µg/ml, respectively.

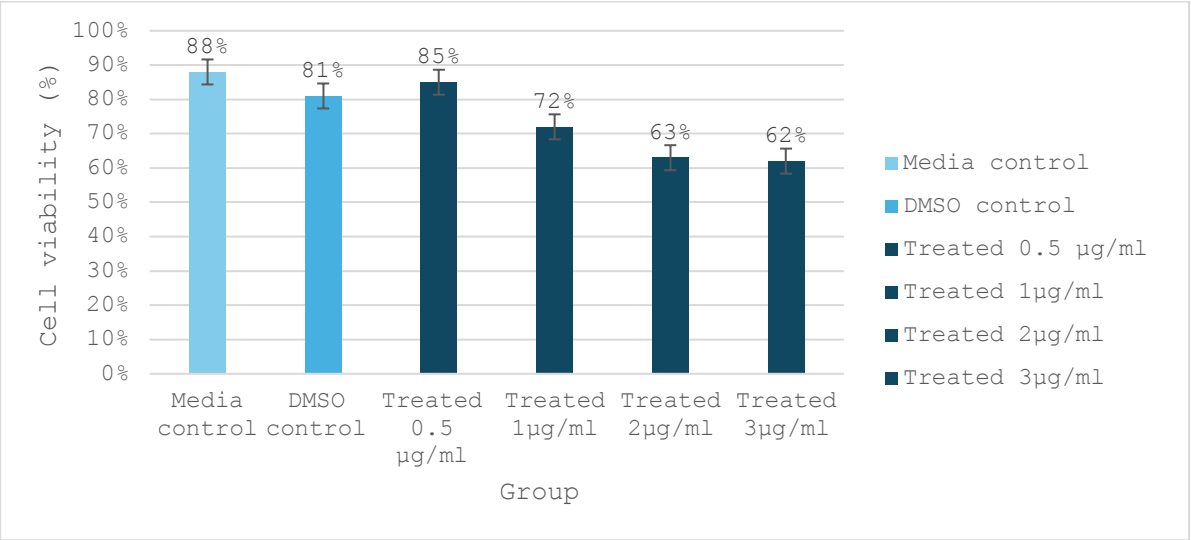


Figure 6.4. The percentage of cell viability (on the y axis) of the cells in the DMEM, DMSO and treated with cytochalasin D group-on the x axis. The key on the right side of the graph shows the colours that were assigned to each group. Six field in each dish was counted and each concentration were repeated three times.

All the different concentrations of cytochalasin D that were tested induced actin disruption (Fig. 6.3E to 6.3H) and transformed the cell morphology (Fig.6.2E to 6.2H) (both of which could halt migration). However, the concentration that showed the highest cell viability was 0,5 µg/ml. Thus, it was concluded that this concentration of cytochalasin D could be used to halt migration without being cytotoxic to the cells.

To confirm the viability of cells treated with 0,5µg/ml of cytochalasin D, the medium containing the cytochalasin D was removed from two cultures after 6hrs and replaced with fresh DMEM. After 2hrs in the DMEM, 13% the cells formed projections and began to assume a stellate shape. After 18hrs in the DMEM some cells developed their projections again (i.e., lamellipodia and filopodia) (Fig. 6.5C), however in the other culture cells maintained their transformed projections (Fig. 6.5F). It should also be noted that there appeared to be fewer cells after recovery.

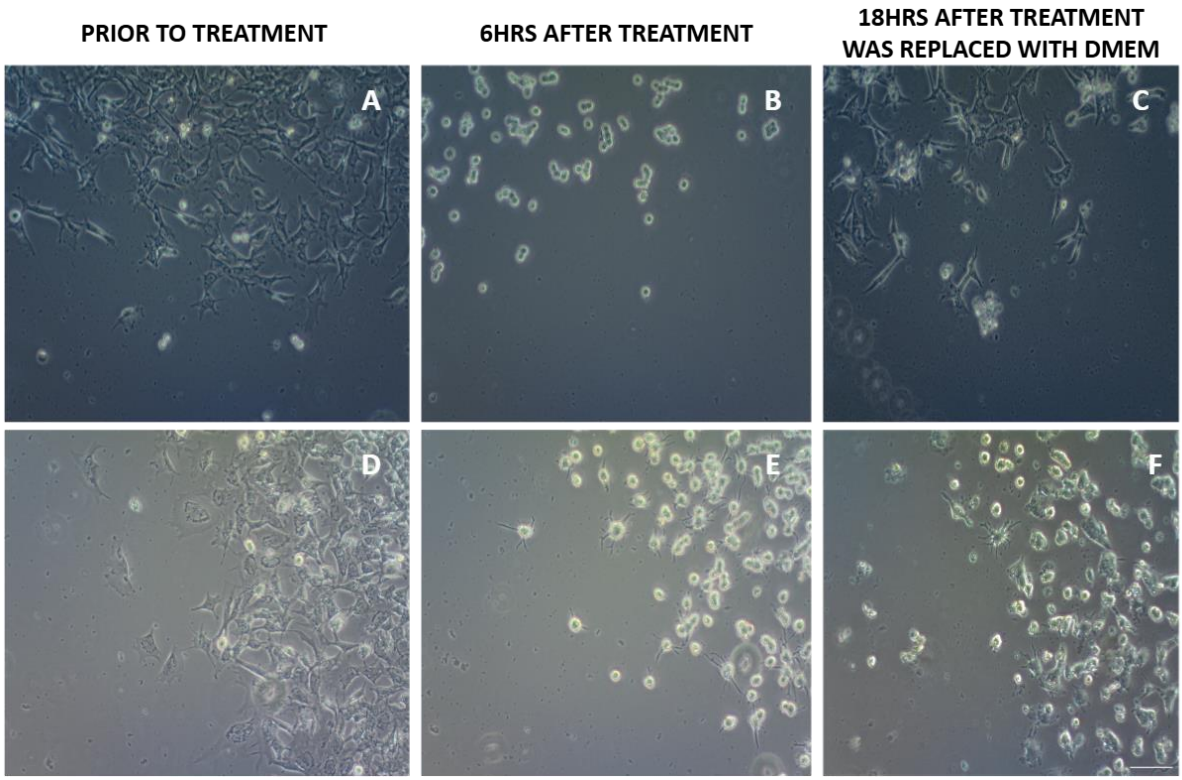


Figure 6.5 Live cells treated with cytochalasin D for 6hrs after which the treatment was replaced was DMEM. Prior to treatment with cytochalasin D, the cells were stellate shaped. After 6hrs of treatment the cells rounded up completely and there were no projections present. The DMEM containing cytochalasin D was replaced with fresh DMEM and after 18hrs in fresh DMEM some cells recovered their projections Fig. C while others maintained their transformed projections Fig. F. (Phase contrast microscopy- 10x objective, scale bar- 200µm)

Appendix 7- Immunocytochemistry solutions and optimisation

Immunofluorescent preparation:

Solutions include:

- PBS (phosphate buffer solution)
- 3,6% paraformaldehyde
- 0,1% Triton X- 100
- 1% BSA solution (bovine serum albumin)

To prepare PBS (phosphate buffer solution): in 800 ml of distilled water.

- 8g of NaCl
- 0,8g of KCL
- 1,44g of $Na_2 HPO_4$
- 0,24g of $KH_2 PO_4$

Adjust the pH of the 800 ml solution to 7,40 thereafter top up solution to 1L.

To prepare 3,6% paraformaldehyde for fixing the NC cultures:

- 10µl of 36% paraformaldehyde was added to 900 µl of PBS.

To prepare 0,1% Triton X-100:

- 10µl of 100% Triton X-100 was added to 10 ml of PBS.

To prepare 1% BSA-PBS solution (the volume of BSA needed was calculated and prepared on the day of experiment):

- 0,10g of BSA powder (Sigma) was added to 10 ml of PBS

Primary antibody

The optimisation for the primary antibody was conducted. Two different anti-HNK antibodies were tested from different sources. HNK-1 (Sigma- C6680 mouse IgM) and HNK-SH5 from Developmental Studies Hybridoma Bank (DSHB).

For the Sigma antibody, a 1:500 dilution was tested. For the DSHB antibody the following concentrations were tested 1:10,1:50, and1:100. The concentrations for the DSHB antibody were according to the following references (Juarez et al., 2014; Kerosoa and Bronner, 2014; Rogers et al., 2012 and Tang et al., 2021)

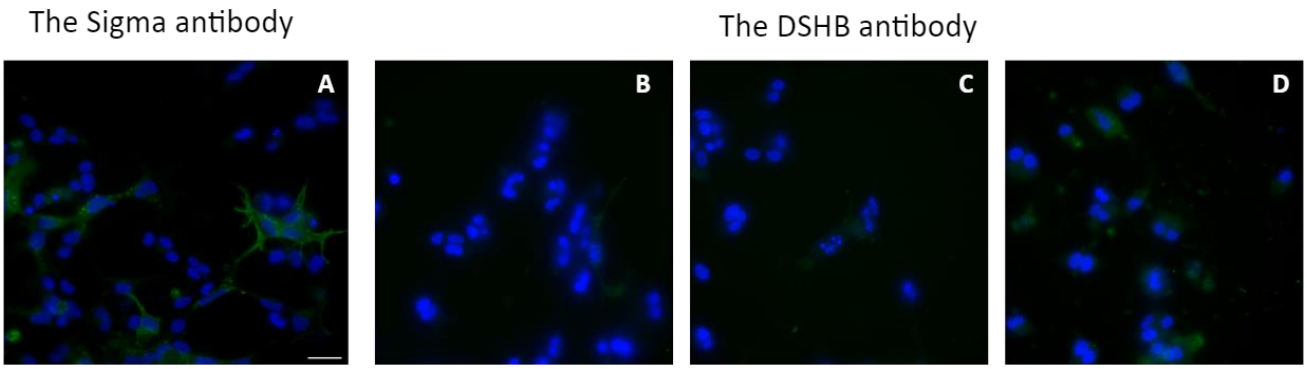


Figure 7.1 Immunolabelling of *in vitro* NC cultures using the antibody DSHB. (At different concentrations). Fig. A Sigma antibody 1:500, Fig. B DHSB antibody, Fig. C DHSB antibody 1:50 and Fig. D DHSB antibody 1:10. The antibody is generally localised along the membrane and within the cell body (as seen in the cells labelled with the Sigma antibody Fig. A). The DSHB antibody does not fluoresce as intensely as the Sigma antibody. In Fig. D some cells are immunolabelled, however the cell boarders are not well defined, and labelling is not definitive. In Fig. B and C the cell boarders can be seen but fluorescent intensity is low. (Fluorescent microscopy, X40, scale bar- 200µm).

From the figures above it was determined that the Sigma antibody at the dilution of 1:500 was the optimal dilution and antibody. All immunolabelling was then performed using the Sigma HNK-1. The primary antibody was diluted in 1% BSA-PBS solution.

Secondary antibody

The secondary goat anti-mouse conjugated to Alexa-Fluor 488 (Thermo Fisher- **A-10680)** was diluted in 1% BSA-PBS solution at the1:1000 concentration. No further dilutions were tested since the 1:1000 concentration was shown to be the optimal dilution. Negative controls were conducted on seven NC cultures, where the fixed cells were permeabilised with Triton X and blocked using BSA, incubated in the secondary antibody only and stained with DAPI.

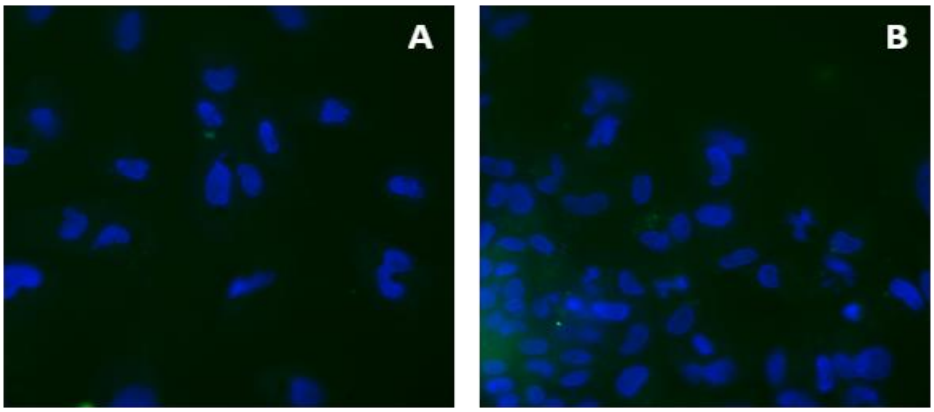


Figure 7.2. Negative immunofluorescent controls (secondary goat anti-mouse conjugated to Alexa-Fluor 488 (Thermo Fisher). Some NC cultures were used as a negative immunofluorescent control. In both figures above, the secondary antibody alone showed no distinct labelling and the fluorescence observed was measured and was subtracted from positive control images to remove the background fluorescence. (Fluorescence microscopy, X40, scale bar- 200µm).

DAPI staining.

The optimised concentration of DAPI that was previously used in the laboratory (Deroubaix et al., 2019) was 1:1000. DAPI was prepared by diluting in PBS in the following dilution (1:1000).

Phalloidin-Atto 590 staining

Phalloidin- Atto 590 was added to the dilution of primary antibody (in BSA-PBS) and incubated for 1 hour at 37°C. Optimisation runs were conducted to determine the optimal concentration of Phalloidin-Atto 590 that stained the actin filaments in the cells. At a concentration of 1:500 which was used previously in the laboratory on NCCs (Deroubaix et al., 2019), the staining intensity was low, and the actin filaments were not well defined. The concentration was increased to 1:200 which stained the actin well. It is possible that there was an increase in the number of migrating cells in quail NC cultures (as opposed to the chicken NC culture in Deroubaix et al., 2019) hence the concentration was increased.

APPENDIX 8- Data was entered into JASP software for analysis

Cell velocity:

Cell velocity,Group
145.02,DMEM
128.32,DMEM
143.61,DMEM
117.57,DMEM
152.65,DMEM
156.24,DMEM
155,DMEM
151.24,DMEM
54.78,DMEM
61.6,DMEM
65.73,DMEM
46.46,DMEM
45.2,DMEM
45.89,DMEM
70.26,DMEM
42.46,DMEM
59.7,DMEM
52.79,DMEM
32,DMEM
37.97,DMEM
80.9,DMEM
60.79,DMEM
37.35,DMEM
50.93,DMEM
37.32,DMEM
49.19,DMEM
125.6,DMEM

72.68,"DMSO "
99.47,"DMSO "
50.17,"DMSO "
71.55,"DMSO "
53.41,"DMSO "
64.2,"DMSO "
65.13,"DMSO "
28.17,"DMSO "
51.05,"DMSO "
38.54,"DMSO "
44.09,"DMSO "
45.82,"DMSO "
22.64,"DMSO "
33.86,"DMSO "
41.22,"DMSO "
40.24,"DMSO "
29.84,"DMSO "
34.73,"DMSO "
37.21,"DMSO "
50.58,"DMSO "
33.01,"DMSO "
22.51,"DMSO "
50.87,"DMSO "
51.9,"DMSO "
45.69,"DMSO "
25.11,"DMSO "
40.28,"DMSO "
40.51,TREATED
45.01,TREATED
46.18,TREATED
46.19,TREATED
36.12,TREATED
47.19,TREATED

47.24,TREATED
43.65,TREATED
47.54,TREATED
17.92,TREATED
36.9,TREATED
19.86,TREATED
16.47,TREATED
9.37,TREATED
26.33,TREATED
20.67,TREATED
35.31,TREATED
18.44,TREATED
42.78,TREATED
38.99,TREATED
50.32,TREATED
53.97,TREATED
49.82,TREATED
50.91,TREATED
54.58,TREATED
39.9,TREATED
50.54,TREATED

Phalloidin Fluorescence:

Phalloidin Fluorescence
,"Group "
3797433.566,DMEM
2449624.417,DMEM
4507067.861,DMEM
3508426.213,DMEM
1791442.373,DMEM
2622678.947,DMEM
6590453.768,DMEM

6590453.768,DMEM
6215081.507,DMEM
1276652.023,DMEM
1143127.356,DMEM
1803926.142,DMEM
1322841.565,DMEM
1743816.522,DMEM
1595265.003,DMEM
856306.1391,DMEM
1693992.261,DMEM
1131443.368,DMEM
4529620.617,DMEM
3077688.783,DMEM
3321814.14,DMEM
4540320.075,DMEM
5706204.149,DMEM
3460073.673,DMEM
2205646.185,DMEM
6736041.657,DMEM
2004489.644,DMEM
668855.038,DMEM
1438164.932,DMEM
1535855.75,DMEM
1430644.391,DMSO
2575009.847,DMSO
1540700.444,DMSO
1915518.023,DMSO
854430.1622,DMSO
1167528.261,DMSO
1913362.112,DMSO
1622363.371,DMSO
2020605.954,DMSO
1818287.618,DMSO

1430644.391,DMSO
2169334.884,DMSO
1612616.401,DMSO
1080100.58,DMSO
995943.9929,DMSO
1459477.16,DMSO
481824.5626,DMSO
1169555.827,DMSO
728829.466,DMSO
758757.0983,DMSO
941485.456,DMSO
2596392.919,DMSO
985853.1911,DMSO
1108221.315,DMSO
1761875.713,DMSO
2717034.99,DMSO
1219181.097,DMSO
1821908.858,DMSO
1018997.998,DMSO
1613072.673,DMSO
1358255.608,TREATED
1571863.38,TREATED
891562.3161,TREATED
1678961.667,TREATED
973668.6645,TREATED
1057520.6,TREATED
1156617.245,TREATED
1620739.942,TREATED
1175803.505,TREATED
1532316.357,TREATED
1910826.568,TREATED
1055741.865,TREATED
620179.1765,TREATED

813255.39,TREATED
1712915.573,TREATED
1249597.06,TREATED
1354707.632,TREATED
1339068.892,TREATED
730868.4103,TREATED
645120.3154,TREATED
1554765.496,TREATED
801280.0192,TREATED
826533.2706,TREATED
2046579.578,TREATED
580149.7359,TREATED
507965.2214,TREATED
510707.7441,TREATED
550379.9834,TREATED
1390383.097,TREATED
685646.8073,TREATED